

3-AXIS ATTITUDE CONTROL OF A GEOSTATIONARY SATELLITE

A THESIS SUBMITTED TO  
THE GRADUATE SCHOOL OF NATURAL AND APPLIED SCIENCES  
OF  
THE MIDDLE EAST TECHNICAL UNIVERSITY

BY

HAKKI ÖZGÜR DERMAN

IN PARTIAL FULFILMENT OF THE REQUIREMENTS FOR THE  
DEGREE OF  
MASTER OF SCIENCE  
IN  
THE DEPARTMENT OF AERONAUTICAL ENGINEERING

DECEMBER 1999

Approval of the Graduate School of Natural and Applied Sciences

---

Prof. Dr. Tayfur Öztürk  
Director

I certify that this thesis satisfies all the requirements as thesis for the degree of Master of Science.

---

Prof. Dr. Nafiz Alemdaroğlu  
Head of Department

This is to certify that we have read this thesis and that in our opinion it is fully adequate, in scope and quality, as a thesis for the degree of Master of Science.

---

Prof. Dr. Yurdanur Tulunay  
Co-Supervisor

---

Assoc. Prof. Dr. Ozan Tekinalp  
Supervisor

Examining Committee Members

Prof. Dr. M. Cevdet Çelenligil

Prof. Dr. Ünver Kaynak

Assoc. Prof. Dr. Yusuf Özyörük

Assoc. Prof. Dr. Mehmet Ş. Kavsaoglu

Assoc. Prof. Dr. Ozan Tekinalp

## **ABSTRACT**

### **3-AXIS ATTITUDE CONTROL OF A GEOSTATIONARY SATELLITE**

Derman, Hakkı Özgür

M.S., Department of Aeronautical Engineering

Supervisor: Assoc Prof. Dr. Ozan Tekinalp

December 1999, 134 pages

In this thesis application of an attitude control system minimising fuel expenditure of a geostationary satellite is studied. The satellite parameters are similar to the actual TÜRKSAT 1B satellite platform. TÜRKSAT 1B Attitude Determination and Control Subsystem is described in detail. Using MATLAB-Simulink computing, modelling and simulation environment, the satellite attitude, under various external and internal disturbances and sensor noise is simulated. A new automatic control system is designed. A PD controller regulates the pitch attitude with strapdown momentum wheels. For yaw/roll attitude regulation, an integral plus full state-feedback controller attitude is designed, and tested various pole locations. Pulse width modulated thruster activation period is also tuned for fuel expenditure minimisation through an extensive parametric search.

Key Words: Attitude Control, Geostationary Satellite, TÜRKSAT 1B, Pulse Width Modulation, Pole Placement Design, State Variable Feedback, Attitude Regulation, Satellite Attitude Simulations.

## ÖZET

YER EŞZAMANLI BİR UYDUNUN 3 EKSENDE DENETİMİ:

Derman, Hakkı Özgür

Yüksek Lisans, Havacılık Mühendisliği Bölümü

Tez Yöneticisi: Doç. Dr. Ozan Tekinalp

Aralık 1999, 134 Sayfa

Bu tezde yer eşzamanlı bir uydunun davranış hareketine yakıt sarfiyatını en aza indiren denetim sisteminin tasarlanması incelenmiştir. Kullanılan uydu modelinin özellikleri gerçek TÜRK SAT 1B uydusununkilere benzemektedir. TÜRK SAT 1B davranış hareketi belirleme ve denetim altsistemi detaylıca tanıtılmıştır. MATLAB–Simulink yazılımı kullanılarak uydunun çeşitli iç ve dış bozucu kuvvetler ve algılayıcı gürültüsü altında davranışı için benzetim çalışması yapılmıştır. Yeni bir denetim yasa tasarlanmıştır. Bir PD denetimcisi yunuslama davranışını momentum tekeri ile ayarlar. Sapma/ yuvarlanma açısız denetimi için bir tüm hal değişkenleri geribeslemesi ile bir integral denetimcisi tasarlanıp değişik özdeğer atama yöntemi ile denenmiştir. Darbe genlik modülasyonu kullanan tepki motorunun faaliyet devresi, yakıt sarfının en aza indirilmesi için kapsamlı parametrik bir tarama yapılarak belirlenmiştir.

Anahtar Kelimeler: Davranış Denetimi, Yereşzamanlı Uydu, TÜRK SAT 1B, Darbe Genlik Modülasyonu, Özdeğer Atama Tasarımı, Durum Değişkenleri Geribeslemesi, Davranış Düzenlemesi, Uydu Davranış Benzetimi.

# TABLE OF CONTENTS

<b>ABSTRACT .....</b>	<b>III</b>
<b>ÖZET.....</b>	<b>IV</b>
<b>TABLE OF CONTENTS .....</b>	<b>V</b>
<b>CHAPTERS .....</b>	
<b>I. INTRODUCTION .....</b>	<b>1</b>
1.1 INTRODUCTION TO “ATTITUDE CONTROL OF A SATELLITE PLATFORM RESEMBLING TO TÜRKSAT 1B” .....	1
<b>II. LITERATURE SURVEY .....</b>	<b>5</b>
2.1 SURVEY SUMMARY.....	5
<b>III. DESCRIPTION OF TÜRKSAT 1B SATELLITE SYSTEM WITH A CONCENTRATION ON ATTITUDE CONTROL SUBSYSTEM.....</b>	<b>11</b>
3.1 TÜRKSAT 1-B ON ORBIT .....	11
3.2 GENERAL DESCRIPTION OF TÜRKSAT 1B SUBSYSTEMS.....	13
3.3 ATTITUDE DETERMINATION AND CONTROL SUBSYSTEM (ADCS).....	13
3.3.1 <i>Overall Electrical Configuration.....</i>	<i>14</i>
3.3.2 <i>TÜRKSAT 1B Attitude Sensor Configuration.....</i>	<i>15</i>
3.3.3 <i>Attitude Determination and Control Electronics.....</i>	<i>19</i>
3.3.4 <i>TÜRKSAT 1B Attitude Control Actuators .....</i>	<i>21</i>
3.3.5 <i>Functions of the ADCS during Transfer Orbit (TO).....</i>	<i>25</i>
3.3.6 <i>Functions of the ADCS during Geostationary Orbit (GO).....</i>	<i>28</i>
3.3.7 <i>Functions of the ADCS in Antenna Pattern Measurement .....</i>	<i>32</i>
3.3.8 <i>Functions of the ADCS in De-Orbiting .....</i>	<i>32</i>
3.3.9 <i>Functions of the ADCS in Safe-Guarding .....</i>	<i>32</i>
3.3.10 <i>Functions of the ADCS in Earth Re-Acquisition with RIGA Attitude Reference .....</i>	<i>33</i>
3.3.11 <i>Functions of the ADCS in Re-positioning.....</i>	<i>34</i>
3.3.12 <i>Functions of the ADCS in Monitoring.....</i>	<i>34</i>

3.4	TÜRKSAT 1B ELECTRICAL POWER SUBSYSTEM (EPS)	34
3.4.1	<i>Solar Panels</i>	35
3.4.2	<i>BAPTA</i>	35
3.4.3	<i>PCU and PCDU</i>	36
3.5	TÜRKSAT 1B UNIFIED PROPULSION SUBSYSTEM (UPS)	36
3.6	TÜRKSAT 1B TELEMETRY, COMMANDING AND RANGING (TCR) SUBSYSTEM	37
3.7	TÜRKSAT 1B REPEATER SUBSYSTEM	38
3.8	TÜRKSAT 1B THERMAL CONTROL SUBSYSTEM	38
3.9	TÜRKSAT 1B MASS PROPERTIES	39
<b>IV. BUILDING OF A SATELLITE ATTITUDE DYNAMICS MODEL SIMILAR TO THE TÜRKSAT 1B GEOSTATIONARY SATELLITE</b>		<b>41</b>
4.1	INTRODUCTION	41
4.2	MASS PROPERTIES OF THE MODEL SPACECRAFT	42
4.2.1	<i>General Description</i>	42
4.2.2	<i>Determination of the Model Inertial Properties</i>	43
4.3	DERIVATION OF THE RIGID BODY ATTITUDE EQUATIONS OF MOTION (EOM)	43
4.3.1	<i>General Equations of Motion Description</i>	43
4.3.2	<i>Model's EOM Description</i>	45
4.4	ENVIRONMENTAL AND INTERNAL DISTURBANCES ON ATTITUDE MODEL	56
4.4.1	<i>Environmental (External) Disturbance Torques</i>	57
4.4.2	<i>Internal Disturbance Torques</i>	64
<b>V. ATTITUDE CONTROL SYSTEM DESIGN</b>		<b>66</b>
5.1	PITCH CONTROL SYSTEM DESIGN	66
5.1.1	<i>Equations for Pitch Motion</i>	66
5.1.2	<i>Actuator Model</i>	67
5.1.3	<i>PD Controller Design: Tuning the Parameters</i>	70
5.1.4	<i>Simulink Program for the Simulation of the Linear Pitch Dynamics Model, together with the Controller</i>	71
5.1.5	<i>Linear Simulation Results</i>	73
5.2	ROLL/YAW CONTROL SYSTEM DESIGN	75
5.2.1	<i>Linearised Equations Of Roll/Yaw Coupled Motion</i>	76
5.2.2	<i>Controller Design for Coupled Linear Roll/Yaw Dynamics</i>	77
5.2.3	<i>Thruster Model</i>	81
5.2.4	<i>Simulink Roll/Yaw Control Model</i>	83
5.2.5	<i>Linear Simulation Results with Fuel Consumption Minimising</i>	86
5.2.6	<i>Linear Simulations with Pulse Width Modulated Actuator</i>	90
5.3	NONLINEAR SIMULATION	94
5.3.1	<i>Nonlinear System Responses with Controllers</i>	95

5.3.2	<i>Description of Nonlinear Simulink Model with Controllers</i> .....	99
<b>VI.</b>	<b>SUMMARY AND CONCLUSION</b> .....	<b>104</b>
	<b>REFERENCES</b> .....	<b>108</b>
	<b>APPENDICES</b> .....	
<b>A.</b>	<b>NONLINEAR BODY DYNAMICS BEHAVIOUR ANALYSES</b> .....	<b>112</b>
A.1.	DISTURBANCE EFFECTS ARE EXCLUDED .....	112
A.1.1.	<i>Simulations without the External Disturbance Torque</i> .....	112
A.2.	SIMULATIONS WITH DISTURBANCE TORQUE MODELS INCLUDED .....	117
<b>B.</b>	<b>LINEARISED ATTITUDE DYNAMICS MODELS</b> .....	<b>124</b>
B.1.	CASE 1; MANUAL LINEARISATION.....	124
B.1.1.	<i>Assumptions for Linearisation</i> .....	125
B.1.2.	<i>Linearisation</i> .....	125
B.1.3.	<i>Stability Analysis</i> .....	128
B.2.	CASE 2; LINEARISATION BY MATLAB .....	129
B.3.	LINEARISATION OF THE SIMULINK MODEL THAT EXCLUDES EXTERNAL DISTURBANCE TORQUE MODEL.....	132
B.4	SHORT DISCUSSION ON LINEARISATIONS IN TERMS OF STABILITY .....	134

# CHAPTER I

## INTRODUCTION

### 1.1 Introduction to “Attitude Control of a Satellite Platform Resembling to TÜRKSAT 1B”

Artificial satellites have become our everyday tools, just like our cars, televisions, mobile phones, and so on. They are used for telecommunication, weather forecasting, geological and interstellar surveys, for defense and spying applications and many others. Mankind achieved to develop many types of artificial spacecraft to satisfy the above indicated and many other needs: Micro satellites, low orbit, high orbit or interstellar/interplanetary surveying satellites, geostationary and special mission satellites like the GPS satellite group with service life varying from weeks to decades. Many special or general use spacecraft are developed and are being developed for a better understanding of the earth, close and far stellar objects, the space and the human himself.

Turkey has also put his step in satellite communication business by TÜRKSAT series of geostationary satellites. This increased Turkish scientists’ and engineers’ interest on spacecraft sciences like satellite communication; space vehicle’s orbit and attitude dynamics, determination and control; celestial mechanics. TÜRKSAT series of satellites brought a chance of technology transfer and development on spacecraft sciences.

Determination of the satellite orbit is research area under celestial mechanics, a branch of astrodynamics. Eskobal [1] define this as “the process of formulating a

first approximation to the orbital parameters”. Astrodynamics in general deals with the particle motion subject to a gravity field, such as body dynamics in the interplanetary space. Celestial mechanics being a specific branch of it concentrates on the natural motion of heavenly bodies.

The attitude dynamics of a spacecraft is another specific branch of astrodynamics. This branch concentrates on the motion of the plant (the controlled space vehicle) about its center of mass. [2] Naturally knowing attitude behaviour of the satellite before production and placing on service orbit enable the designers to propose the best control method to warrant its mission to be performed within specifications. Here we notice two basic problems: Attitude / Motion dynamics determination and proper control of the plant. This thesis work concentrates on spacecraft attitude control.

TÜKSAT 1B, on its orbit continuously stay on specific latitude and longitude, and pointed to earth to cover certain transmission area. These types of spacecraft are placed on a geostationary orbit about 36000 to 42000 km away from earth. “A geostationary satellite is subjected to various disturbances. As such it can not keep its geostationary orbit and drifts from its required positions. Consequently, the position and orbit parameters of the satellite must be corrected periodically by the commands sent from a ground station. Orbit correction of TÜRKSAT 1B is conducted from Gölbaşı and METU ground stations.” [3] Attitude correction is done autonomously via the built in automatic control system of the satellite, the ADCS (Attitude Determination and Control Sub-system). Orbit and attitude control specifications are stringent for a telecommunication satellite to achieve its mission. Space systems cost millions of US Dollars including launching, on orbit servicing and the ground control services. Hence the modern space plants’ stability, robustness, reliability, tracking/pointing performance, service life and other constraints have become more stringent in comparison to land/sea vehicle systems and to previously designed space vehicles.

Introduction of modern control theory with various feasible techniques became popular in spacecraft control problems as well. For example, gain scheduling, pole

placement, Linear Quadratic Gaussian (LQG) techniques took attention mostly for their robustness properties. [4] In real life the sensors are still noisy, plant dynamics are still hard to model precisely, and the disturbances, as always, are still existent. Various linear and nonlinear control methods are proposed to solve these problems.

Development of electronics and computer sciences enabled faster and faster onboard computing which led to more enhanced control strategies. A giant step in digital control applications was realised by the introduction of online, discrete time modeling of the process. This enabled many filtering (like Kalman Filter) and plant prediction methods. Soon this was followed by the minimum variance control (MVC) approach that is based on these prediction models under noisy conditions. [5] These methods formed the background of optimization theory and its control applications. [4]

Donald E. Kirk, at his book *Optimal Control Theory; An Introduction*, states the basic differences between classical and optimal control theories as at the following paragraph [6]:

Classical control system design is generally a trial-and-error process in which various methods of analysis are used iteratively to determine the design parameters of an "acceptable" system. Acceptable performance is generally defined in terms of time and frequency domain criteria such as rise time, settling time, peak overshoot, gain and phase margin, and bandwidth. Radically different performance criteria must be satisfied, however, by the complex, multiple-output systems required to meet the demands of modern technology. For example, the design of a spacecraft attitude control system that minimizes fuel expenditure is not amenable to solution by classical methods. A new and direct approach to the synthesis of these complex systems, called optimal control theory, has been made feasible by the development of the digital computer.

The objective of optimal control theory is determine the control signals that will cause a process to satisfy the physical constraints and at the same time minimize (or maximize) some performance criterion.

In this thesis Optimal Control problem is not addressed. However, the controller sought for is desired to provide low fuel expenditure. Thus, we can state the purpose of this thesis work completely; Design of a Control System for plant model resembling to TÜRKSAT 1B satellite, with low fuel expenditure satisfying various predefined attitude control constraints like keeping satellite pointing within specified angle range. In shorter words this thesis is a study on “Attitude Control of a Satellite Platform Resembling to TÜRKSAT 1B.” Controlled and uncontrolled attitude behaviour of the satellite model is simulated via MATLAB-Simulink software.

We shall briefly introduce our computing/modeling/simulating environment the MATLAB 5.2: MATLAB is a technical computing environment for high-performance numeric computation and visualization. MATLAB integrated numerical analysis, matrix computation, signal processing, and graphics in an easy-to-use environment where problems and solutions are expressed just as they are written mathematically- without traditional programming. The name MATLAB stands for Matrix Laboratory. MATLAB also features a family of application-specific solutions called “toolboxes”. We will make use of optimization and control system toolboxes and Nonlinear Control Design Blockset of MATLAB during this thesis work. Finally we introduce the SIMULINK: Simulink is a tool for modeling, analyzing and simulating a vast variety of physical and mathematical systems, including those with nonlinear elements and those which use continuous and discrete time. As an extension of MATLAB, Simulink adds many features specific to dynamic systems while retaining all of MATLAB’s general-purpose functionality. Using Simulink, we model a system graphically, sidestepping much of the nuisance associated with conventional programming.

A competitor program to MATLAB can be the MATRIX-X program, but unlike MATLAB it is not so widely available to academic areas, and modeling with MATRIX-X is more difficult in comparison with simple usage of Simulink.

## CHAPTER II

### LITERATURE SURVEY

This section summarises the recent literature on attitude dynamics and control of spacecraft. The publications from 1991 up to 1997 are compiled in this chapter. The number of similar journals are very restricted, however most relative ones are presented here.

#### 2.1 Survey Summary

Liu and Singh [7] studied the fuel/time optimal control design of an inertially symmetric spacecraft undergoing “rest-to-rest” maneuvers. They proposed both time optimal and fuel/time optimal control problem solutions by a modified Switch Time Optimization (STO) algorithm. Numerical STO algorithm integrates state equations forward in time, and the costates (or adjoints) backward in time. Since final time ( $t_f$ ) is set free and switching time depend on  $t_f$ . Errors and final constraints update iterative algorithm. Bang-off-Bang type control and optimal number of switching are simulated. They used quaternion method to represent body dynamics (state equations).

Similar to Liu & Singh, Bilimoira and Wie studied time optimal 3-axis control of an inertially symmetric rigid spacecraft [8]. Time optimal solution is found to be Bang-Bang type of control with optimal number of switching. Again quaternion method is used to describe attitude dynamics of the spacecraft. Singular control search yielded the necessity of saturation of at least one actuator. They simulated the attitude behaviour by using a numerical approach: Multiple shooting algorithm

with modified control constraint approach. Multiple shooting algorithm is for two-point boundary value problems and is used with state-costate equations. Modified control constraint approach is needed to determine control structure itself. Minimum time 180° “rest-to-rest” maneuver control is simulated at the end of their work.

Seywald et al. [9] present the fuel optimal solutions to reorient an inertially symmetric rigid spacecraft from specified initial conditions to fully or partly prescribed terminal conditions. First attitude dynamics are represented in terms of quaternions, but in a different way than of Ref. [7] & Ref. [8] . They perform a transformation on costate dynamics so that state-costate system dimension is reduced. Defining the optimal control problem with related optimality conditions, solutions for optimal and singular optimal control are investigated. Detailed analysis for finite order and infinite order singular control is performed. Numerical simulation results are presented at the end. Different from Ref. [7] & Ref. [8] they present necessary conditions for numerical methods but selection of any particular algorithm is left to the reader. Finally they compare all possible control logic.

Hablani [10] developed a pole placement technique to remove magnetic disturbance torque from earth pointing spacecraft. Developed method is compared with classical linear and Bang-Bang  $\mathbf{H} \times \mathbf{B}$  control methods. ( $\mathbf{H}$ : excess angular momentum vector,  $\mathbf{B}$ : geomagnetic field vector.) This technique is an alternative method since magnetic momentum removal on some spacecraft can also be managed by gravity gradient torque design.

Herman and Conway at their letter published in ‘Engineering notes’ [11] present their work on the method of direct collocation and nonlinear programming which is applied to the optimal control problem of satellite attitude control. Mission is to recover a high orbit disabled satellite via a remotely operated satellite. The work determines optimal open loop control histories for detumbling a disabled satellite. The cost function becomes the integral square control, which is very similar to well-known minimum energy performance index.

$$J = \frac{1}{2} \int_{t_0}^{t_f} (\underline{u}^T \mathbf{B} \underline{u}) dt \quad (2.1)$$

$\underline{u}$ : control vector,  $\mathbf{B}$ : weighting matrix,  $t_0$ : fixed,  $t_f$ : free

Byrnes and Isidori investigated the existence of the smooth state feedback control law, asymptotically stabilizing a rigid spacecraft with only two actuators (thrusters) in operation [12]. It is shown that without any failure on the three actuators state feedback law can asymptotically stabilize the system. EOM (Equations of Motion) are defined by Euler's equations. Additionally desired control is derived using methods from a general nonlinear feedback design theory with rootlocus study. They used topological methods to prove the related theorems.

Pittelkau developed optimal control algorithms for autonomous magnetic roll/yaw control of polar orbiting, earth oriented momentum bias spacecraft [13]. Optimal design is required due periodic nature of roll/yaw dynamics. Linearized pitch dynamics are developed from roll/yaw dynamics and found to be time invariant. Design of a Linear Quadratic Gaussian (LQG) Control enabled disturbance rejection. Including pitch control into performance index he suggests

$$J = \int_0^T (u^T R_c u + x^T Q x) dt \quad (2.2)$$

which can be solved by Ricatti differential equation numerically. The term  $x^T Q x$  implies state feedback design and preceding term implies minimum energy problem. State estimator design is solved via MATLAB. Simulation of closed loop dynamics is presented at the end.

The paper by H. Weiss presents two-loop control of rate and attitude of a rigid body [14]. The inner velocity loop controls the rate and the outer loop controls the

angular position. The structure of a quaternion based rate/attitude tracking system is presented with the discussion of the eigenaxis rotation in case of Proportional (P) or Proportional + Integral (PI) error quaternion controllers. The stability of this augmentation + attitude control system is studied. Finally he discusses application of the proposed tracking system to gimbal attitude control.

The control problem solved by Nicosia and Tomei depends on measurement of only angular positions [15]. In case of all the actuators are momentum wheels their velocity measurements are also needed, to overcome this need they construct a nonlinear observer by exploiting some structural properties of spacecraft model. Spacecraft dynamics are represented by Euler angles. Then they derive a dynamic output feedback controller and define a region of asymptotic stability. Finally they design output feedback controller with reduced order estimator and simulate results of observer, error dynamics, and controlled attitude dynamics.

Sun pressure produces significant effects on high altitudes like where geostationary satellites are positioned. Venkatachalam proposes control of the pitch attitude of a high altitude spacecraft by two-plate solar pressure controller as the actuators [16]. No thruster activity is needed. He defines attitude and orbital dynamics of unsymmetrical satellite with its center of mass moving in a circular orbit about the earth center. He proposes simple output feedback controllers for various values of final pitch angles and rates. The feedback constants are obtained by solution of two-point boundary value problem. Also he studies the size effect of the actuator on attitude dynamics.

Mathematical models of spacecraft dynamics are highly nonlinear and always include idealizations. These handicaps prevent direct application of linear control theory and also cause deviations from actual motion. Hence Lee et al. propose a robust sliding-mode control law to handle not only the attitude reorientation problem but also the tracking maneuver problem [17]. The two advantages of this method are; first it can reject external disturbances, second it is robust to system parameter changes. Spacecraft rigid body dynamics model is composed of two sets of equations; the kinematics and dynamic equations in vector form. No frame

transformation is used. Control law is designed with attitude dynamics on body fixed frame. Lyapunov stability theory is used both for development and for stability analysis of sliding mode control law. Robust control law is derived in two consecutive steps. Finally simulations are performed to verify robustness and appropriateness of control vector on a spacecraft mathematical model using only thrusters as actuators.

Dodds and Walker propose sliding mode control for three-axis attitude control of a rigid body spacecraft with unknown dynamics parameters [18]. They model spacecraft dynamics in body coordinates only; using moment inertia matrix, change of angular momentum magnitude and direction vectors and the kinematics equations. Optical sensors and accelerometers do the attitude measurement. Accelerations are directly measured, and angular rates and positions are estimated. Only actuators are the tetrahedrally arranged reaction wheels. Actuator dynamics are included the controller design but sensor dynamics are set undetermined. Sliding control law comprises a linear state feedback section. Switching sequence determination is performed. Finally simulation of controlled dynamics is performed.

An adaptive control scheme to simulate the attitude and momentum management of gravity gradient stabilized spacecraft is designed by Parlos and Sunkel [19]. Fully coupled nonlinear EOM are systematically linearized around an operating point. Rigid body EOM (both orbital dynamics and attitude dynamics) is derived in state space form. Only actuators are the momentum wheels. Gain scheduled adaptive controller based on LQR (Linear Quadratic Regulator) design with pole placement is proposed for attitude control of spacecraft undergoing mass properties variations. Simulation results for a case study 'Space Station Freedom' are discussed in the final part.

Most common spacecraft attitude control method is the momentum management via reaction wheels. Attitude error defines the control moment to be applied by the actuators. When attitude errors are large systems show long term and large oscillations. Piper and Kwatny show that matching nonlinear actuator dynamics

(saturation) and controller dynamics (switches) properly, it is possible to reach a globally stable equilibrium [20]. They uncouple pitch axis motion and design a linear SISO (single input single output) pitch controller containing nonlinear elements like switches. Proposed SISO controller is a simple PI controller when pitch attitude error is below a threshold and a simple P when above the threshold. It is shown that when actuators are saturated stability is lost.

Sharony and Meirovitch design an optimal controller for the control of perturbations experienced by a spacecraft with a rigid hub and a flexible appendage during minimum time maneuver [21]. Linear time varying set of ordinary differential equations defines the model of vibration ad deviations from rigid body EOM. Nonlinear two-point boundary value problem is encountered in minimum time control formulation of nonlinear reduced order model. These yield a different performance index, like:

$$J = e^{\beta \cdot t} z^T S z + \int_{t_i}^{t_f} e^{\beta \cdot t} (z^T S z + u^T R u) \quad (2.3)$$

Where  $z$ : states,  $u$ : control, then the problem is converted into standard LQR problem to be solved by Ricatti matrix equation via transformation  $z^*(t) = e^{\beta t} z(t)$ .

The high orbit geosynchronous satellite three-axis stabilization is generally achieved by using bias momentum wheels along the pitch axis. The paper by Schwarzschild and Rajaran study on an attitude acquisition system for geostationary satellites [22]. Main concern for us is the use of Euler angles and quaternions for attitude acquisition control. The method uses direct rate quaternion feedback to despin the spacecraft and to align the momentum wheel axis along the orbit normal. Maneuver is designed to be performed along Euler axis.

## CHAPTER III

### DESCRIPTION OF TÜRKSAT 1B SATELLITE SYSTEM WITH A CONCENTRATION ON ATTITUDE CONTROL SUBSYSTEM

Procurement of TÜRKSAT series of satellites was initiated in 1989 by an international contract led by Turkish PTT (now Turk Telecom). The French Company Aerospatiale being a European consortium was contracted on December 1990 for the delivery of 2 satellites on orbit. This on orbit delivery also included launching of satellites by Ariane rockets, delivery of 2 ground control stations, providing support for operations, personnel training, program financing and insurance. Aerospatiale's shareholders for the program were:

From France: ALCATEL Escapce, Execorp, Arianespace

From Germany: MBB (DASA)

From Turkey: Teletaş –Alcatel Espace's subsidiary

Both the ground stations are located in Ankara, major station in Gölbaşı and a spare in METU campus.

#### 3.1 TÜRKSAT 1-B On Orbit

Before starting detail descriptions at satellite system it's better to summarize phases and location of satellite itself was transformed to. On August 1994 it was launched with Ariane rocket to 200-km altitude where is the perigee of its elliptical transfer orbit. (Figure 1 [3]) The apogee point at the transfer orbit is 36000 km distant to Earth. The next step was the firings of the apogee boost rocket of the satellite with high thrust to move from transfer to drift orbit (near-synchronous orbit). The small 10 N thrusters are activated to perform four manoeuvres to reach the satellite's service orbit -the geosynchronous or the geostationary orbit. There it

co-rotates with the earth in the equatorial plane for its telecommunication activities. For basic representation of the above stages refer to Figures 1 and 2. Figure 1 is specifically for TÜRSAT 1B arrangement and Figure 2 [23] is a generic procedure. As noticed from Figure 1 TÜRSAT 1B service orbit is completely circular. It is located at 42 ° East longitude with zero inclination with respect to the earth's equatorial plane.

TÜRSAT 1B is in service since October 1994 and it will be un-operational with an application of de-orbiting phase at the end of its life. It will be carried out to a higher orbit with the remaining fuel.

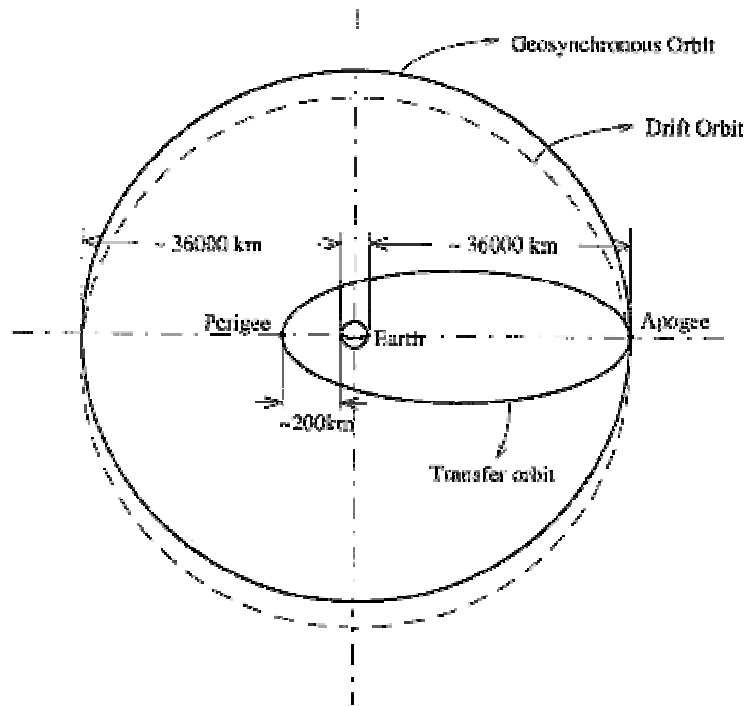


**Figure 1 TÜRSAT 1B Orbital Properties**

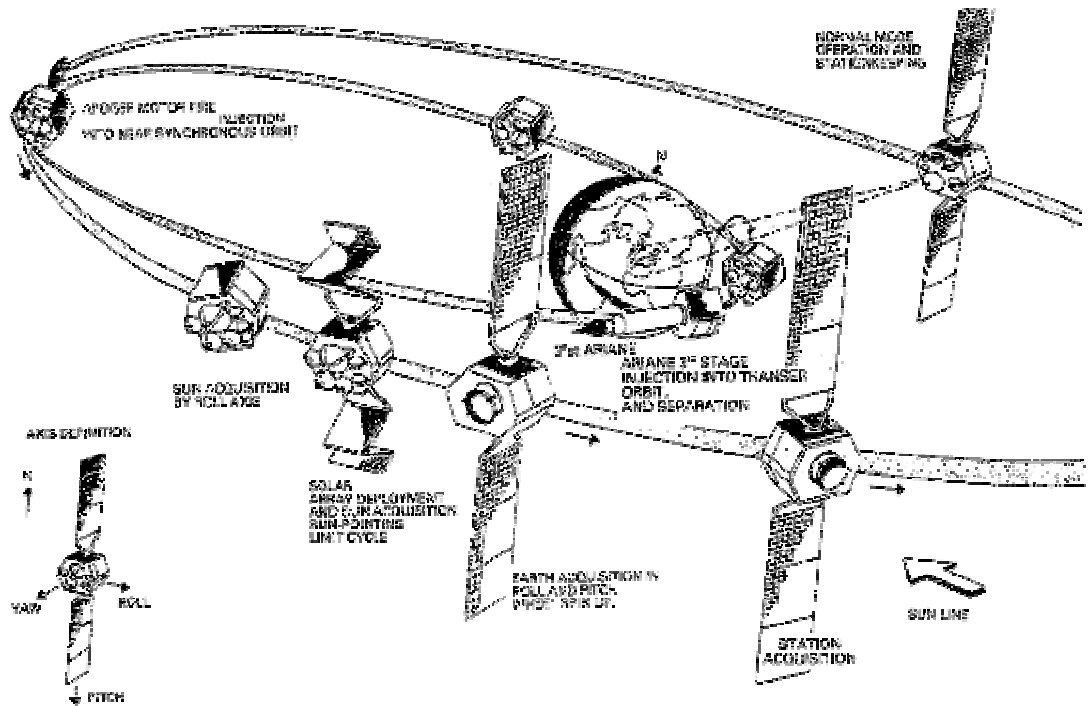


**Figure 2 Generic Phases for Orbital and Attitude Modes**

### **3.2 General Description of TÜRKSAT 1B Subsystems**

TÜRKSAT 1B is composed of the following subsystems that we will describe next:

- 3 Attitude Determination and Control Subsystem (ADCS)
- 4 Electrical Power Subsystem
- 5 Unified Propulsion Subsystem
- 6 Telemetry, Commanding and Ranging Subsystem
- 7 Repeater Subsystem
- 8 Thermal Control Subsystem

### **3.3 Attitude Determination And Control Subsystem (ADCS)**

ADCS is first described in terms of the hardware with the operational properties it consists of and then the ADCS functions and their operation modes.

TÜRKSAT 1B ADCS is an optimized combination of the necessary (most are redundantly coupled) hardware and relevant software for autonomous or ground controlled manoeuvring. Its main mission is to maintain the spacecraft's attitude within its specifications. Sun and earth sensors assemblies, rate integrated gyro assembly provide signals to determine the current attitude of the space vehicle and the actuators (hydrazine thrusters and momentum wheels) act under ADCS's command to manoeuvre the satellite to rearrange its attitude.

During most of the satellite service life ADCS is responsible from on station antenna pointing by station keeping manoeuvres. Another task assigned to ADCS is the transmission of systems monitoring data to ground stations through the Telemetry, Commanding and ranging Subsystem. [24]

Next we will introduce the ADCS hardware (sensors, actuators, and so on) then their functionality will be described by ADCS mission descriptions by various satellite operation modes.

TÜRKSAT 1B ADCS Hardware Configuration described in detail through section 3.3.1 to section 3.3.4

### 3.3.1 Overall Electrical Configuration

ADCS has four electrical interfaces with other subsystems. Two power busses connect two redundant ADSC equipment packages for reliable operation. The Attitude Determination and Control Electronics (ADCE) unit receives the Telecommand and transmits the Telemetry data. ADCE can also command to the thruster and isolation valves. When a hardware protection criterion is triggered ADCS command Hardware Safe Mode for proper system reconfiguration and solar array orientation. Electrical distribution web can be visualized by Figure 3 [24]. Also notice that almost all the electronic equipment are duplicated and fed by

separated power busses for electrical redundancy as well. Figure 6 shows schematic placement of the ADCE on satellite structure. [24]

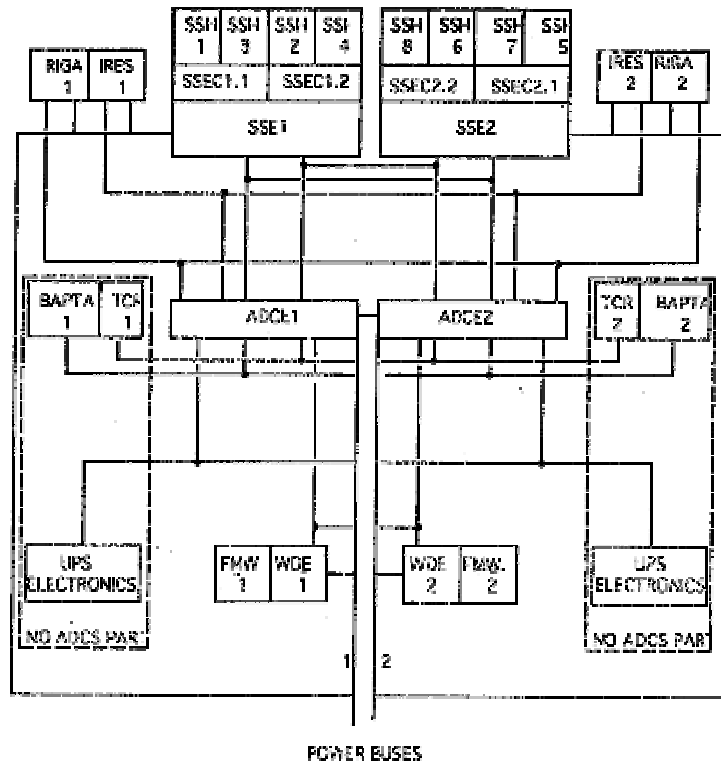


**Figure 3 Overall Electrical Configuration with Redundant Electronic Architecture**

### 3.3.2 TÜRKSAT 1B Attitude Sensor Configuration

Two types of radiation sensors are used; Sun and Earth Sensors. Two redundant sets of sun sensors each composed of four sensor heads, detect either pitch or roll/yaw axis' attitude only. Two units of earth sensors are used to detect pitch and roll attitude. Earth sensor assembly is also named Infrared Earth Sensors (IRES). A rate integrated gyroscope assembly formed of two redundant sets of gyros is also implemented for attitude measurement when sun and earth sensors are not available. Figure 6 shows schematic placements of various sensors and actuators on the satellite. Refer to Figure 3 for related electrical connection between the sensors and the ADCE.

### 3.3.2.1 Infrared Earth Sensor (IRES) Assembly

IRES measure the roll and pitch bias angles by two redundant units, which are located on earth looking side of the satellite with their yaw (Z) axis pointing towards earth. Like many other units these sensors are duplicated, in case a failure occurs in one of the sensors the other set can continue the mission.

IRES system is composed of 2 sets of optical bolometers to sense the infrared radiation from earth and the respective signal modulating/processing electronics. Earth's infrared radiation is much higher than the space's, hence bolometers can clearly detect infrared radiation from the earth horizon and these signals are modulated to ADCE. With two scanning modes IRES can detect the space-earth and the earth-space crossing. Along the pitch axis-scanning frequency is 10 Hz with amplitude  $\pm 9^\circ$  in wide scan (WS),  $\pm 5^\circ$  in narrow scan (NS) modes. [25]

ADCE receive 3 types of signals from IRES assembly; Roll, Pitch and Earth Presence (EP) information. Figure 4 [24] shows the schematic placements of the infrared detector heads (bolometers). Pitch and roll data is derived from the logical combination of the couples of these sensors: Pitch information is derived from the sensor couples 1,3 or 2,4 and roll data is derived from the sensor couples 1,2 or 3,4. Figure 4 also indicate the sign convention of the detectors; When the earth is along south (+Y) direction, ADCE gets a positive roll signal, and when the earth is along west (+X) direction, a positive pitch signal is delivered to ADCE. Bolometers sense infrared radiation; therefore, what happens when any one of them is interfered by infrared radiation of the sun or the moon? Then the respective sensor is inactivated from the detecting logic and the other couple of sensors are used for attitude signal derivation. [24]

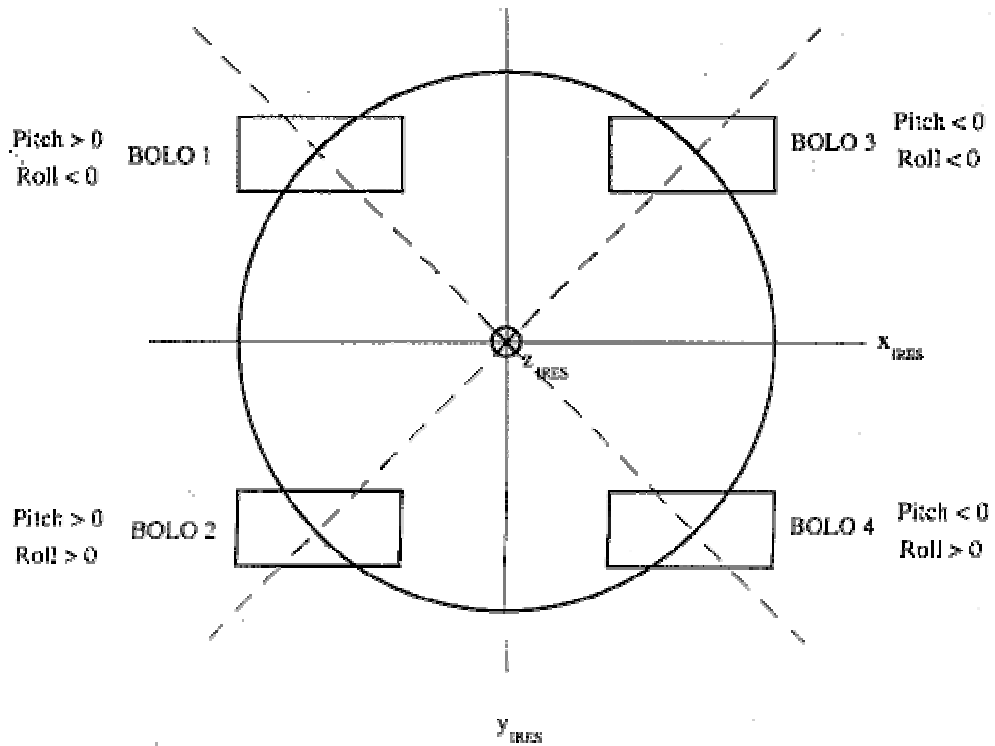


**Figure 4 IRES Configuration and Sign Convention**

Earth Presence (EP) information is derived by use of all the four sensors in narrow scan (NS) by “AND” logical operator combination. Each bolometer produces the Earth Capture (EC) signal to combine the (EP) output:

$$EP = EC_1 * EC_2 * EC_3 * EC_4$$

Where  $EC_{i=1,2,3,4}$  is the Earth Capture signal of respective  $i^{\text{th}}$  detector and the “\*” represents the logical “AND” operation.

In Wide Scan (WS) mode the logic is altered as:

$$EP = EC_1 * EC_2 + EC_3 * EC_4$$

Where this time “+” represents the logical “OR” operation.

WS mode is selected when earth acquisition has not been established and is to be reached. NS mode is selected when the earth acquisition is already established. Naturally this mode provides more accurate data. [3]

### 3.3.2.2 Sun Sensor Assembly (SSA)

Similar to the earth sensor assembly, SSA is composed of two sets of Sun Sensor Heads and two separate Sun Sensor Electronics (SSE). [25] Each set of SSH is composed of 4 detectors located on the spacecraft structure with different view angles. Studying Figure 5 [3] we notice those 2 sets of SSH combined with two redundant SSE Channels (SSEC) from a 4x4 redundant SSA architecture. Four of the SSH are for nominal usage the rest is the back up. SSA control logic includes switching operations. SSEC activates one SSH by switching on, hence operation of a SSH requires a multi-step operation. Physical location of the SSH couple determine which pair is to be activated during manoeuvre phase. After appropriate pair is switched on, one of the SSH of the enabled pair is selected for angle computation.

The signals produced by SSA are proportional to the out of and in plane of the spacecraft sun vector. SSH 1 and 5 determine the out of plane component and the rest derive the in plane vector. These two signals are used to compute the yaw/roll deviations of the satellite attitude. Nominal SSH are the ones on the left (SSE1) of the Figure 5 and the ones at the right side are backup. SSA is not used during nominal operation, because spacecraft attitude is kept with control application on pitch and roll axis only, and the IRES provide information for these angles' bias. On the other hand for relatively more critical manoeuvres like station keeping, yaw angle needs to be crosschecked. Therefore, a SSH is activated for the on-board yaw angle computation. SSH can scan an area of  $\pm 60^\circ$  with  $0.05^\circ$  resolution and  $0.063^\circ$  accuracy. Figure 6 shows the schematic placement of the SSE on satellite. [24]

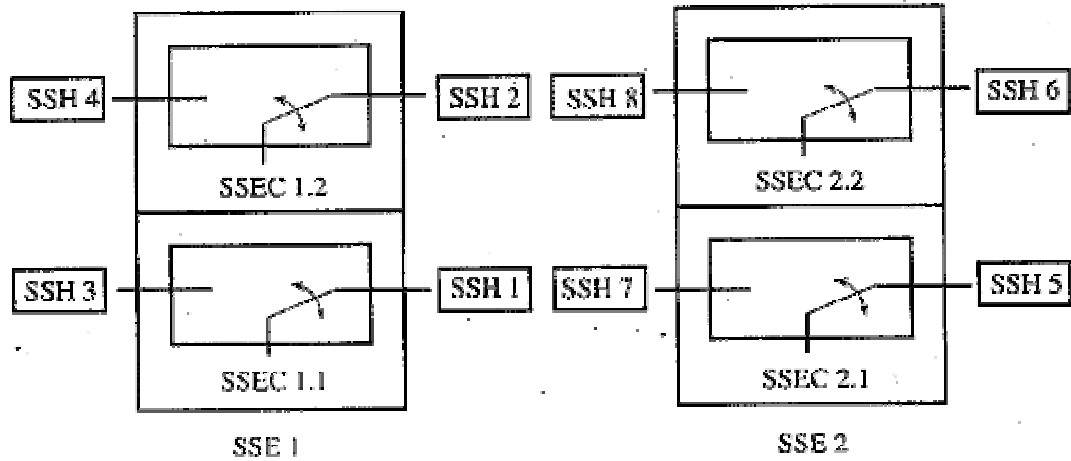


**Figure 5 Sun Sensor Operation Logic**

### 3.3.2.3 Rate Integrated Gyro Assembly (RIGA)

RIGA is composed of two redundant three-axis gyroscope packages, which measure the angular rates of the satellite rotation and angular motion with respect to the universal reference frame. Each gyro unit is formed of three gyroscopes with associated electronics. They produce analog output signals in the form of pulse trains for each control axis. The two separate RIGAs are located on north panel of the satellite. And are kept in OFF mode during normal mode. RIGA because of its error growth nature, it needs calibration regularly. Hence they are used when IRES or SSA can not be relied on. Another problem with RIGA is that, its performance highly depends on how stable the RIGA temperature is. Sudden changes in its temperature cause it to produce more erroneous signals. RIGA's linear range is limited to  $\pm 2^\circ/\text{s}$  and has a pulse train of 1 second. ADCE use a clock time of 100 ms; therefore, pulse trains are counted at 10 Hz Frequency. Figure 6 shows the schematic placement of the assembly on the satellite structure. Figure 3 shows the electrical connection between the RIGA and the ADCE. [24]

### 3.3.3 Attitude Determination and Control Electronics

Like all other systems ADCE units are redundantly coupled, both located on north panel at the satellite structure. ADCE acts as the main coordination center of the ADCS, and is composed of control electronics, connecting interface, and the microprocessor that all the control logic is loaded in. Main missions of the ADCE are as follows: [24]

- a) Selection and conditioning of sensor data.
- b) Selection and control of the torque
- c) Application of the control laws associated to each ADCS mode.
- d) Ground command conditioning and distribution to the relevant parts of the subsystem.
- e) Data collection from all parts of the subsystem for telemetry
- f) Orbit manoeuvres execution
- g) Failure detection of the subsystem and safety measures initiation.
- h) Bias generation.

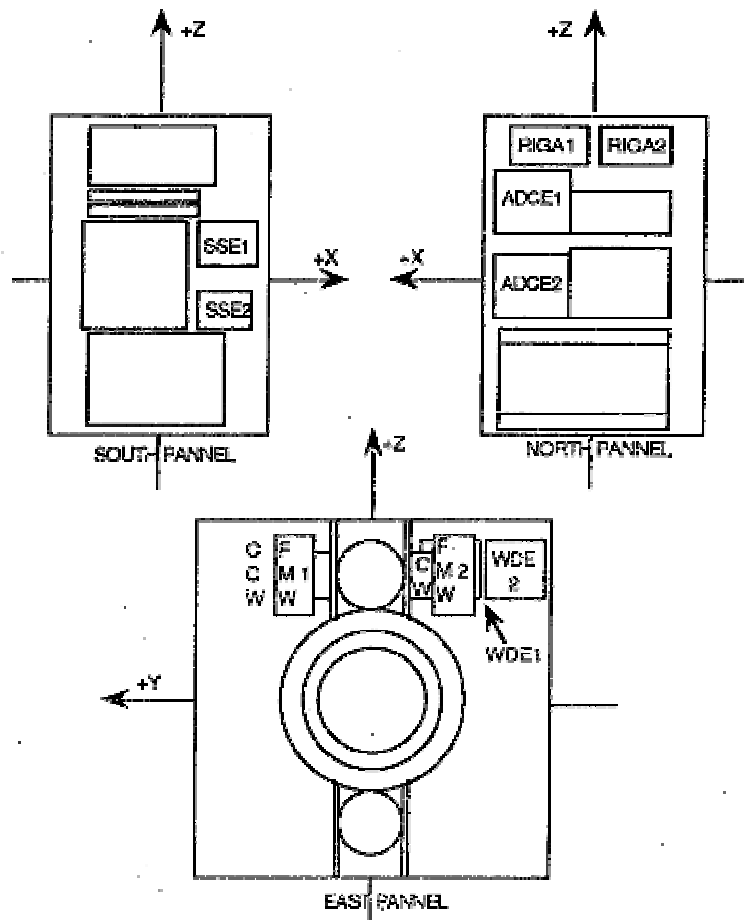


**Figure 6 Component Locations of the ADCS**

### 3.3.4 TÜRKSAT 1B Attitude Control Actuators

TÜRKSAT 1B attitude is controlled via a Momentum Wheel Assembly and twelve hydrazine thrusters.

#### 3.3.4.1 Fixed Momentum Wheel Assembly (FMWA)

This actuator system is composed of two redundant FMWs; one being the nominal and the other back up. FMWs are also associated with two redundant Wheel Drive electronics (WDE). [25] See Figure 6 for schematic location on the satellite structure. Both the rotating disks are mounted in the spacecraft structure in such a way that, their corresponding kinetic momentum is aligned with the satellite negative pitch (-Y) axis, North pointed in the geosynchronous position. As noticed from Figure 6, the first FMW rotates counter-clockwise (CCW) with location on the satellite south web; the second FMW rotates clockwise (CW) with location on North web of the satellite. Therefore both FMW produce angular momentum vector along (-Y) axis.

In addition to FMW, WDE there is a current controller providing continuous control on the wheel current. These altogether form the FMWA. There are two basic missions for the FMWA: [24]

- a) FMWA controls the pitch motion/attitude of the satellite via rotational deceleration/acceleration of the reaction wheel. Figure 7 shows a generic momentum wheel (or reaction wheel) structure. [26]
- b) FMWA stabilizes the roll and yaw motion of the spacecraft with the gyroscopic effects of the fast rotating disc with specific alignment on the structure.

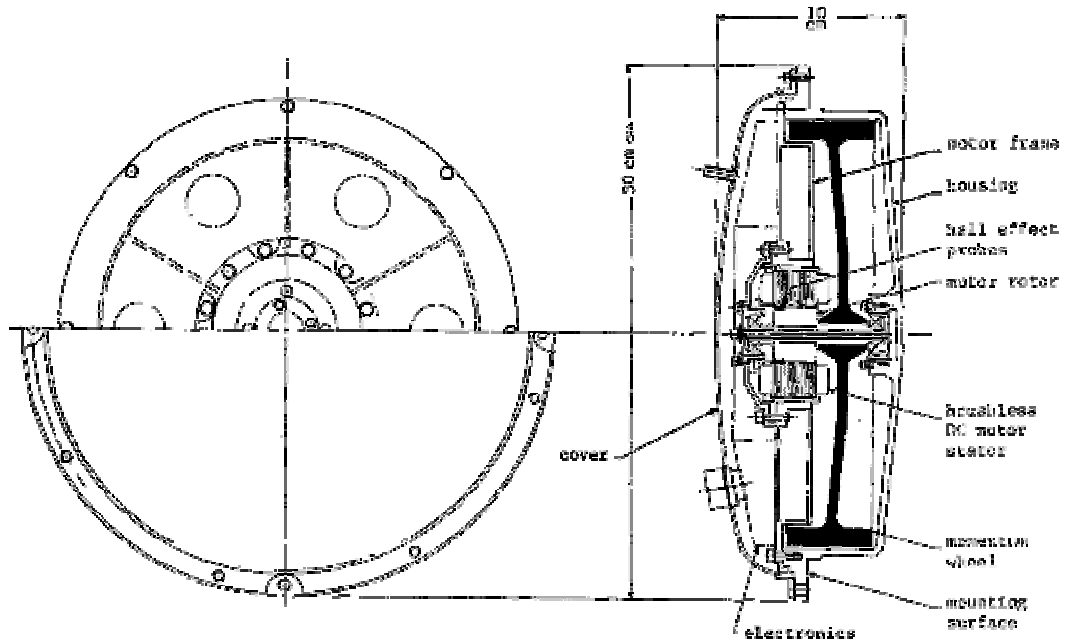


**Figure 7 A Sample Momentum or Reaction Wheel Structure**

FMWA operates with five modes: [24]

- a) **Torque Control Mode:** During this mode of FMWA, the pitch motion/attitude is controlled via FMW action only, no thruster is activated. This action is enabled during Normal Mode (NM) of the spacecraft. (Modes of the satellite will be described in detail with the complete functional task description of the ADCS.) Rotational torque of the reaction wheel is gradually altered within its specifications to control the satellite pitch motion/attitude.
- b) **Speed Control Mode:** The rotation speed of the wheel is fixed to a specific value, which is called the commanded wheel speed. Since no acceleration/deceleration of the wheel rotation is experienced, the 10 N pitch thrusters on the East Panel control pitch motion/attitude.
- c) **Brake Mode:** With this mode triggered wheel rotation is decreased to zero as quick as possible. When there is need for hardware reconfiguration brake mode is activated autonomously. There is no need for ground commanding for this mode.
- d) **Run Up mode:** This mode is triggered by a ground command signal and wheel speed is increased to a pre-determined value.

- e) Run Down Mode: Similarly wheel speed is reduced to a pre-selected value by a ground telecommand.

### 3.3.4.2 Attitude Control Thrusters (10 N Thrusters)

ADCS also activates the twelve 10N thrusters to maintain the satellite attitude, and keep it up within a window on orbit. (See Fig 10 as well) Attitude thrusters are located on the satellite structure as follows; 4 Roll thrusters are located on South panel 2 Pitch and 2 Yaw thrusters are mounted on East ad West Panels respectively. A simple schematic view of these thrusters location with respect to spacecraft specific coordinate system can be seen at Figure 8. [24]

These thrusters use Hydrazine as fuel. It is a very poisonous material, which is also used in most of the aircraft auxiliary/emergency power units. In fact exact thrust values are a bit different than 10 N. Some thrusters produce different thrust values because of their plume impingement characteristics based on their orientation / location. On orbit the solar panels are always directed normal to the sun light. Their continuous movements affect the thrust-impinged areas, hence the thruster plume impingement force/torque values are altered periodically. (See Fig 9 as well)

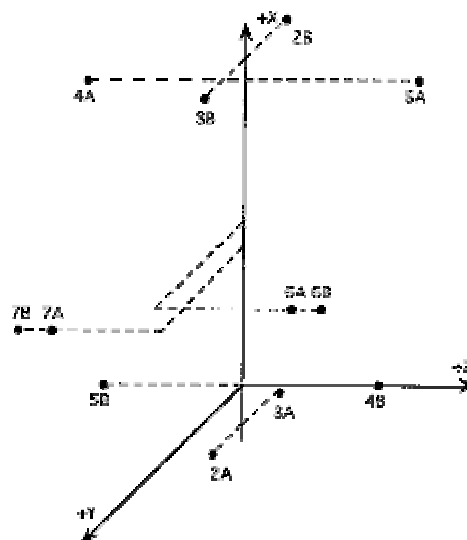


**Figure 8 Thruster Schematic Locations**

Thrusters 6A, 6B, 7A, 7B are the South thrusters. 2B, 3B, 4A and 5A are the East thrusters and the rest are the West thrusters.

Thrusters are not affected from center of gravity shift during satellite life; therefore nominal thrust values during (BOT and EOT) also during (BOL and EOL) are identical. (BOT: Beginning of Transfer, EOT: End of Transfer, BOL: Beginning of Life; EOL: End of Life). There is no west reflector hence west (yaw) thrusters are not subject to an impingement distortion from 10N nominal thrust. On the other hand both the pitch thrusters on East Panel the roll thrusters on South Panel experience minor impingement thrust alterations during BOT (=EOT) and BOL (=EOL) due to solar panels, antennas and other geometrical surfaces of the structure. During service life (Geostationary Orbit) Solar panel is continuously kept normal to the sunrays hence roll-thrusters also periodically (twice a day) experience additional distortions. Each hour with twice a day periodicity impingement forces / torques are altered. However on transfer orbit sun panels are not fully employed hence south thrusters do not experience this periodicity between BOT–EOT. In general in comparison to 10N nominal thrust impingement effect the net thrust around +0.9N and –0.5N. Figure 9 demonstrates how sun collectors are cyclically rotated on Geostationary Orbit and defines periodic daily time zones. (Also see Figure 2)

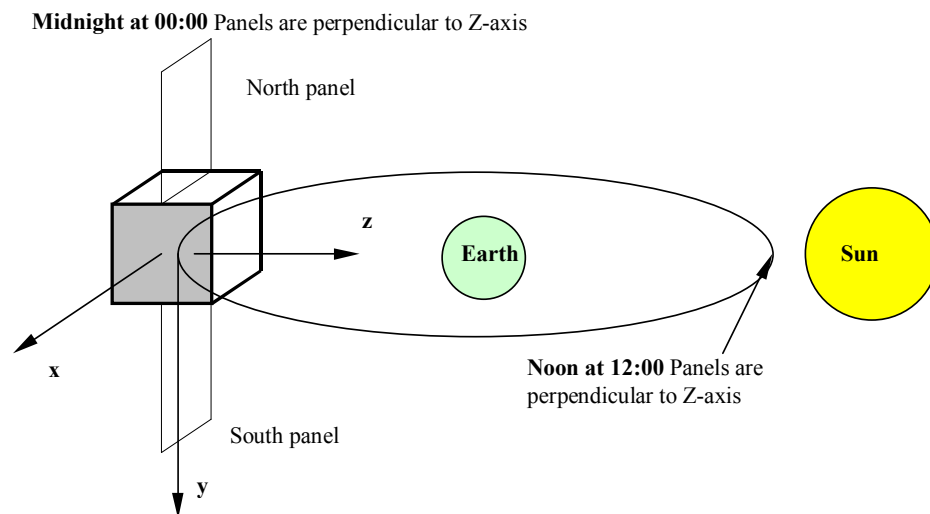


**Figure 9 Satellite Periodic Time Notation and Attitude Representation**

The thruster nozzle exits are not aligned in accordance with the satellite body axes rather all are given various bias angles (all are not symmetric). Defining XT, YT, and ZT as the nozzle exit plane center in the spacecraft axis system, nozzles are biased with  $\alpha$  as the nominal angle of the thruster aligned in XY plane, and with  $\beta$  as the nominal thruster angle out of XY plane. Studying the roll thrusters' alignment it is seen that the nominal 10 N force is divided into 3 components in X-Y-Z directions. [24]

Functions of TÜRKSAT 1B ADCS at its various segments on orbit and service life and its respective operation modes are described in detail through the following sections:

### 3.3.5 Functions of the ADCS during Transfer Orbit (TO)

TÜRKSAT 1B ADCS missions during Transfer Orbit (TO) phase are to orient the satellite with respect to sun and earth. These orientation sequence are needed to realise all the operations leading to synchronous orbit by subsequent firings of the big apogee burst rocket. This TO mission sequence is composed of three modes: Sun Acquisition, Gyro Drift, and the Earth Acquisition modes.

#### 3.3.5.1 Sun Acquisition and Sun Pointing Mode

After ADCS receive a ground command this mode procedures are activated. Satellite is rotated around roll axis till at least one sun sensor start to receive appropriate sun position signal. If required spacecraft is automatically rotated about the pitch axis, ADCE produce pitch and yaw command signals with the west sun sensor reference signals.

After first initialization of this mode by ground telecommand the manoeuvre can be activated by separation strap, or by autonomous safety logic or again by a

ground command. Separation strap means after the satellite is separated from the Ariane last stage rocket it autonomously switches to this mode to orient negative roll (-x) axis towards the sun. Automatic safety logic triggers to this mode when any one of the hardware checks results in an error signal. [24]

For orientation of the (-x) axis of the spacecraft to the sun, following four phases are activated automatically: [24]

PHASE 1: If the sun can not be detected by SHH 2/6<sup>1</sup> or SHH 3/7, all the initial body angular rates are damped. Later controlled rotation about the roll axis is started to detect the sun direction. Total view of the SHH is larger than 180 ° hence sun will be eventually in the detecting field of them, unless it is already.

PHASE 2: If the sun presence (SP) is not yet detected by SSH 2/6 then the following sequence is activated. After the sun is viewed by SSH 3 satellite is rotated about the pitch axis to capture the SP by SHH 2/6 where initially SP was not detected by SHH 2/6.

PHASE 3: SP is captured on SHH2/6 but not yet on SHH 1/5 and rotation about y-axis is kept up.

PHASE 4: When the SHH 1/5 and SHH 2/6 both capture the SP (-x) negative roll axis is maintained towards sun and satellite rotates once more to get the solar panels face the sun perpendicularly.

### 3.3.5.2 Gyro Drift Determination and Compensating Mode

With the initiation of the sun-pointing mode, satellite low frequency spin is removed by ground telecommand (See Fig. 2). The benefit of this spin was the stabilization at TO. The 3 (XYZ) gyro rates are zeroed, with the yaw and pitch loops triggered by SHH1 and 2 reference signals, the spacecraft keeps up its initial attitude: X axis pointing towards the sun.

---

<sup>1</sup> The SHH number preceding “ / “ implies that it is the nominal one and the left one is the back-up

The gyro yaw integrated signal is stored and used to evaluate yaw drift by comparison with sun sensor signals. This calculation is used to determine the appropriate telecommand for gyro yaw drift compensation. All these operations are enabled/accessed via ground command.

### 3.3.5.3 Earth Acquisition Mode (EAM)/ Acquisition of Injection Attitude/ Apogee Boost Mode (ABM)

After SAM, satellite's attitude is X-axis sun-pointing, and it rotates around X-axis with  $0.5^\circ$  Hz frequency. ADCS command an offset bias signal in pitch and yaw to set the satellite into an appropriate attitude to scan the sky and capture the Earth Presence data. The commanded bias corresponds to the sun vector in satellite coordinates in the target attitude for the estimated time of EAM. (Phases 1 and 2) After the EAM, Spacecraft has an orientation with its Z-axis pointing towards earth and X-axis is in the orbit plane. Following EAM injection attitude acquisition and finally ABM sequences are activated. Following phases summarise these: [24]

PHASE 1 (EARTH SEARCH): Satellite is rotated conically about sun reference vector. Then the IRES with a direction along satellite Z-axis search and detect the EP.

PHASE 2 (EC): When the IRES detects the appropriate EP signal, pitch and roll control loops are closed with the IRES produced reference data to point the +Z-axis towards earth.

PHASE 3 (YAW SLEWING): After the second phase satellite +X-axis is oriented towards west, hence a slew of  $180^\circ$  around Z-axis (earth pointing) is required to orient -X-axis towards west. This slew command loop uses yaw gyro information.

PHASE 4 (YAW CAPTURE): When the SHH 3/7 detect sun presence information, the yaw reference can be provided from either SHH 3 or 7 and similarly pitch and roll loops are closed via IRES signals.

Appropriate biasing is determined on ground and telecommanded to the satellite ADCE.

Phases 1, 2 are the EAM sub-modes, phases 3, 4 are the Sub-modes for injection attitude acquisition. Coming to ABM:

The yaw bias is telecommanded to the satellite to rearrange orbit inclination according to the three-apogee boost maneuvers prediction. In case of colinearity between the earth, the satellite and the sun during apogee maneuver, the actual sun sensor yaw data is transferred to the yaw rate integrated gyro electronics before starting firing of the apogee boost rockets. ABM is then controlled by the yaw gyro reference.

After EAM and injection acquisition, satellite fires apogee motors for three Apogee maneuvers to reach the GO from TO. During these phases ADCS provides pitch bias capability of  $\pm 2^\circ$ .

### 3.3.6 Functions of the ADCS during Geostationary Orbit (GO)

The ADCS main function in GO is to keep up the satellite attitude for on-station antenna pointing. Also ADCS maintains the spacecraft within its specific orbital window by the orbital manoeuvres required for acquiring the satellite orbital position (See Figure 10). These functions are completed by the following three operation modes:

#### 3.3.6.1 Normal Operating Mode (NM)

The ADCS function in NM is to provide accurate on station pointing during GO lifetime. This mode is accomplished by completely automatic commands of the ADCS, no ground telecommanding is required. This mode has three basic control loops: [25]

a) Pitch Control Loop with Automatic Wheel Unloading:

In NM pitch attitude is maintained by controlled deceleration/acceleration of the FMW operating in the torque mode. The reaction torque due to the fast rotation of the FMW disk controls the satellite's pitch rate/position. The wheel reaches its highest and the lowest speed limits of its operational range because the accumulated angular momentum from external disturbance torque is just neutralised by FMW. Whenever this case occurs an automatic logic signal is issued to provide wheel unloading by the preset pitch thruster firings as pulses. A built-in time-limited thruster firing algorithm inhibits repeated thruster firings before the wheel dynamics can respond. Thruster firing in two cases activates wheel unloading:

- i. When a transition from NM to SKM is realised,
- ii. When the wheel reaches its operation boundaries. ( $\pm 10\%$  range of its nominal rotation speed : 4140-5060 rpm)

During the NM, roll and pitch reference information is provided by IRES; on the other hand yaw reference is not measured, because yaw motion is not actively controlled.

b) Roll / Yaw Control Loop:

The roll / yaw attitude control in NM combines both the FMWA and the roll thrusters on the south web. Roll thrusters vectorial aligning with respect to satellite coordinate system has an offset to produce an opposite yaw component of control torque. The FMW provides gyroscopic stiffness (increases satellite stability) required to implement the WHECON principle. As soon as  $\pm 0.05^\circ$  error in the roll attitude is detected with IRES reference information, ADCE initiates an 8 ms roll thruster firing.

Yaw motion is not actively controlled. The pitch reaction wheel produces a gyro-compassing effect, transforming yaw attitude errors into roll errors with

six hours periodicity. Then this is detected as roll error signal creating a roll coupling on yaw motion enabling passive control of yaw attitude (in the inertial frame). Additionally roll control torque by roll thrusters has a yaw offset component (coupling about 15%). Both this thruster bias alignment and the FMWA are used to control yaw attitude passively without any direct measurement on yaw attitude. Then roll bias signal is processed to activate the south thrusters within its specified deadband.

#### c) Nutation and Angular Momentum Control Mode (NAMC)

In addition to the standard WHECON mode, ADCS pointing performance is improved with this mode. Roll bias is still determined from IRES, but this time yaw error is computed on-board from the information provided by SSHA, with decoupling performed by IRES signals.

FMW is not used, but roll and yaw thrusters are used as actuators. During NM this mode does not require any ground command more frequently than once a day, except for IRES inhibition due to sun or moon interference. The ADCS keep the attitude in the range of  $\pm 0.5^\circ$  for roll and  $\pm 1.5^\circ$  for pitch with a resolution of  $0.01^\circ$ . [24]

#### 3.3.6.2 Station Keeping Mode (SKM)

On GO, satellite has to be kept in a prespecified contact window for accurate communication between the satellite and the ground- the accurate coverage of the transmission area. (See Figure 10 [23]) SKM is also used to provide the final position in the drift orbit and de-orbit the satellite at the end of its service life. ADCS at these control loops provide three-axis stabilization of the satellite during North/South (N/S) and East/West (E/W) orbit correction manoeuvres. [24]

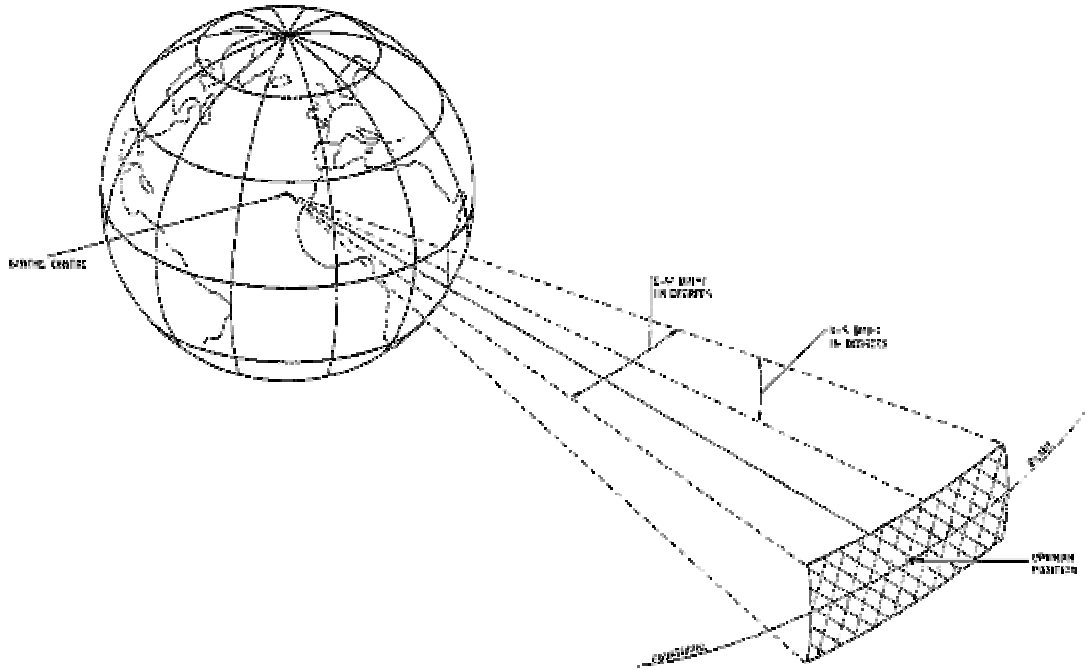


**Figure 10 Station Keeping Window**

For yaw reference data SHHA is used except for colinearity region where the satellite is then aligned close to earth-sun line. There are two possibilities for orbit correction in these colinearity regions: Either yaw reference is provided by the RIGA with a previous specific on-orbit Gyro-calibration accomplished, or the manoeuvre is postponed (off node strategy). In either case, the ADCS design is compatible with the two kinds of reference input. The appropriate reference setting is done in an orbital position when SSHA provide accurate yaw reference information. For E/W and N/S corrections on orbit, control thrusters are activated as appropriate pairs simultaneously. During these orbit correction manoeuvres with 10N control thrusters, attitude control is achieved by thruster-off-modulation to produce reaction torques in addition to the velocity increment. Also the thrusters, which do not contribute to orbit corrections are on-modulated for attitude keeping.

Mini-pulses control strategy is implemented for N/S, E/W orbit correction maneuvers, in order to minimize overshoots. [24]

Following the Station Keeping Maneuvers, before the NM command, residual angular rates are reduced by use of transition regulator characteristics with small impulse bits to the thrusters. [24]

### 3.3.7 Functions of the ADCS in Antenna Pattern Measurement

Antenna mapping mode is designed to accomplish the antenna pattern measurements from ground station during the satellite in-orbit tests. At nominal attitude (Z axis aligned toward earth center and Y-axis is normal to the orbital plane) it is possible to offset the satellite up to  $\pm 6^\circ$  in pitch and  $\pm 5^\circ$  in roll attitude. However these limits are outside the linear range for the IRES measurements. Hence the RIGA achieves the reliable attitude detecting, but it requires calibration before and during operation.

The 10N thrusters provide 3-axis control and commanded by the SKM roll, yaw, pitch regulator algorithms. Additionally pitch motion/attitude can be controlled with FMW in torque mode using the NM pitch control loop. In case of the required bias is within IRES linear range, SKM is used. [24]

### 3.3.8 Functions of the ADCS in De-Orbiting

At the end of satellite's service life, it is transferred to 150 km higher GO, as its cemetery orbit. Using SKM pitch thrusters are activated to generate  $\sim 5.5$  m/s excess velocity to reach the higher orbit. [24]

### 3.3.9 Functions of the ADCS in Safe-Guarding

The basic responsibility of this phase is to provide the capability for an automatic acquisition of a safe satellite attitude in case of an emergency. The algorithm incorporates two modes: [24]

### 3.3.9.1 Hardware Safe Mode

This mode performs full reconfiguration sequence and has the SP (Sun Presence), EP, Thruster on time, and ADCE health check criteria permanently under control. Except for ADCE check, the rest can be skipped/disabled by ground command. If this mode is activated, satellite automatically passes on directly to Sun Pointing mode after reconfiguration sequence finishes. Returning to NM needs command of EAM and Wheel Spin up. [24]

### 3.3.9.2 Software Safe Mode (SSM)

This mode acts as a software monitoring/protecting module for NM, Antenna mapping, NAMC, and SKM. This mode gives a recovery time to the satellite in case of a failure. Hence benefits to prevent the initiation of a complete hardware reconfiguration, which starts with SAM. This software algorithm is triggered when the roll, yaw, or pitch thresholds exceed 300 ms. If the SSM fails to recover, SAM is initialised by ground command. When an equipment error is detected with the initialization of SSM, pre-selected IRES, RIGA and Unified Propulsion System Electronics are used for recovery. NM is started when the roll, yaw and pitch transition conditions are satisfied. [24]

### 3.3.10 Functions of the ADCS in Earth Re-Acquisition with RIGA Attitude Reference

ADCS main function in this mode is to perform the earth search. Satellite is rotated about a reference vector. This mode is based on the fact that the nominal EAM can not be used all along the orbit due to limitations of pitch sun sensor. This mode is composed of five steps: [24]

- X-axis rotation is zeroed.

- SSH transition
- Adjustment of Sun reference Vector
- Earth Search
- Earth Capture

### 3.3.11 Functions of the ADCS in Re-positioning

At this mode on-station longitude is changed within the specified orbital arc through the SKM, with E/W and W/E manoeuvres. [24]

### 3.3.12 Functions of the ADCS in Monitoring

In this mode ADCS transmit data to the ground to determine the satellite attitude during all orbital operations with accuracy sufficient to monitor ADCS operations. The data is delivered via Telemetry, Commanding and Ranging (TCR) Sub-System. [24]

## **3.4 TÜRKSAT 1B Electrical Power Subsystem (EPS)**

EPS provides electrical power to all the systems on the satellite (See Figure 11 [24] for general arrangement) The electric source of the satellite is the solar panels. They are always pointed normal to sunrays by the BAPTA –Bearing and Power Transmission Assembly. Power Conditioning Unit (PCU) regulates the output voltage obtained at solar panels. Again two redundant buses transmit the DC electric power to Power Control and Distribution Unit (PCDU), where then the electricity reaches to all required systems. Two sets of 27 celled Nickel / Hydrogen batteries are the only electrical source when the satellite enters the moon's or the earth's shadow (eclipse period), and prior to deployment of solar panels. They also help to equalise the voltages on both busses. [24]

Two redundant BAPTA Mechanisms (BAPTA-M) rotate the solar array wings to provide their normal alignment towards the sun. BAPTA-M are controlled by two internally redundant BAPTA-Electronics (BAPTA-E) [24]

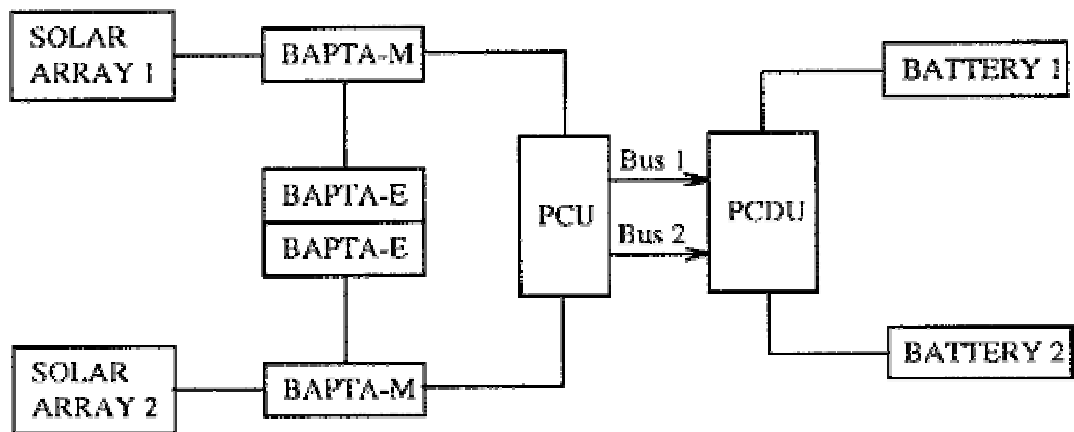


**Figure 11 Electrical Power Subsystem**

### 3.4.1 Solar Panels

The sun energy is converted into DC electrical power by the solar cells placed on the wing/panel structure mounted on south and north panels of the satellite structure. On launch phase the solar arrays remain stowed on those panels. On TO only one segment of the two solar panels are deployed. On GO all four sections of each of the solar arrays are deployed for full power requirement. See Figure 2 for general arrangement of the solar panels on the satellite. Position of the wing like panels also name the Y-axis as in aircraft the Pitch axis.

### 3.4.2 BAPTA

This assembly is constituted of the two BAPTA-M and one BAPTA-E with two internally redundant parts. It rotates the solar panels continuously with respect to sun and also serves as a bridge for signal and electrical power transmission between solar panels and satellite units. [24]

BAPTA operates in three specific modes:

- a) Cruise mode; one revolution per day in NM,
- b) Acquisition mode; one revolution per 40 minutes,
- c) Hold mode; panels fixed, no rotation.

### 3.4.3 PCU and PCDU

Each solar wing is composed of four panels of solar cells. Their total current output is regulated by PCU. Shunting the current from all the sections to ground with control of an error amplifier stabilizes the regulation of the voltage on two buses. PCDU distributes the obtained electrical power to the satellite units. Additionally it manages battery charging, controls temperature, and interfaces telemetry between all the equipment of EPS and TCR Subsystem. See Figure 3 for electric distribution for units of satellite systems. [24]

## 3.5 TÜRKSAT 1B Unified Propulsion Subsystem (UPS)

TÜRKSAT 1B benefits from the UPS based on reaction control logic. Except the pitch control by FMW in NM all rotational (attitude) and translational (orbit) maneuvers are actuated by the UPS. From TO- to drift orbit satellite is transferred by means of three maneuvers actuated by 400 N apogee boost motors. From drift orbit to GO 10N thrusters actuate N/S and W/S maneuvers. Orbit corrections are ground commanded but attitude control is done automatically by onboard algorithms of the ACDS. [24]

UPS is incorporated of the following units: [24]

- a) One 400 N ABM motor
- b) Twelve 10N thrusters
- c) Two propellant tanks
- d) One pressurant tank

- e) A set of valve control system
- f) Two electronics units : UPSE (Also see Figure 3)

Total fuel and oxidiser has a mass of 942.8 kg, which is to be completely consumed after de-orbiting. TÜRKSAT 1B uses monomethyl hydrazine, as fuel and nitrogen tetroxide with 1% dissolved NO as oxidiser.

400 N ABM engine is used only for transmission from TO- to drift orbit, then sealed and isolated from the UPS completely. Valve system of the boost motor and the 10N thrusters also vary: 400 N motors use shut-off valves whereas 10N thrusters use electrically powered on/off valves. UPSE serve as being an interface between UPS and ADCS. [24]

### **3.6 TÜRKSAT 1B Telemetry, Commanding and Ranging (TCR) Subsystem**

This subsystem is mainly an interface between the satellite and the ground stations. It performs three main functions: the telemetry, commanding and ranging to control the operating mode which includes monitoring and command sending and determination of the satellite orbit.

TCR subsystem equipment for on-station phase is: [24]

- a) Communication antenna (also apart of the repeater subsystem)
- b) Low noise amplifier (also apart of the repeater subsystem)
- c) Couplers of telecommand signal for attenuation or amplification
- d) Three receivers
- e) Two transmitters
- f) Two beacons
- g) Switches for receive, transmit, beacon, and ranging redundancy arrangements
- h) Two authentication units.

The receivers operate in hot redundancy, but transmitters and beacons operate in cold redundancy. Hot redundancy means; in case of the nominal equipment fails, the back up automatically switches on to continue the mission. On cold redundancy ground commanding activates the back up equipment. [25]

### **3.7 TÜRKSAT 1B Repeater Subsystem**

The main task of this subsystem is to receive the communication input signals that are sent from earth, then to amplify them for transmitting back on the selected coverage zones. In addition to this communication transmission task, the reception of telecommand in GO, and telemetry transmission in TO and in emergency cases are accomplished by this subsystem. [3]

### **3.8 TÜRKSAT 1B Thermal Control Subsystem**

As its name implies its main task is to regulate, and maintain the temperature; or in other words to provide a comfortable temperature environment within the satellite. All the components, units in the satellite has its specific operational temperature range, hence this subsystem keeps all the equipment within their reliable operational temperature limits. Temperature regulation is achieved by two functional types of elements: Active and Passive thermal controllers. [3]

Passive thermal control elements are; radiator panels with heat sinks or heat pipes, optical solar reflectors, multilayer isolation blankets or foils, black or white paints, interfillers, and shields.

Active elements are; the heaters, thermostats, and the thermistors. Class I heaters are for temperature regulation of UPS components, sensors and batteries. Class II heaters are for Repeater Subsystem. Thermostats are for IRES, RIGA, SSH

heaters. Thermistors are the temperature sensors to initiate the routine or emergency heater on/off switching.

### 3.9 TÜRKSAT 1B Mass Properties

Table 1 below summarises the mass property evolution during whole life of TÜRKSAT 1B: [24]

**Table 1**

PHASE	EVENT	MASS (kg)
LAUNCH	All appendages stowed	1783.678
B.O.T	Solar array partially deployed Reflector deployed	1783.678
E.O.T	Solar array partially deployed Reflector deployed	1082.578
B.O.L	Solar array deployed Reflector Deployed	1082.578
E.O.L	Solar array deployed Reflector Deployed	835.898

(Where BOT: Beginning of Transfer, EOL: End of Life, EOT, and BOL are as similar.)

With the above mass change satellite also experience changes in moment of inertia values and naturally satellite center of gravity (CG) is also altered during satellite life. Maximum CG shift from BOT to EOL can be summarised in satellite coordinates as: in x direction  $\Delta X=79.51$  mm,  $\Delta Y=2.66$  mm,  $\Delta Z=1.38$  mm. As noticed total GC variation is very limited in Z and Y direction in comparison with X direction. Similarly because of configuration and mass changes in TO, drift and GO mass moment of inertia about the satellite principal axes are subject to large changes. [24]

Continuous regulation of the sun collector panels heading also has an effect on the moment of inertia about the Roll (X) and Yaw (Z) axes. But keep in mind that the panels are of thin light weight material and are not too long due to structural (vibration, and so on) restrictions. Therefore cyclic change in the inertial values will be very small. This attribute is sketched as Figure 12. This behaviour has small impact on nominal thrust value of each thruster (impingement distortion).

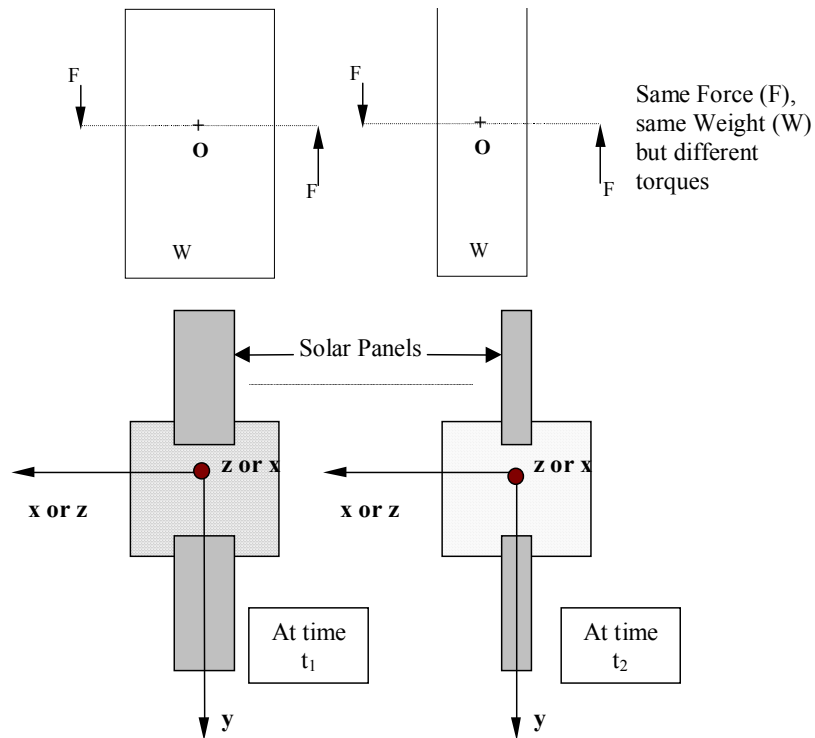


**Figure 12 Reason how  $I_{xx}$  and  $I_{yy}$  change periodically**

## **CHAPTER IV**

### **BUILDING OF A SATELLITE ATTITUDE DYNAMICS MODEL SIMILAR TO THE TÜRKSAT 1B GEOSTATIONARY SATELLITE**

#### **4.1 Introduction**

Construction of a reliable attitude model for spacecraft is a vital step in development of the automatic attitude control system. Careful building of the motion equations is the first step of a simulation work. Simulations of a system prior to functional component testing mock-up and/or prototype manufacturing specifically for satellite production play very important roles. Simulation capabilities are utilised for development time and cost reduction, validation and verification, and also for reduction of training and maintenance costs.

Unlike aviation industry spacecraft industry, does not encounter mass production. Hence an in-orbit prototype is not made, however an on-ground full-scale engineering model for functional component and overall testing is manufactured. The system designers and the manufacturer both appreciate the detection of design errors early in design, and initialisation of the designed controllers' optimisation. Computer simulations also give a deeper insight into component functional tests and the prototype or the manufactured item acceptance tests.

In this chapter, a mathematical model representing rigid body attitude dynamics of a geostationary satellite platform similar to the TÜRKSAT 1B is derived for the purposes of automatic control system design. First mass related properties are

introduced, later equations of motion (EOM) using Newtonian mechanics with definitions of reference coordinates and respective coordinate transformations are derived, next actuator dynamics are also modelled, and finally environmental disturbance torque are discussed to complete a full nonlinear attitude dynamics model.

## **4.2 Mass Properties of the Model Spacecraft**

### **4.2.1 General Description**

TÜRKSAT 1B has a continuously decreasing mass behaviour, due to fuel expenditure by thruster firings. Also inertial properties are affected from deployment of solar panels. (Inertia values between Beginning of Transfer (BOT) to End of Life (EOL) is variable due to mass loss) We will design our model with mass properties similar to that of TÜRKSAT 1B. The control system we will design concentrates on Geostationary Orbit (GO) attitude control. Therefore mass and inertia values are selected with consideration of TÜRKSAT 1B BOL and EOL properties. TÜRKSAT 1B experience about 250-kg mass reduction between BOL and EOL. This results in a CG movement in XYZ directions of body coordinates as:  $\Delta X \approx 37\text{mm}$ ,  $\Delta Y \approx 1\text{mm}$ , and  $\Delta Z \approx 1\text{ mm}$ .

The developed model assumes the Rigid Body representation of the satellite structure is applicable. This representation neglects the effects of body elastic modes. Rigid body model assumes the distance between any two points on the satellite structure is constant.

Considering the CG movement of the TÜRKSAT 1B it is safe to assume that on GO our model has a fixed CG location on the satellite structure. For a mass about 2000 kg CG movement of a few mm can be neglected for development of the EOM and design of the controller. Hence attitude dynamics can be modelled as rotational kinematics around the CG. Also this thesis we assume fixed moment of

inertia values for design. Later it is possible to test the controller's robustness to changes in mass, CG locations and inertial parameters.

#### 4.2.2 Determination of the Model Inertial Properties

In her thesis work Uslu [3] proposed the following inertia tensor:

$$I = \begin{bmatrix} I_{xx} & -I_{xy} & -I_{xz} \\ -I_{xy} & I_{yy} & -I_{yz} \\ -I_{xz} & -I_{yz} & I_{zz} \end{bmatrix} = \begin{bmatrix} 3600 & 0 & 0 \\ 0 & 600 & 0 \\ 0 & 0 & 4000 \end{bmatrix} kg.m^2 \quad (4.1)$$

It is noticed that she used principal axis frame where Product Mass Moment of Inertia (PMMOI) values disappear. This is a valid approximation since TÜRKSAT 1B on its specific spacecraft coordinate frame PMMOI values are negligible in comparison with Principal Moment of Inertia (PMOI) values. Uslu also proposed PMOI values, which are also typical for geostationary satellites. Here our proposed values are also close to those typical values, but also more specifically to TÜRKSAT 1B to catch up its mass change effects. Again we will define the body fixed reference frame also be principal. The following inertia tensor is used to develop rigid body equations of motion:

$$I = \begin{bmatrix} I_{xx} & -I_{xy} & -I_{xz} \\ -I_{xy} & I_{yy} & -I_{yz} \\ -I_{xz} & -I_{yz} & I_{zz} \end{bmatrix} = \begin{bmatrix} 3770 & 0 & 0 \\ 0 & 730 & 0 \\ 0 & 0 & 4020 \end{bmatrix} kg.m^2 \quad (4.2)$$

### 4.3 Derivation of the Rigid Body Attitude Equations of Motion (EOM)

#### 4.3.1 General Equations of Motion Description

Newtonian mechanics is used to derive satellite rigid body EOM. In order to derive EOM, an inertial reference frame is required, in which the Newtonian mechanics is valid. The definition of an inertial frame states that the frame should ideally be fixed, or be in uniform rectilinear translational motion relative to distant stars. In this thesis “Earth fixed” reference frame can be taken as the inertial reference, because our model satellite like TÜRKSAT 1B stay fixed on a specific (42° East) longitude with zero inclination to earth equatorial plane in a circular orbit with synchronous rotation with earth. (Always stays on same point as seen by an earth observer.) Earth fixed coordinate system can be defined with the following parameters: Its origin is the origin of spherical earth model with  $X_E$  and  $Z_E$  on equatorial plane and  $Y_E$  pointing south. (See Figure 13)

To define the motion with respect to an observer on the satellite, the body fixed reference frame, which is initially defined as a principal axes system, is used. The body rates, moments, forces can easily defined in this frame. The origin of this frame is the CG of the satellite. The x (roll) axis is aligned tangent to circular orbit towards the satellite motion direction, y (pitch) axis is normal to the orbit plane and directed towards south, z (yaw) axis is in the orbit plane and directed to earth center.

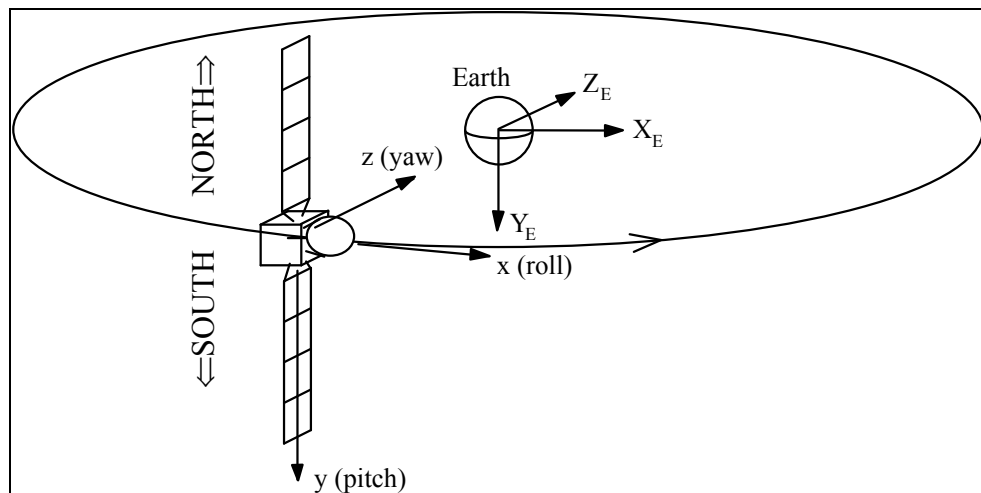


**Figure 13 Reference frame definitions**

Where x, y, z represent the body fixed reference frame and  $X_E$ ,  $Y_E$ ,  $Z_E$ , earth fixed reference frame.

Figure 13 [3] shows the orientation of the body fixed and the earth fixed reference coordinate frames. Both these systems are defined as right-handed and orthogonal. Earth fixed coordinate frame together with the satellite body-fixed frame rotates with respect to an inertial frame at the orbit rate of one revolution per day ( $\omega_0=7.272 \cdot 10^{-5}$  rad/s)

The earth centered inertial reference frame is used for dynamic system of equation derivation. As the set of states, the common practice is to choose angular velocity components and attitude variables to define the 3-DOF (degrees of freedom) rotational EOM. (The 3 translational components are not studied since this thesis does not study orbital correction manoeuvres)

#### 4.3.2 Model's EOM Description

The angular momentum of a rigid body around its center of mass (here CG is assumed to coincide with center of mass) determined by the following relation:

$$\vec{H} = \int \vec{r} \times (\vec{r} \times \vec{\omega}) dm \quad (4.3)$$

Where the integration is done over the whole mass body as represented in a generic way by Figure 14. In this generic formula  $\vec{r}$  (or equivalent representation by “**r**”) denotes the location vector of a particle inside the body, and  $\vec{\omega}$  (or equivalent representation by  $\omega$ ) is the angular velocity vector of the body defined by “**B**”.

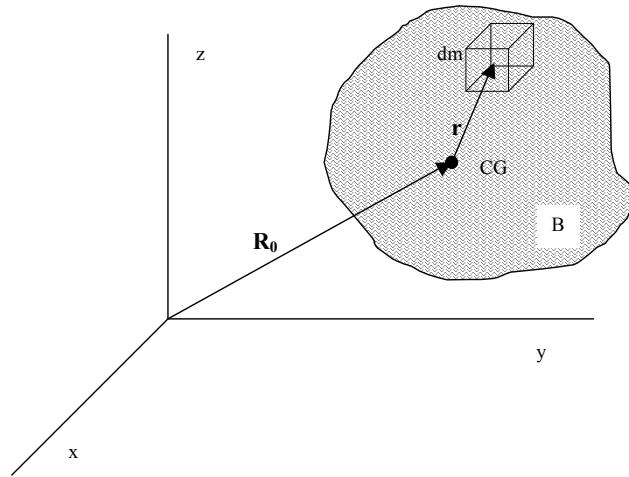


**Figure 14 Generic sketch for EOM derivation**

Evaluating the above vectorial integral and decomposing, we obtain the angular momentum of the body B. Here  $\omega_{x,y,z}$  are the body angular rates.

$$h_x = I_x \omega_x - I_{xy} \omega_y - I_{xz} \omega_z \quad (4.4.a)$$

$$h_y = -I_{xy} \omega_x + I_y \omega_y - I_{yz} \omega_z \quad (4.4.b)$$

$$h_z = -I_{xz} \omega_x - I_{yz} \omega_y + I_z \omega_z \quad (4.4.c)$$

Inertia tensor is very simplified by use of the principal axes. PMMOI components of the inertia matrix vanished, hence the angular momentum vector simplifies to:

$$h_x = 3770 \omega_x \quad (4.5.a)$$

$$h_y = 730 \omega_y \quad (4.5.b)$$

$$h_z = 4020 \omega_z \quad (4.5.c)$$

The total applied torque (T) on the system about its center of mass is equal to the time rate change of the angular momentum.

$$\mathbf{T} = d\mathbf{H}/dt \quad (4.6)$$

or

$$\mathbf{T} = \left( \frac{d\mathbf{H}}{dt} \right)_{\text{body}} + \boldsymbol{\omega} \times \mathbf{H} \quad (4.7)$$

where  $\left( \frac{d\mathbf{H}}{dt} \right)_{\text{body}}$  defines the derivative in body axis frame.

Without adding the momentum wheel effect the Euler equations yield:

$$T_x = I_x \dot{\omega}_x + (I_z - I_y) \omega_y \omega_z \quad (4.8.a)$$

$$T_y = I_y \dot{\omega}_y + (I_x - I_z) \omega_x \omega_z \quad (4.8.b)$$

$$T_z = I_z \dot{\omega}_z + (I_y - I_x) \omega_x \omega_y \quad (4.8.c)$$

with the addition of inertia values the torque equation becomes:

$$T_x = 3770 \dot{\omega}_x + 3290 \omega_y \omega_z \quad (4.9.a)$$

$$T_y = 730 \dot{\omega}_y - 250 \omega_x \omega_z \quad (4.9.b)$$

$$T_z = 4020 \dot{\omega}_z - 3040 \omega_x \omega_y \quad (4.9.c)$$

At the above derivation there exists no explicit disturbance effect. The thruster control torque values shall appear on the left side inside  $T_{x,y,z}$  torque components. (Momentum wheel effect is separately discussed in the following section. Right hand side of the equations represents undisturbed free body motion in principal axis frame.

We reference the satellite attitude to earth fixed reference frame hence to obtain angle data from angular velocity in body fixed frames we need a conversion method to integrate the velocity vector correctly.

For small angular variations Euler angle transformation is easily implemented, and also it is easy to understand from its construction geometry.

#### 4.3.2.1 Euler Angle Transformation

Euler angle transformation gives the attitude of the spacecraft with respect to an Earth-Fixed observer. Starting from earth's axes, with three rotations in a specific order, it is possible to obtain attitude representation of the satellite in body-fixed axes. These angles are defined as follows:

$\phi \rightarrow$  Roll angle about (x) axis

$\theta \rightarrow$  Pitch angle about (y) axis

$\psi \rightarrow$  Yaw angle about (z) axis

The transformation is not a commutative operation hence the order of the transformation is important. Different sequences yield different resultant matrices. For our model we select the rotation sequence about the angles: yaw ( $\psi$ ), roll ( $\phi$ ) and finally pitch ( $\theta$ ).

We define the body fixed principal (xyz) coordinate system with  $\mathbf{e}_{\text{body}}$  vector and an orbital frame fixed on the satellite (XYZ)<sub>orbit</sub> as the  $\mathbf{E}_{\text{orbit}}$ . (See Figure 15. [26])

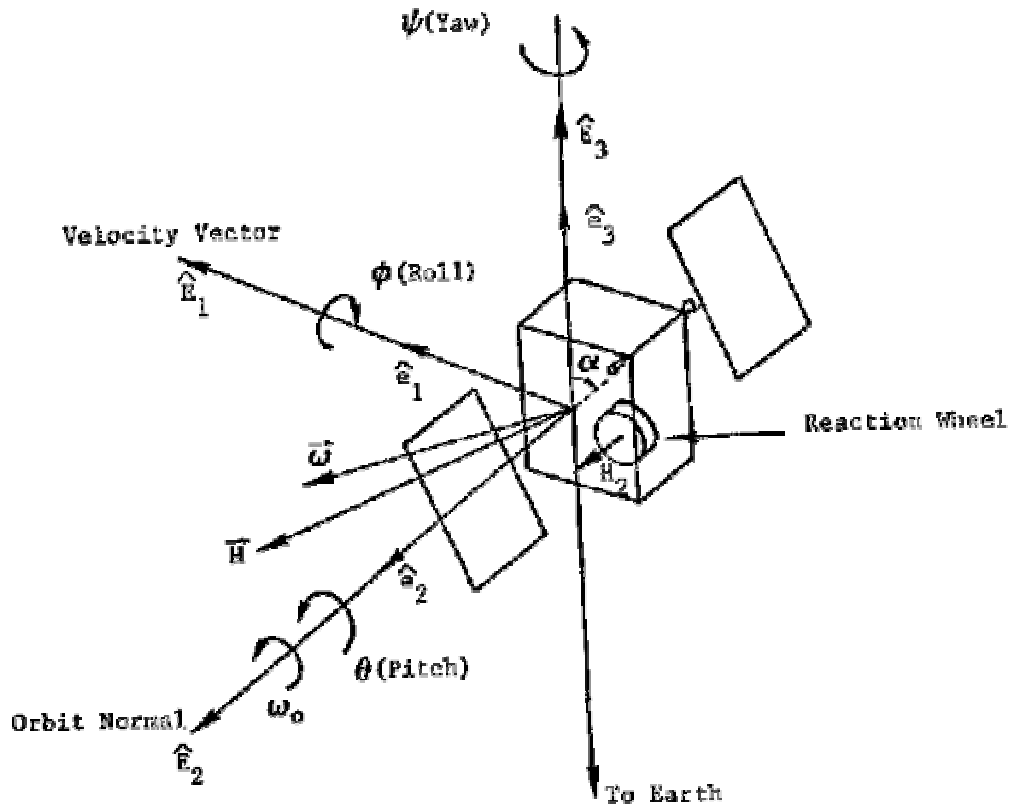


Figure 15 Geometry for orbital axis definition

$$\begin{pmatrix} e_1 \\ e_2 \\ e_3 \end{pmatrix}_{body} = \mathbf{R}_\psi \mathbf{R}_\phi \mathbf{R}_\theta \begin{pmatrix} E_1 \\ E_2 \\ E_3 \end{pmatrix}_{orbital} \quad (4.10)$$

Rotation sequence can be visualized as below Figures 16 and 17:

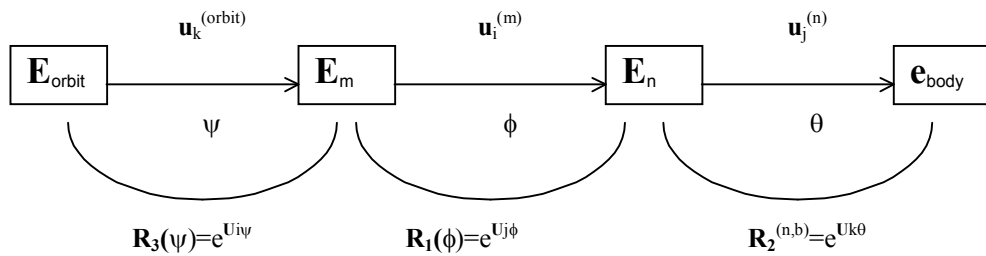
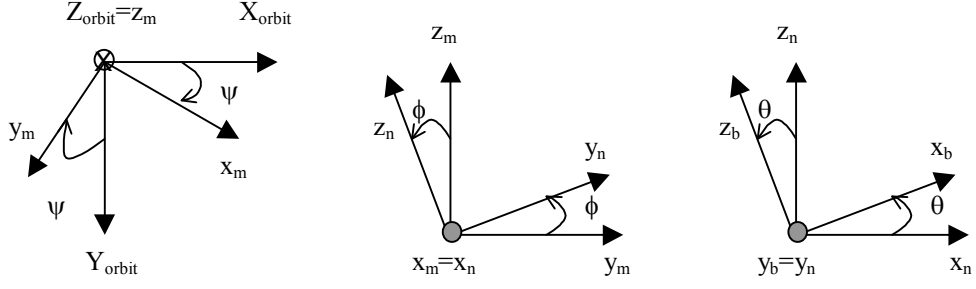


Figure 16 Transformation sequence



**Figure 17  $\psi$ - $\phi$ - $\theta$  Rotation sequence from orbit fixed to body fixed frame**

There we obtain the following rotation matrices:

$$\mathbf{R}_3(\psi) = \begin{bmatrix} c\psi & -s\psi & 0 \\ s\psi & c\psi & 0 \\ 0 & 0 & 1 \end{bmatrix}, \quad \mathbf{R}_1(\phi) = \begin{bmatrix} 1 & 0 & 0 \\ 0 & c\phi & -s\phi \\ 0 & s\phi & c\phi \end{bmatrix}, \quad \text{and} \quad \mathbf{R}_2(\theta) = \begin{bmatrix} c\theta & 0 & s\theta \\ 0 & 1 & 0 \\ -s\theta & 0 & c\theta \end{bmatrix} \quad (4.11 \text{ a, b, c})$$

Where the  $s(\cdot)$  and  $c(\cdot)$  define the sine and cosine functions respectively.

The individual rotations can be expressed as:

$$\begin{bmatrix} X \\ Y \\ Z \end{bmatrix}_{orbit} = \mathbf{R}_3(\psi) \begin{bmatrix} x \\ y \\ z \end{bmatrix}_m, \quad \begin{bmatrix} x \\ y \\ z \end{bmatrix}_m = \mathbf{R}_1(\phi) \begin{bmatrix} x \\ y \\ z \end{bmatrix}_n, \quad \text{and} \quad \begin{bmatrix} x \\ y \\ z \end{bmatrix}_n = \mathbf{R}_2(\theta) \begin{bmatrix} x \\ y \\ z \end{bmatrix}_b \quad (4.12)$$

The angular velocity components  $\omega_1$ ,  $\omega_2$ ,  $\omega_3$  in the spacecraft principal body fixed reference frame are given by,

$$\begin{bmatrix} \omega_1 \\ \omega_2 \\ \omega_3 \end{bmatrix} = \begin{bmatrix} 0 \\ 0 \\ \dot{\psi} \end{bmatrix} + \mathbf{R}_3(\psi) \begin{bmatrix} \dot{\phi} \\ 0 \\ 0 \end{bmatrix} + \mathbf{R}_3(\psi) \mathbf{R}_1(\phi) \begin{bmatrix} 0 \\ \dot{\theta} \\ 0 \end{bmatrix} + \mathbf{R}_3(\psi) \mathbf{R}_1(\phi) \mathbf{R}_2(\theta) \begin{bmatrix} 0 \\ \omega_0 \\ 0 \end{bmatrix} \quad (4.13)$$

Where  $\omega_0$  is the earth rotation rate of  $7.272 \cdot 10^{-5}$  rad/sec. And performing the respective matrix multiplication the body rates yield the following result,

$$\begin{bmatrix} \omega_1 \\ \omega_2 \\ \omega_3 \end{bmatrix}_{body} = \begin{bmatrix} \omega_x \\ \omega_y \\ \omega_z \end{bmatrix} = \begin{bmatrix} \dot{\phi} \cos(\psi) + (\dot{\theta} + \omega_0) \sin(\psi) \cos(\phi) \\ -\dot{\phi} \sin(\psi) + (\dot{\theta} + \omega_0) \cos(\psi) \cos(\phi) \\ \dot{\psi} - (\dot{\theta} + \omega_0) \sin(\phi) \end{bmatrix} \quad (4.14)$$

Defining  $(\dot{\theta} + \omega_0) = \dot{\theta}_1$  we can take the inverse left part of the above equation to get,

$$\begin{bmatrix} \dot{\phi} \\ \dot{\theta}_1 \\ \dot{\psi} \end{bmatrix} = \begin{bmatrix} \omega_x \cos(\psi) - \omega_y \sin(\psi) \\ \omega_x \frac{\sin(\psi)}{\cos(\phi)} + \omega_y \frac{\cos(\psi)}{\cos(\phi)} \\ \omega_x \sin(\psi) \tan(\phi) + \omega_y \cos(\psi) \tan(\phi) + \omega_z \end{bmatrix} \quad (4.15)$$

replacing  $(\dot{\theta}_1 - \omega_0) = \dot{\theta}$

$$\begin{bmatrix} \dot{\phi} \\ \dot{\theta} \\ \dot{\psi} \end{bmatrix} = \begin{bmatrix} \omega_x \cos(\psi) - \omega_y \sin(\psi) \\ \omega_x \frac{\sin(\psi)}{\cos(\phi)} + \omega_y \frac{\cos(\psi)}{\cos(\phi)} - \omega_0 \\ \omega_x \sin(\psi) \tan(\phi) + \omega_y \cos(\psi) \tan(\phi) + \omega_z \end{bmatrix} \quad (4.16)$$

This is the final equation representing Euler rates in body coordinates. As noticed from the above set of equations the system is singular at 90° roll angle ( $\phi=90^\circ$ ), since  $1/\cos(90^\circ)$  is infinity. For different selections of the rotation sequences any of the rotation angles may experience this singularity. Above set is selected to avoid a singularity at pitch angle specifically. Having limitations on these angles does not interrupt us, because satellite is to offset maximum  $\pm 6^\circ$  as previously noted on section 3.3.7 and on NM pitch and roll attitudes are maintained within  $\pm 0.05^\circ$  bias. [3] As a result satellite is not expected to experience high changes in roll/pitch attitude during service orbit life.

Another way of representing the attitude information is the "quaternion" technique. Quaternion representation has the advantage of not having the singularity in

coordinate transformations. Also it increases the on-board computation speed which is critical for navigation, strapdown systems. Unfortunately with this method, it is hard to visualise the actual angles. In this thesis there is no need to use the quaternions. Euler representation is reliable, simple and accurate enough.

#### 4.3.2.2 Including the Momentum Wheel Torque to Euler Equations

The previously derived

$$T_x = 3770\dot{\omega}_x + 3290\omega_y\omega_z \quad (4.9.a \text{ -repeated})$$

$$T_y = 730\dot{\omega}_y - 250\omega_x\omega_z \quad (4.9.b \text{ -repeated})$$

$$T_z = 4020\dot{\omega}_z - 3040\omega_x\omega_y \quad (4.9.c \text{ -repeated})$$

equations excluded the momentum wheel torque. Similar to TÜRKSAT 1B arrangement we select a momentum wheel whose total torque is aligned with  $-y$ -axis (negative pitch axis) of the satellite. In vectorial representation the angular momentum equation is modified as follows in Cartesian representation ( $\mathbf{i}, \mathbf{j}, \mathbf{k}$  representing unit vectors along the  $x, y, z$  directions):

$$\mathbf{H} = I_x\omega_x \mathbf{i} + (I_y\omega_y - h_w) \mathbf{j} + I_z\omega_z \mathbf{k} \quad (4.17)$$

Where  $h_w$  represents the nominal torque of the momentum wheel. ( $h_w=60$  N.m just as Reference [3] proposed) Then with the application of Euler angular momentum law (Equation 4.7) we get the following result:

$$T_x = 3770\dot{\omega}_x + 3290\omega_y\omega_z + 60\omega_z \quad (4.18.a)$$

$$T_y = 730\dot{\omega}_y - 250\omega_x\omega_z - \dot{h}_w \quad (4.18.b)$$

$$T_z = 4020\dot{\omega}_z - 3040\omega_x\omega_y - 60\omega_x \quad (4.18.c)$$

Here  $\dot{h}_w$  represent the time rate of change of wheel angular momentum, which defines the pitch control law. In case no pitch control is applied it vanishes ( $\dot{h}_w = 0$ ).

#### 4.3.2.3 Thruster Geometry and Torque Definitions

Similar to TÜRKSAT 1B our model also uses the offset oriented thrusters to get coupling for passive yaw control. The generic orientation can be visualized by the following Figure 18:

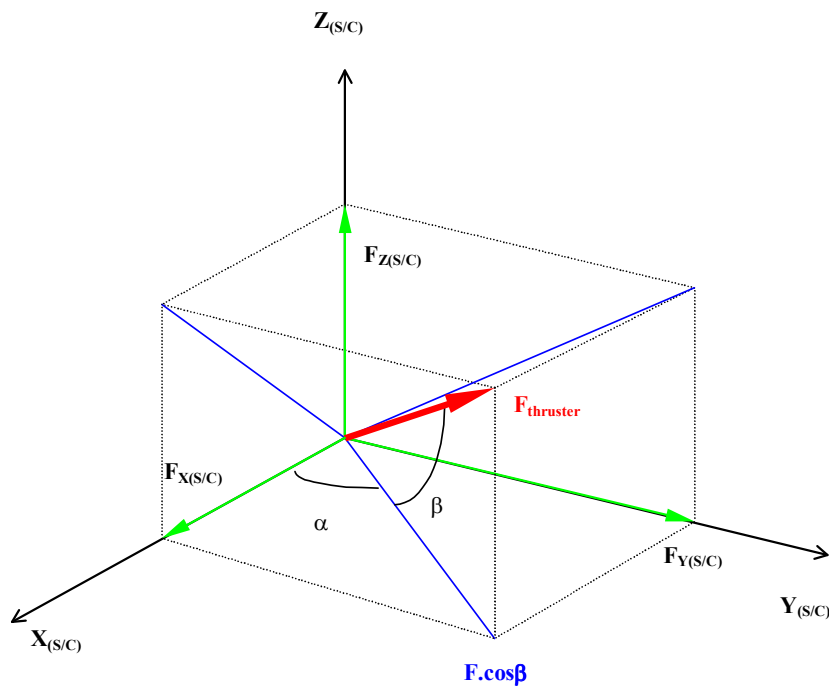


**Figure 18 Generic thruster orientation angles**

Where the (S/C) denote the spacecraft coordinate frame. We can easily conclude from the above Figure that the  $X_{(S/C)}$ ,  $Y_{(S/C)}$ ,  $Z_{(S/C)}$  components of the force vector  $F_{thruster}$  are:

$$F_{thruster} = F \text{ (10N nominal)} \quad (4.19.a)$$

$$F_{X(S/C)} = F \cdot \cos\beta \cdot \cos\alpha \quad (4.19.b)$$

$$F_{Y(S/C)} = F \cdot \cos\beta \cdot \sin\alpha \quad (4.19.c)$$

$$F_{Z(S/C)} = F \cdot \sin\beta \quad (4.19.d)$$

We computed the exact torque components of the TÜRKSAT 1B with the inclusion of impingement forces. The value arising from the impingement characteristics were negligible (less than 1% of maximum component) Also Reference [3] notes this feature, hence in this thesis we also exclude impingement characteristics.

This thesis will use canted roll thrusters with similar location and alignment to that of TÜRKSAT 1B. The control system will be designed in accordance with use of only roll thrusters, which is the nominal case in NM during GO.

Nominal thrust magnitude is 10 N. Thruster 4A, 4B, 5A, 5B of TÜRKSAT 1B are used. On/off valves similar to TÜRKSAT 1B control the attitude thrusters of our model. .

In TÜRKSAT 1B the orientations of the south thrusters are as at Table 2:

**Table 2 TÜRKSAT 1B Roll Thruster Properties**

Thruster	Locations			Thruster Orientation	
	X (mm)	Y (mm)	Z (mm)	$\alpha$ (deg)	$\beta$ (deg)
4A	2200	0	-1100	0	-16
4B	0	0	900	180	7
5A	2200	0	1380	0	26
5B	0	0	-900	180	-7

However with above location coordinated CG is not at the origin. A Microsoft Excel worksheet calculates the net torque over our model of satellite with the CG at the origin of satellite body fixed coordinates. (Tables 3-5) In TÜRKSAT 1B CG change during BOT to EOL also changes the moment arms of the thrusters, which causes alterations on the effective torque values of the thrusters. However since our model assumes a fixed CG location, moment arm length is fixed for our study during NM at GO (BOL to EOL). Our model has the below thruster characteristics where moment arms (the location of thruster's nozzles with respect to the satellite CG) are approximately nominal to that of TÜRKSAT 1B. The average CG

between BOL and EOL of TÜRKSAT 1B is the satellite axis origin of our model, hence thruster location values at the below Table 3 are a bit different in comparison to Table 2. Angle alignments are taken just as at Table 2.

**Table 3 Roll Thruster Nozzle Locations of the Model**

Thruster Distance with respect to CG at Axis Origin (m)			
Thruster	x	y	z
4A	1.1403	0.0054	1.1047
4B	1.1127	0.0044	0.9053
5A	1.1363	0.0054	1.3943
5B	1.1127	0.0054	0.9007

**Table 4 Roll Thruster Force Components**

Force Components (N)			
Thruster	x	y	z
4A	11.319	-4.5E-05	1.337
4B	-10.003	-2.7E-05	3.964
5A	10.216	4.1E-05	6.106
5B	-11.044	-1.9E-05	-1.099

**Table 5 Roll Thruster Torque Components**

Net torque Components (Nm)			
Thruster	x	y	z
4A	11.3193	-4.5E-05	1.3367
4B	-10.0034	-2.7E-05	3.9644
5A	10.2156	4.12E-05	6.1057
5B	-11.0438	-1.9E-05	-1.0992

Notice that as will be seen in section 5.2.3 for simulation purposes a single pair of thruster model is implemented on controller design, rather than using 4 thrusters as above tables indicate. For the actuator design of the controller above values gives a direction, about the magnitude and proper alignment of the nozzles. We can approximately accept following values,  $T_x \approx 10 \text{ Nm}$ ,  $T_y \approx 10^{-5} \text{ Nm}$ ,  $T_z \approx 3 \text{ Nm}$  as nominal thruster torque components.

#### 4.3.2.4 MATLAB-Simulink Uncontrolled Behaviour Graphical Results

This uncontrolled attitude dynamics simulation study is represented at APPENDIX A where we also included the discussion of the results by comparisons. Next step is to explain environmental (external) and internal disturbance effects on the satellite dynamics.

#### **4.4 Environmental and Internal Disturbances on Attitude Model**

The primary environmental disturbing effects concerning the spacecraft attitude are the solar radiation pressure, gravity gradients, aerodynamic and magnetic disturbing torques on satellite body. These are the external disturbances, and the other group of perturbations is the internal ones; which primarily includes the effects associated with internal moving hardware, thrust misalignment, propellant leakage or slosh effects, and so on.

From the environmental perturbation group, the solar radiation pressure is significant on both attitude and trajectory biases of the satellite for altitudes higher than 1000 km. The gravity gradient disturbance torques, result from the extended dimensions of the geostationary satellite. The magnetic perturbations arise by interaction of the satellite magnetic materials with earth's magnetic field and are most significant below 1000 km. Similarly Aerodynamic perturbations are most significant below 500 km and are negligible over 1000-km altitudes. These effects are visualised by the Figure 19. ( [26] and [30] )

As for the other group, the internal perturbation torques group, the torques arising from internal moving parts have several causes such as, rotating wheels, scanning devices, circulating fluids, and so on. These effects must be included in the general equations of motion of the satellite attitude. Propellant slosh, leakage, and misalignment of the momentum exchange actuators (thrusters, momentum wheels and so on) cause deviation on satellite kinetic energy and momentum distribution among components affecting its attitude. [26]

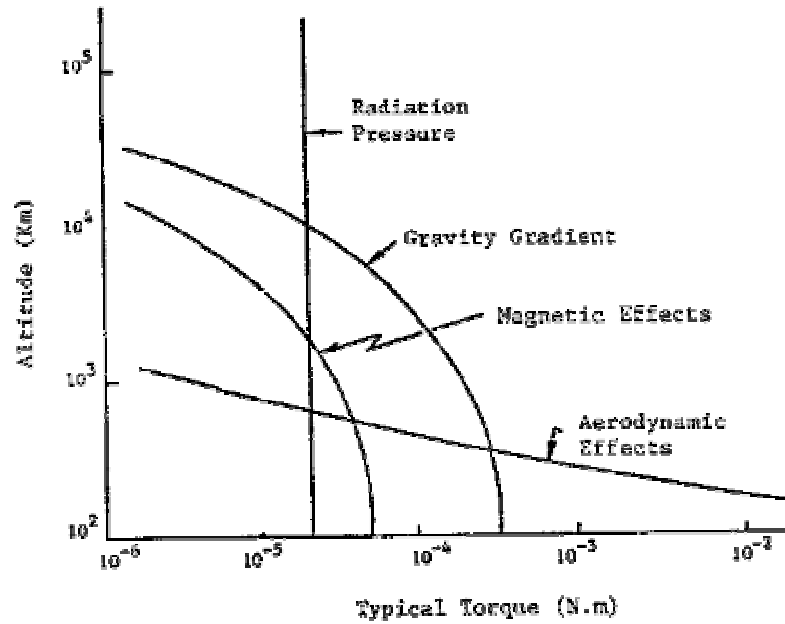


**Figure 19 Typical perturbation torques as a function of altitude**

#### 4.4.1 Environmental (External) Disturbance Torques

Here we present the mathematical models for environmental disturbing torques on satellite attitude. On the simulation model only solar radiation and gravity gradient torques have significant effects because TÜRSAT 1B has a high altitude of 36000 km on its geostationary orbit. Also refer to Figure 19.

##### 4.4.1.1 Solar Radiation Pressure Torque

The photons from the sun produce a net torque with their impingement on the various distinct surfaces of the satellite structure. According to the satellite attitude with respect to sun and its geometrical shape the incident photons produce net force components on each distinctive satellite segment. The total net perturbing torque is a result of these components, which are biased with satellite center of mass. This disturbance torque mainly depends on the following factors: [26] and [2]

- a) Satellite Geometric Configuration. This configuration influences the degree of shading and the net moment arm of the net force with respect to satellite mass center.
- b) Shading Effects. Some components of the satellite structure surely will not be exposed to sunrays due to the other component's shades over them. Satellites with large protruding parts experience significant effects of shading.
- c) Optical Reflection Properties of the Satellite Surface.
- d) Satellite-Sun Vector Orientation. The time history of the satellite, the orbital position and inclination with respect to sun, affects the shading and the total amount of solar radiation absorbed/reflected.

The solar radiation torque on a satellite is in the form: (Chobotov [26])

$$\vec{T}^{(solar)} = \int_{e.s} \vec{r} \times d\vec{f} \quad (4.20)$$

Where  $\vec{r}$  is the vector directed from the satellite center of mass to the area element  $d\mathbf{A}_i$  for the  $i$ -th surface, and e.s represents the sun exposed surface

The latter differential force vector may be modelled assuming that the incident radiation of the sun is either reflected (specularly or diffusively) or absorbed, or some combination of these. The following formula is given [3].

$$d\vec{f}_{total} = -P \int \left[ (1 - C_a) \vec{S} + 2(C_s \cos(\theta) + \frac{1}{3} C_d) \vec{N} \right] \cos(\theta) dA \quad (4.21)$$

Here coefficients  $C_a$ ,  $C_s$ ,  $C_d$  define the percentage of the absorbed, specularly reflected and diffusively reflected radiation, respectively.  $P$  is the mean momentum flux,  $\vec{S}$  is the unit vector from the satellite to the sun,  $\vec{N}$  is the unit vector along the normal of the exposed surface, and  $\theta$  is the angle between  $\vec{S}$  and  $\vec{N}$ . The integral is taken over the surface area ( $dA$ : infinitesimal area element).

However it's very difficult to apply these relations to our case of Geostationary Satellite.

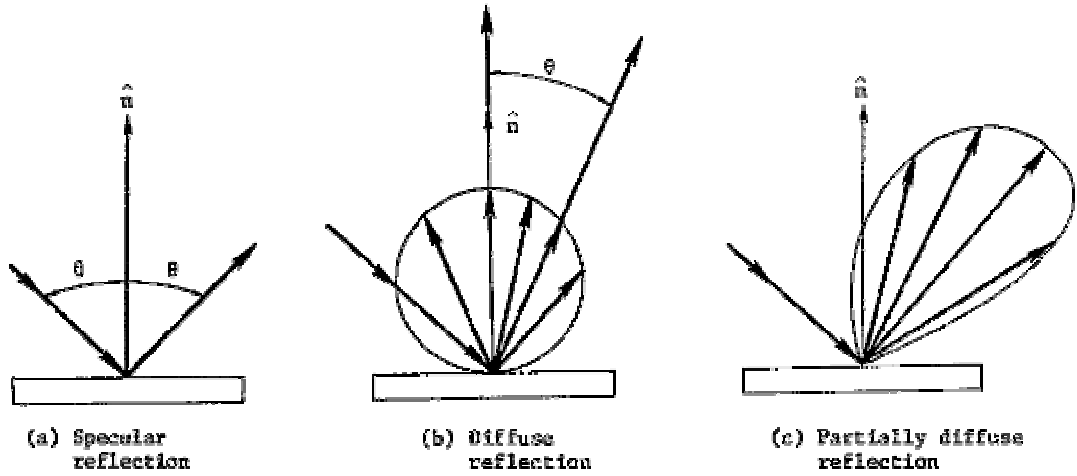


Figure 20 Reflection types [26]

Chobotov also proposes the following general formula for a geosynchronous satellite for a given season [26]. The fundamental Fourier components of solar torque about the body axes are:

$$T_1^{(s)} = A + B \cos(\omega_0 t) + G \sin(\omega_0 t) \quad (4.21 \text{ a})$$

$$T_2^{(s)} = E + F \cos(\omega_0 t) + I \sin(\omega_0 t) \quad (4.21 \text{ b})$$

$$T_3^{(s)} = C + D \sin(\omega_0 t) + H \cos(\omega_0 t) \quad (4.21 \text{ c})$$

where A to H are constants.

Kaplan ([27]) proposes a more explicit model. A cyclic model for a three-axis stabilised satellite configuration. The model resembles to the above set of equations proposed by Chobotov.

$$T_x = 2 \cdot 10^{-5} [1 - 2 \sin(\omega_0 t)] \quad (4.22 \text{ a})$$

$$T_x = 10^{-4} \cos(\omega_0 t) \quad (4.22 \text{ b})$$

$$T_x = -5 \cdot 10^{-5} \cos(\omega_0 t) \quad (4.22 \text{ c})$$

This model is used for this thesis, at the Matlab-Simulink simulation model. The above set of equations are transferred into Matlab-Simulink as follows:

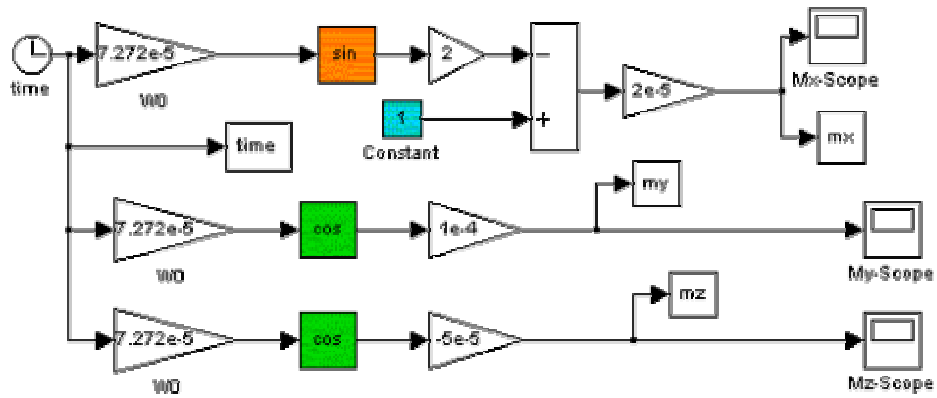


**Figure 21 Solar pressure disturbance, simulink implementation**

The time history of the perturbation torque is:

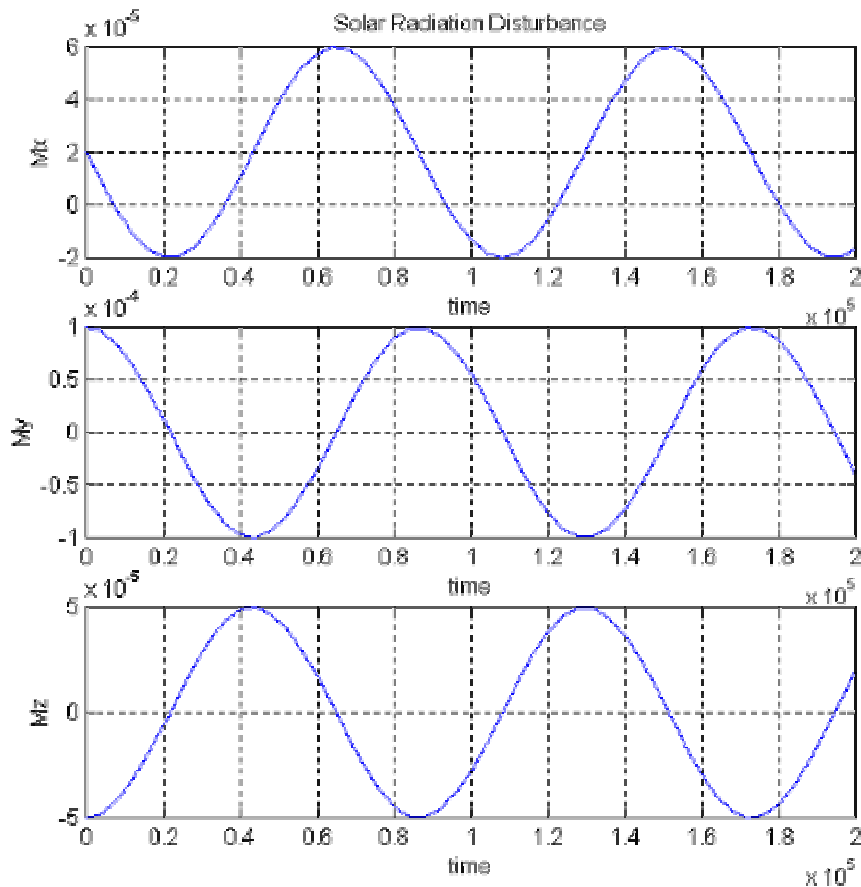


**Figure 22 Solar radiation pressure time history (torque in Nm)**

#### 4.4.1.2 Gravity Gradient Torque

This perturbation torque occurs because of the small difference in the strength of the earth gravitational field over the satellite structure.

Hughes [28] proposed the following mathematical relation, the gravity gradient torque acts on a general body with principal moments of inertia  $I_1, I_2, I_3$  as:

$$\mathbf{g} = -3(GM / R^3)[(I_2-I_3) \theta_1, (I_1-I_3) \theta_2, 0] \quad (4.23)$$

where  $\theta_1, \theta_2, \theta_3$ , represent the small rotation angles about the principal axes. For circular (as in the case of geostationary) orbit  $GM/R^3$  is equal to the square of orbital angular velocity,  $\omega_0$ .  $R$  is the distance between the earth and the satellite mass center.

Chobotov proposes a more complex model with principal body axes; the gravity gradient torque in component form is as follows:

$$T_1^{(g)} = K (I_{33}-I_{22}) a_{21} a_{31} \quad (4.24 a)$$

$$T_2^{(g)} = K (I_{11}-I_{33}) a_{11} a_{31} \quad (4.24 b)$$

$$T_3^{(g)} = K (I_{22}-I_{11}) a_{11} a_{21} \quad (4.24 c)$$

where  $K=3\mu/R^3$  and  $a_{ij}$  ( $i, j=1,2,3$ ) are the elements of the transformation matrix (i.e., direction cosines). ( $\mu=GM$  the earth gravitational constant). This equation also simplifies to equation set 4.26 with proper assumptions.

The location of the satellite center of gravity (CG) changes according to its attitude, which is the angular arrangement with respect to gradient of the potential field and the distance between the satellite and the attraction center (the earth). [29] This yields a net torque in addition to the attraction force, and is called gravity gradient torque.

Rimrott proposes a very similar form of equations like Chobotov. With the small satellite assumption the torque of the Kepler force about the satellite's mass center the following set of equations result:

$$\mathbf{M} = 3\Omega^2 \begin{bmatrix} e_x & e_y & e_z \end{bmatrix} \begin{bmatrix} (C-B)\cos(\gamma)\cos(\beta) \\ (A-C)\cos(\gamma)\cos(\alpha) \\ (B-A)\cos(\alpha)\cos(\beta) \end{bmatrix} \quad (4.25)$$

where  $\alpha$ ,  $\beta$ ,  $\gamma$  are the direction angles between the position vector  $\mathbf{p}$  and the satellite principal axes.  $A$ ,  $B$ ,  $C$  are the components of the inertia tensor along the principal axes.  $\Omega^2 = \mu/\rho_C^3$  and  $\rho_C$  is the distance between satellite mass center and the earth center. Note that small satellite approximation yields the following approximation:  $\mu/\rho_C \rho_G^2 \approx \mu/\rho_C^3 = \Omega^2$ . When position vector and the principal axis directions coincide, this equation takes the simple form of the model proposed by Kaplan [27], which we are to present next:

Kaplan [27] simplifies the above stated general formulas to yield following set of linearised equations in component form:

$$T_x^{(g)} = -3\omega_0^2(I_y - I_z) \phi \quad (4.26 \text{ a})$$

$$T_y^{(g)} = -3\omega_0^2(I_x - I_z) \theta \quad (4.26 \text{ b})$$

$$T_x^{(g)} = 0 \quad (4.26 \text{ c})$$

Kaplan derives this set of equations using the simple form of the motion equation,

$\mathbf{G} = \frac{d\mathbf{h}}{dt}$  where  $\mathbf{G}$  is the gravity gradient net torque vector, and  $\mathbf{h}$  is the net angular momentum vector of the rigid satellite.

Finally Bryson [30] proposes the above relation with minor symbology difference:

$$\vec{Q}_g = 3 \frac{g}{R} \left[ (I_z - I_y) \phi \hat{i} + (I_z - I_x) \theta \hat{j} + (I_x - I_y) \phi \theta \hat{k} \right] \quad (4.27)$$

where he also states that the multiplication  $\phi\theta$  is negligible and  $3g/R \approx \omega^2_0$ .

As Uslu [3] Kaplan and the others we are going to use this model (4.26) of gravity gradient disturbance torque for the simulations by Matlab-Simulink. Inserting the model inertia values we finally obtain the following set of equations for gravity gradient perturbing torque:

$$\begin{bmatrix} G_x \\ G_y \\ G_z \end{bmatrix} = \begin{bmatrix} 5.21975 \cdot 10^{-5} \phi \\ 3.96637 \cdot 10^{-6} \theta \\ 0 \end{bmatrix} \quad (4.28)$$

#### 4.4.1.3 Aerodynamic and Magnetic Disturbance Torques

- *Aerodynamic Torque*

This perturbation force is most dominant for low altitude satellites orbiting below approximately 400-500 km. The drag force components created by the air molecule interaction with the satellite body produce a net torque about the satellite center of mass. The satellite passes through an atmosphere of density  $\rho$  with a velocity vector  $\mathbf{v}$ . The magnitude of the aerodynamic drag force  $\mathbf{F}^{(a)}$  is then given as:

$$\mathbf{F}^{(a)} = \frac{1}{2} \rho \mathbf{v} \cdot \mathbf{v} A C_d \quad (4.29)$$

where  $A$  is the reference area of the satellite (i.e., cross-section along  $\mathbf{v}$ ) and  $C_d$  is the drag coefficient. Then the total torque is given by:

$$\mathbf{T}^{(a)} = \frac{1}{2} \rho v^2 l S C_d \quad (4.30)$$

where  $l$  is the length of the perpendicular from the mass center to the force line of action. Chobotov offers some estimates on  $C_d$  and air densities.

Uslu [3] offers the same formula in differential form. Uslu and Hughes and Chobotov emphasize that the aerodynamic torque becomes comparable with the gravity gradient perturbation on low altitudes between 100-600 km. For TÜRKSAT 1B geostationary satellite which is at high altitude (~36000 km) this perturbing torque can safely be neglected. Refer to Figure 19 as well.

- *Magnetic Disturbance Torque*

Magnetic disturbance torques on a satellite result from the interaction of the spacecraft's residual magnetic field and geomagnetic field. Let  $\mathbf{M}$  be the sum of all magnetic moments in the satellite the torque acting on it is: ([3] and [26])

$$\mathbf{T}^{(m)} = \mathbf{M} \times \mathbf{B} \quad (4.31)$$

where  $\mathbf{B}$  is the geomagnetic field vector (also named as geocentric magnetic flux density). Generally  $\mathbf{M}$  is caused by permanent and induced magnets or by satellite generated current loops.

As emphasised by Uslu and Chobotov this perturbation is also negligible for a geostationary satellite at high orbit. Refer to Figure 19 as well.

#### 4.4.2 Internal Disturbance Torques

The internal torques that we will shortly describe here show completely random behaviour. Therefore we are unable to propose explicit mathematical models as in the case of environmental effects. Also their perturbing magnitudes are small in comparison to external torques hence they are neglected for the simulations.

#### 4.4.2.1 Mass Expulsion Torque

They are the results of the propellant or other mass ejection from the satellite. They can be investigated in two groups according to their sources: [3]

- a) Unintentional control system torques. These include the fuel leakage, thrust vector misalignment, anomaly in the thruster firing time, reaction forces due to plume impingement.
- b) Torques due to sources intended to expel mass. These include dumping residual propellant, payload separation, payload ejection, equipment jettison, and orbital manoeuvre's impact.

One note on plume impingement is that for TÜRKSAT 1B the measured maximum plume impingement of the roll thrusters is about 1% of the nominal control torque which is also neglected when we represented the model satellite's actuator properties. (Section 4.3.2.3)

#### 4.4.2.2 Propellant Slosh Torque

The rotational or the translational accelerations of the satellite causes sloshing of the fluids inside the satellite which is generally only the propellant in partially filled fuel tank and pipes. The duration and magnitude of the sloshing depends on the propellant properties, tank/pipe geometry, the amount of fluid in the tank/pipes, and the acceleration field [2] , [3].

#### 4.4.2.3 Moving Hardware Torques

Motions of some satellite components like antennas, solar array wings, hardisk of the microcomputers also produce disturbance torques.

## CHAPTER V

### ATTITUDE CONTROL SYSTEM DESIGN

#### 5.1 Pitch Control System Design

Initially the pitch motion is decoupled from the yaw/roll dynamics, then the equations are converted into state space representation.

##### 5.1.1 Equations for Pitch Motion

At Appendix 2 the nonlinear governing motion equations are linearised. The decoupled pitch attitude equation is :

$$T_y + 3.8722 \cdot 10^{-7} \theta = 730 \ddot{\theta} + \dot{h} \quad (5.1)$$

where  $T_y$  is only the solar pressure perturbation torque, and  $\dot{h}$  is the momentum wheel control law – basically the momentum wheel acceleration/deceleration value. Without the control  $\dot{h}$ , pitch motion is unstable. The gravity gradient perturbing torque shifts the body dynamics system from double poles at origin to, one positive one negative real pole close to origin. (See the eigenvalues calculation in Appendix 2.) The pitch motion equation is converted into state space formulation for better representation in Simulink program. Setting the states  $X_1 = \theta$  and  $X_2 = d\theta/dt$ , we get the state equation in form  $\dot{\mathbf{X}} = \mathbf{A} \mathbf{X} + \mathbf{B} u$  and the output equation in form  $y = \mathbf{C} \mathbf{X}$ . Where the system representing matrices are as follows:

$\mathbf{A} = \begin{bmatrix} 0 & 1 \\ 5.3043 \cdot 10^{-10} & 0 \end{bmatrix}$  is named as system matrix, and its eigenvalues determine the stability characteristics.

$\mathbf{B} = \begin{bmatrix} 0 \\ 1.369863 \cdot 10^{-3} \end{bmatrix}$  is the input matrix.

The outputs of the system are the states, hence the respective measurement matrix  $\mathbf{C}$  is a 2x2 unity matrix,  $\mathbf{C} = \begin{bmatrix} 1 & 0 \\ 0 & 1 \end{bmatrix}$ .

Finally  $u$  is the control law  $\dot{h}$ , which is determined by the following sections.

One remark may be that the rate information ( $d\theta/dt$ ) is assumed to be measured by rate gyros and the attitude ( $\theta$ ) information is measured by optical earth/sun sensors. Here our model differs from the original TÜRKSAT 1B control configuration. We propose a controller that needs measurement of both rate and attitude information for precise attitude regulation whereas original TÜRKSAT 1B controller needs measurement of attitude only.

### 5.1.2 Actuator Model

Second order DC motor representation is selected for accurate torque control. Both Ogata [31] and Kuo [32] uses this second order model throughout their control books for position control purposes. The model is modified for torque control to get the angular moment output rather than angular position output. The block diagram is given in Figure 27. The physical parameters of the DC motor for TÜRKSAT 1B was not available hence in this thesis an actuator model is assumed. Various stabilizing parameters are determined by rootlocus analysis however many of them require very high gains for the PD controller hence one of

most feasible configuration is represented here. The 'load actuator' block in the main program for control of linearised pitch dynamics is used to test various DC models for transient responses. It is a simple Matlab m file that loads motor parameters into Matlab Workspace when clicked on the respective block in main Simulink program.

Physical parameters of designed actuator are:

$L_a=0.005$ (H) Armature inductance,

$K_i=0.3$  (N-m/A) Torque constant,

$K_b=0.3$  (V/rad/s) Back EMF constant,

$B_m=0.002$  viscous-friction coefficient;

$J_w=0.12456$  (kg m<sup>2</sup>) total (rotor+wheel) inertia of motor,

$R_a=5$  ( $\Omega$ ) Armature resistance

The following transfer function represents the DC motor model. It has the system poles at  $-999.86$  and  $-0.16059$ , and the system zero is at  $-1.6057 \cdot 10^{-2}$  locations.

$$\frac{60 s + 0.96339}{s^2 + 1000.016 s + 160.5652} \quad (5.2)$$

The satellite dynamics is represented by the transfer function (5.3). The system has one stable pole at  $-2.3031 \cdot 10^{-5}$  and one unstable pole at  $2.3031 \cdot 10^{-5}$ .

$$\frac{1.3699 \cdot 10^{-3}}{s^2 - 5.3044 \cdot 10^{-10}} \quad (5.3)$$

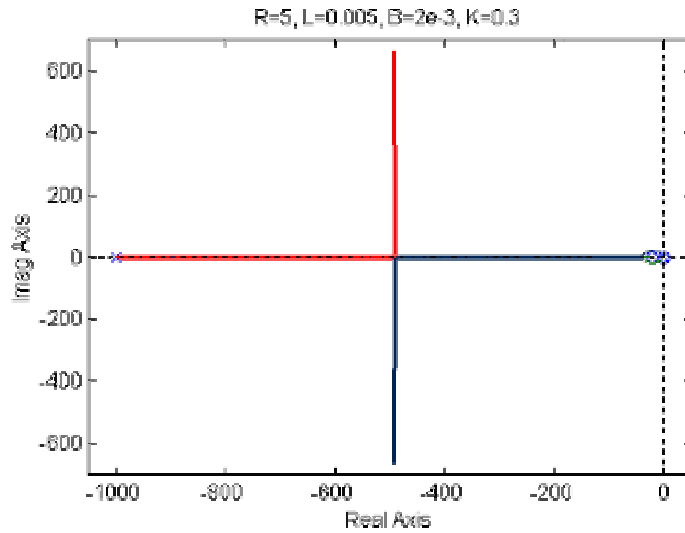
Finally the transfer function for the PD controller is  $(K_d s + K_p)$ , which introduces a zero to the closed loop system at  $-K_p/K_d$ .

The following m file is written to obtain the rootlocus plot of the actuator, satellite, PD Controller blocks together;

```

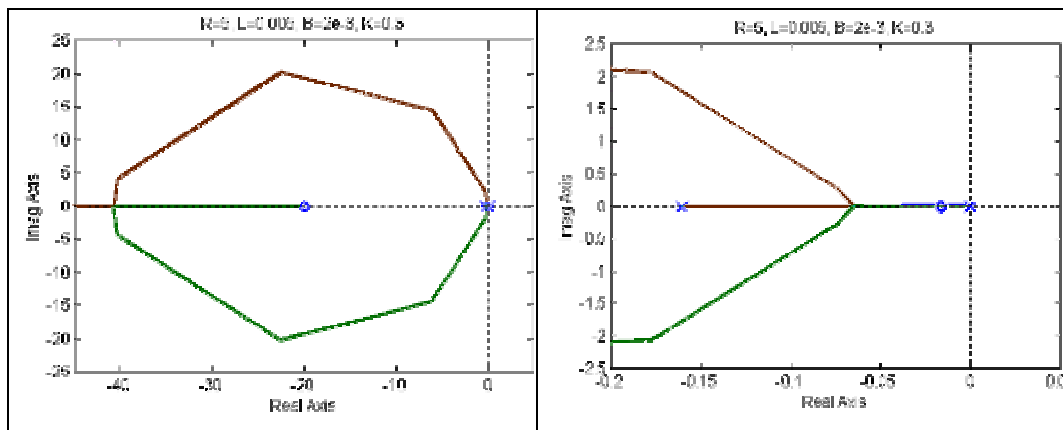
KpKd3=-20;
Z3=[-1.6057e-2 KpKd3];
P3=[-2.3031e-5 2.3031e-5 -999.86 -1.6057e-1];
SYS3=ZPK(Z3,P3,1);
rlocus(SYS3)
title('R=5, L=0.005, B=2e-3, K=0.3')

```



**Figure 23 Rootlocus diagram for controlled pitch attitude**

Below set of figures show various zoomed sections of above Figure 23. Each zoomed section present the regions about system poles (defined by an X mark) and system zeros (defined by an O mark).



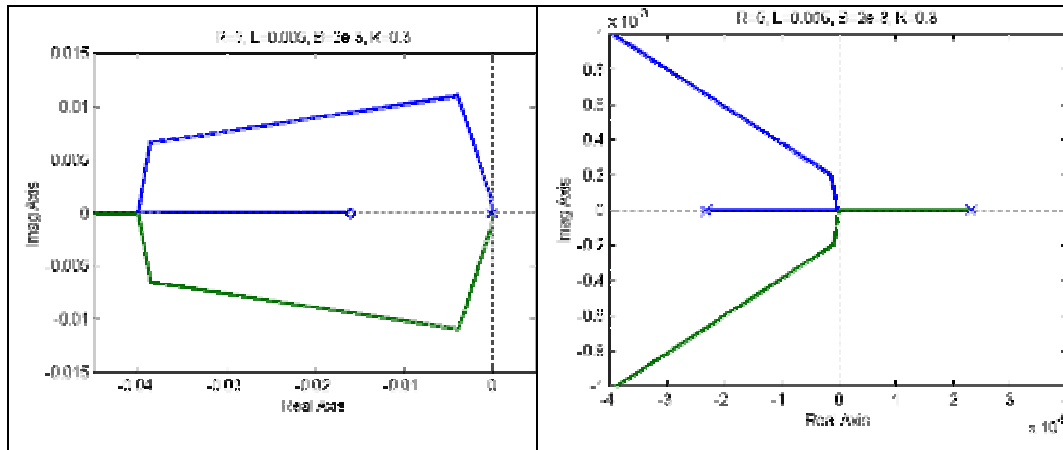


**Figure 24 Zoomed sections of Figure 23**

Actuator poles are at,  $s_1=-999.86$  and  $s_2=-0.16059$  and the zero is at  $z=-1.6057 \cdot 10^{-2}$ . The actuator itself is stable with relatively fast dynamics in comparison with satellite attitude dynamics whose unstable poles are placed at  $s_{1,2}=\pm 2.3031 \cdot 10^{-5}$ . Figures 23 and 24 are the overall closed loop rootlocus diagrams with PD controller zero at  $-20$  ( $-K_p/K_d$  zero location for controller,  $K_p=50$ ,  $K_d=2.5$  is found appropriate after several trials on Simulink model).

### 5.1.3 PD Controller Design: Tuning the Parameters

From the Rootlocus analysis the most appropriate location for the zero defined by the PD controller ( $K_p + K_d \cdot s$ ) is between the actuator most right pole and the most left pole. This configuration gives a stable pitch behaviour.

Also with the help of NCD (Nonlinear Control Design) optimisation built-in-block of Simulink, a neutrally stable configuration can be obtained. This design is later refined by tuning the gains of the PD controller. After several such trial and error study,  $K_p \geq 50$  and  $K_d \approx 2.5$  is found satisfactory to keep the satellite's maximum controlled pitch attitude for expected disturbances between  $0.8336 \pm 0.05^\circ$ . Lesser  $K_p$  values result in single overshoot at initial seconds to initial position errors, whereas higher  $K_d$  requires higher  $K_p$  which both multiplies the measurement

errors. Also higher  $K_d$  may result in several oscillations before settling around the nominal angle.

Solar radiation pressure disturbance is also successfully suppressed by the above selection of  $K_p$ , and  $K_d$  control variables. The control system short term response to both positive and negative biases around nominal settling angle and long term response to solar radiation are represented through Figures 31-35.

Measurement process is assumed to be noisy hence 'Band Limited White Noise' blocks are added to system outputs (Roll angle and rate). The magnitude of the measurement error is assumed to be on the order of maximum ( $\pm 0.00005^\circ$  and  $\pm 0.00001$  °/s).

As a result PD controller with ( $K_p=50$ ,  $K_d=2.5$ ) gains can damp  $\pm 0.1^\circ$  bias from nominal without any overshoot and dangerous oscillations. Also this selection is satisfactory to suppress solar radiation cyclic disturbances and can reject the random measurement errors of about ( $\pm 0.00005^\circ$  and  $\pm 0.00001$  °/s). These gains are also experimented with the final nonlinear model and are found satisfactory.

#### 5.1.4 Simulink Program for the Simulation of the Linear Pitch Dynamics Model, together with the Controller

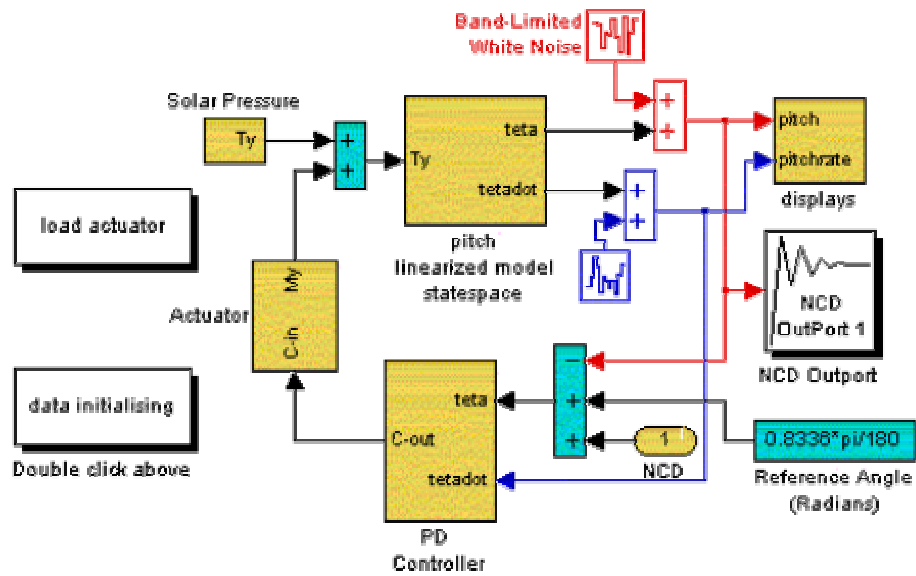


Figure 25 The main Simulink model for control of linearised pitch dynamics

The yellow blocks are the sub-systems represented at Figures 26-30.

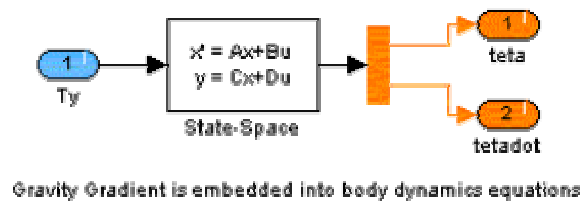


Figure 26 Linearised state space representation of pitch dynamics

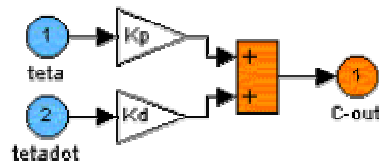


Figure 27 PD controller

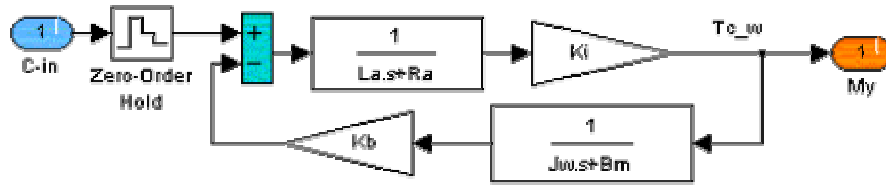


Figure 28 Second order DC motor (actuator) model

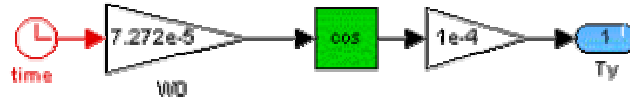


Figure 29 Solar radiation pressure disturbance model

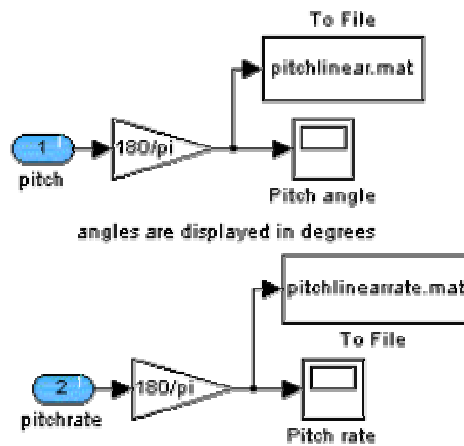
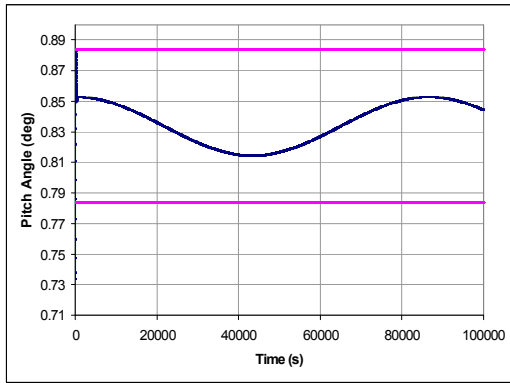


Figure 30 Data storage and displays model

### 5.1.5 Linear Simulation Results

Figures 31-35 show time histories of the controller's response to two different initial attitude bias angles and to external disturbance torque of solar pressure radiation and gravity gradient. Two cases for initial attitude bias are defined as follows:

CASE 1  $\theta_0=0.8336-0.1^\circ$  and CASE 2  $\theta_0=0.8336+0.1^\circ$ . Figures 31 and 33 are simulations for CASE 1, Figures 34, 35 are for CASE 2.



**Figure 31 Pitch attitude long-term response for CASE 1**

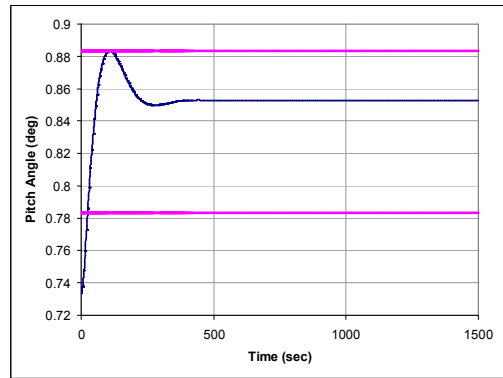


**Figure 32 Pitch attitude zoomed (0-1500 sec) response for CASE 1**

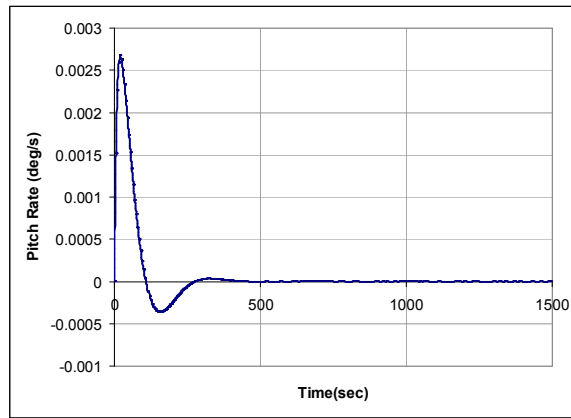


**Figure 33 Pitch rate zoomed (0-1500 sec) response for CASE 1**

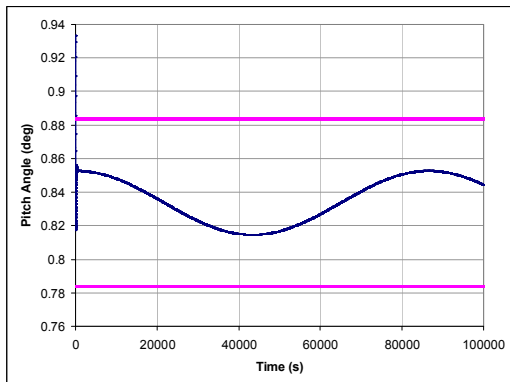


**Figure 34 Pitch attitude long-term response for CASE 2**

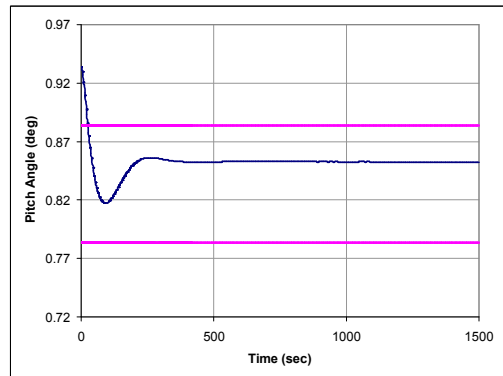


**Figure 35 Pitch attitude zoomed (0-1500 sec) response for CASE 2**

The selected gains ( $K_p=50$ ,  $K_d=2.5$ ) for the pitch controller can suppress both long-term solar radiation disturbance and short term initial attitude bias successfully. Also below Figure 36 shows that the actuator is not saturated with this selection of control gains. The produced torque is not very high to saturate the actuator.

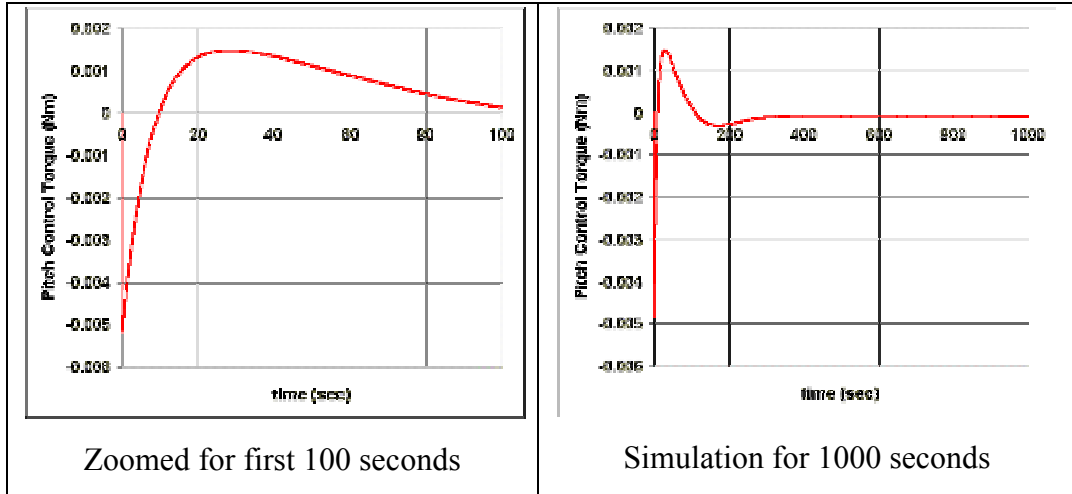


**Figure 36 Pitch actuator output torque**

## 5.2 Roll/Yaw Control System Design

The Roll/Yaw coupled equations of motion are linearised in Appendix B. The eigenvalues analysis in Appendix B shows that, the uncontrolled system is marginally stable with relatively low frequencies. (Both the roll and yaw have imaginary poles with no real parts). Since the actuators are the thrusters, they shall be modelled as nonlinear on-off type modulators for Simulink model. This introduces nonlinearity to the simulation, which requires careful design. After presenting the respective motion equations required for satellite body dynamic model, control law development, and actuator implementation are discussed. Finally the control parameter tuning for best control with fuel minimisation in mind, is presented.

## 5.2.1 Linearised Equations Of Roll/Yaw Coupled Motion

Equation (5.4) represents the roll/yaw coupled linear attitude dynamics.

$$0 = \begin{bmatrix} 3770 & 0 \\ 0 & 4020 \end{bmatrix} \begin{bmatrix} \ddot{\phi} \\ \ddot{\psi} \end{bmatrix} + \begin{bmatrix} 0 & 60.1604 \\ -60.0091 & 0 \end{bmatrix} \begin{bmatrix} \dot{\phi} \\ \dot{\psi} \end{bmatrix} + \begin{bmatrix} -1.37 \cdot 10^{-3} & 0 \\ 0 & -1.36 \cdot 10^{-3} \end{bmatrix} \begin{bmatrix} \phi \\ \psi \end{bmatrix} \quad (5.4)$$

This equation can be put into state space formulation, which is used in Simulink model more conveniently.  $\dot{\mathbf{X}} = \mathbf{A} \mathbf{X} + \mathbf{B} u$  and the output equation in form  $y = \mathbf{C} \mathbf{X} + \mathbf{D} u$ .

This time since the motion is coupled, matrix dimensions are increased. The states are defined as  $X_1 = \phi$ ,  $X_2 = \psi$ ,  $X_3 = \dot{\phi}$ ,  $X_4 = \dot{\psi}$ . Then the respective  $\mathbf{A}$ ,  $\mathbf{B}$ ,  $\mathbf{C}$ ,  $\mathbf{D}$  matrices are as follows:

$$\mathbf{A} = \begin{bmatrix} 0 & 0 & 1 & 0 \\ 0 & 0 & 0 & 1 \\ 3.6342 \cdot 10^{-7} & 0 & 0 & -1.595767 \cdot 10^{-2} \\ 0 & 3.3911 \cdot 10^{-7} & 1.49276 \cdot 10^{-2} & 0 \end{bmatrix} \quad (5.5)$$

$$\mathbf{B} = \begin{bmatrix} 0 \\ 0 \\ 2.6525 \cdot 10^{-4} \\ 0.3 \times 2.4876 \cdot 10^{-4} \end{bmatrix} \quad (5.6)$$

Here we again aim to design a controller which needs all the states' information, hence the output relation becomes,  $\mathbf{C} = 4 \times 4$  unity matrix and  $\mathbf{D} = [0 \ 0 \ 0 \ 0]$ .

The B matrix is 1x4 vector. We selected the thruster similar of TÜRK SAT 1B which also have "canted" set of roll/yaw thrusters. That is 'roll' thruster firing also accompanied by a yaw torque due to the alignment of the thruster with respect to

satellite frames. The degree of thruster coupling is selected to be 0.3 after several controller designs for various thrust coupling levels. Thus, 1Nm torque in the roll axis causes 0.3 Nm torque in the yaw axis. This value is also close to that of actual TÜRKSAT 1B configuration.

### 5.2.2 Controller Design for Coupled Linear Roll/Yaw Dynamics

Since the body dynamics are coupled even in the linearised equations we best make use of modern control methods. The uncontrolled system is marginally stable, hence control law shall not only track the zero input but also stabilise the overall system. That is overall system poles shall be at the left-hand side of the s-plane, or in other words we shall have the system eigenvalues with negative real parts. The imaginary parts impose oscillation to the system, which shall be minimised as well.

The uncontrolled system's eigenvalues for roll/yaw dynamics were computed in Appendix B,

$$\lambda_{(3,4)}=0 \pm 1.5422 \cdot 10^{-2} i \quad \text{and} \quad \lambda_{(5,6)}=0 \pm 2.2764 \cdot 10^{-5} i \quad (5.7 \text{ a,b})$$

Natural oscillations of the linear system seems relatively small enough, hence changing the order of magnitudes is not a necessity while designing the state feedback controller.

The methodology for servo system design can be found in many feedback control books. A general figure of a state feedback with integral control system is as follows [31],

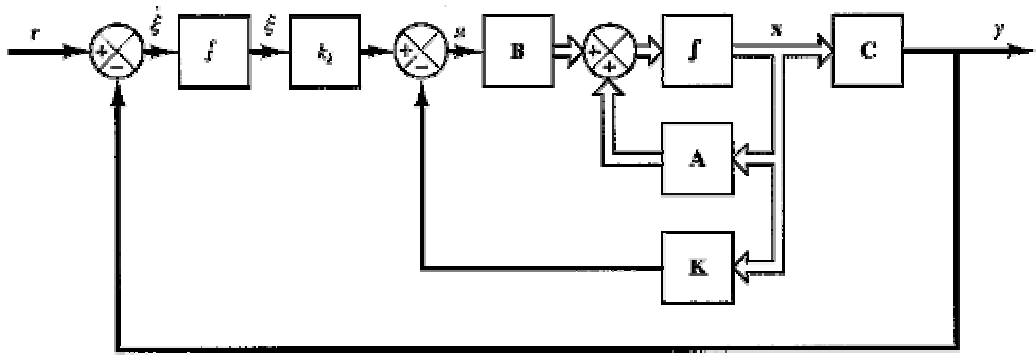


**Figure 37 Generic integral plus state variable feedback attitude control system**

From the diagram we can deduce:

$$\dot{\mathbf{X}} = \mathbf{A} \mathbf{X} + \mathbf{B} u \quad (5.8 a)$$

$$y = \mathbf{C} \mathbf{X} + \mathbf{D} u \quad (5.8 b)$$

$$u = -\mathbf{K}\mathbf{X} + K_i \xi \quad (5.8 c)$$

$$\dot{\xi} = r - y = r - \mathbf{C}\mathbf{X} \quad (5.8 c)$$

where  $u = \mathbf{T}x$ ,  $\xi$  is the output of the integrator (additional state variable),  $r$  is the reference input signal (zero for regulation),  $\mathbf{K}$  is the state feedback gain matrix,  $K_i$  is the integral gain, and matrices  $\mathbf{A}$ ,  $\mathbf{B}$ ,  $\mathbf{C}$ ,  $\mathbf{D}$  are as defined before.

The new closed loop system can be represented as:

$$\begin{bmatrix} \dot{\mathbf{X}}(t) \\ \dot{\xi}(t) \end{bmatrix} = \begin{bmatrix} \mathbf{A} & \mathbf{0} \\ -\mathbf{C} & 0 \end{bmatrix} \begin{bmatrix} \mathbf{X}(t) \\ \xi(t) \end{bmatrix} + \begin{bmatrix} \mathbf{B} \\ 0 \end{bmatrix} u(t) + \begin{bmatrix} \mathbf{0} \\ 1 \end{bmatrix} r(t) \quad (5.9)$$

defining  $u_e(t) = -\mathbf{K}\mathbf{X}_e(t) + K_i \xi_e(t)$  we can rewrite above equation as:

$$\begin{bmatrix} \dot{\mathbf{X}}_e(t) \\ \dot{\xi}_e(t) \end{bmatrix} = \begin{bmatrix} \mathbf{A} & \mathbf{0} \\ -\mathbf{C} & 0 \end{bmatrix} \begin{bmatrix} \mathbf{X}_e(t) \\ \xi_e(t) \end{bmatrix} + \begin{bmatrix} \mathbf{B} \\ 0 \end{bmatrix} u_e(t) \quad (5.10)$$

defining a new (4+1)<sup>th</sup> order state vector,

$$\mathbf{e}(t) = \begin{bmatrix} \mathbf{X}_e(t) \\ \xi_e(t) \end{bmatrix} \quad (5.11)$$

then the state equation becomes:

$$\dot{\mathbf{e}}(t) = \hat{\mathbf{A}} \mathbf{e} + \hat{\mathbf{B}} u_e \quad (5.12)$$

where

$$\hat{\mathbf{A}} = \begin{bmatrix} \mathbf{A} & \mathbf{0} \\ -\mathbf{C} & 0 \end{bmatrix}, \quad \hat{\mathbf{B}} = \begin{bmatrix} \mathbf{B} \\ 0 \end{bmatrix}, \quad (5.13 \text{ a,b})$$

$$\text{and } u_e = -\hat{\mathbf{K}} \mathbf{e} \quad (5.14)$$

where

$$\hat{\mathbf{K}} = [\mathbf{K} \quad -K_i] \quad (5.15)$$

The basic idea of designing a servo controller is to design a stable (n+1)<sup>th</sup> order regulator system that brings the new error vector  $\mathbf{e}(t)$  to zero.

A Matlab program is prepared for the determination of the state feedback gains and the integral control gain. The program uses Ackermann's formula for pole placement. [31] First the state equations are defined, then the system controllability check is done. Next the desired pole locations for closed loop system is entered finally by Ackermann's formulation the control gains are determined. The Matlab m file for these operations is listed below:

```
%Roll/Yaw system matrices are
```

```

a=[0 0 1 0; 0 0 0 1; 3.6342e-7 0 0 -1.595767e-2; 0
3.39113e-7 1.492764e-2 0];
b=[0 ; 0; 2.6525e-4; 0.3*2.4876e-4];
c=[1 0 0 0];
d=[0];

%enter the new state representation for output feedback

A1=[a zeros(4,1); -c 0];

B1=[b;0];

% define controllability matrix M

M=[B1 A1*B1 A1^2*B1 A1^3*B1 A1^4*B1];
rank(M)

disp('if rank is of order 5 then the system is
controllable')

% rank(M)=5,

% Hence arbitrary pole placement is possible
% This m file uses Ackermann's formula

% system eigenvalues: (eig(A1))=
%
%          0
% 3.4746e-018 +1.5411e-002i
% 3.4746e-018 -1.5411e-002i
% -5.1388e-021 +2.2779e-005i
% -5.1388e-021 -2.2779e-005i

%enter the desired characteristic polynomial by defining
%the following matrix J and computing poly(J)

J=[-0.004-0.0015*i 0 0 0 0;
0 -0.004+0.0015*i 0 0 0;
0 0 -0.0001-(1e-5)*i 0 0;
0 0 0 -0.0001+(1e-5)*i 0;
0 0 0 0 -4.5];

Ja=poly(J); roots(Ja)

% enter the characteristic polynomial PHI

phi=polyvalm(Ja, A1);

% the statefeedback gain matrix K and integral gain
constant Ki are:

KK=[0 0 0 0 1]*(inv(M))*phi

K1=KK(1), K2=KK(2), K3=KK(3), K4=KK(4), Ki=KK(5),

```

```

% KK = -6.5710e+001    3.8203e+000    1.2144e+004
1.7247e+004    9.2214e-003

```

Above program also checks for the system controllability. First the controllability  $M$  matrix is defined with the new system and input matrices.

$$\mathbf{M} = [\mathbf{B1} \quad \mathbf{A1} * \mathbf{B1} \quad \mathbf{A1}^2 * \mathbf{B1} \quad \mathbf{A1}^3 * \mathbf{B1} \quad \mathbf{A1}^4 * \mathbf{B1}] \quad (5.16)$$

The original system matrix  $\mathbf{A}$  is of order 4 and the modified system matrix  $\mathbf{A1}$  is of order 5, hence rank of the controllability matrix shall be 5 for controllability. Above Matlab program's run shows that the system is controllable with the state variable feedback plus integral controller.

The obtained control gains depend on the closed loop poles defined by  $\mathbf{J}_a$  matrix in the program. Best feedback gain configuration can be determined by comparing responses of several designs.

### 5.2.3 Thruster Model

Before going into details of feedback controller design we would better define thruster model. As the yaw/roll actuator TÜRKSAT 1B uses on-off thrusters. One alternative could be the proportional thrusters, which are very difficult to built and subject to extreme strict operation conditions. They usually have large amount of hysteresis. Furthermore proportional gas jets need to open a small amount to produce the small torques required for control. As a result, dirt and ice particles tend to stick in the valve openings. They do not shut down properly, causing continuous gas leak to produce internal disturbance torque and consuming fuel rapidly. Therefore most appropriate thruster selection will be the bang-bang or on-off type. The valves are either completely closed or open for a controlled period of time. Large springs may be used to hold valves shut, thereby reducing leakage; the closing "bang" jars loosen any ice or dirt particles as well. [26] & [30]

On-off valves can be operated to stay open as little as a few milliseconds and can be operated over a million times reliably. The valves stay open for a finite length of time causing a discrete angular velocity change with each firing. To prevent opposing gas jets from fighting each other, there must be a deadband- a finite interval for off state. This in addition helps for fuel economy. [26]

Here we used a Pulse Width Modulation technique to simulate the actuator operation. The sampled control signal integral is equated to the actuator firing magnitude times the operation time. Hence for each sample of control input signal to actuator, it produces different pulses. This behaviour is shown by Figure 37.

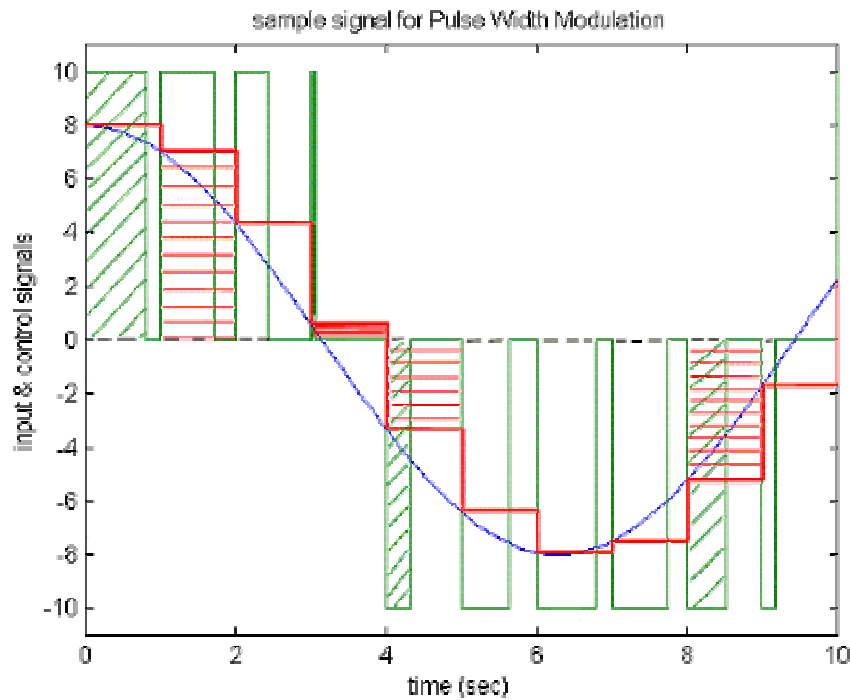


**Figure 38 PWM sample signal**

Green pulses with  $\pm 10$  magnitude are the output signals, red signal is the sampled input signal, and blue curve is the continuous input cosine wave. Details of this block can be seen on definitions of nonlinear Simulink model (Figures 67 and 68).

## 5.2.4 Simulink Roll/Yaw Control Model

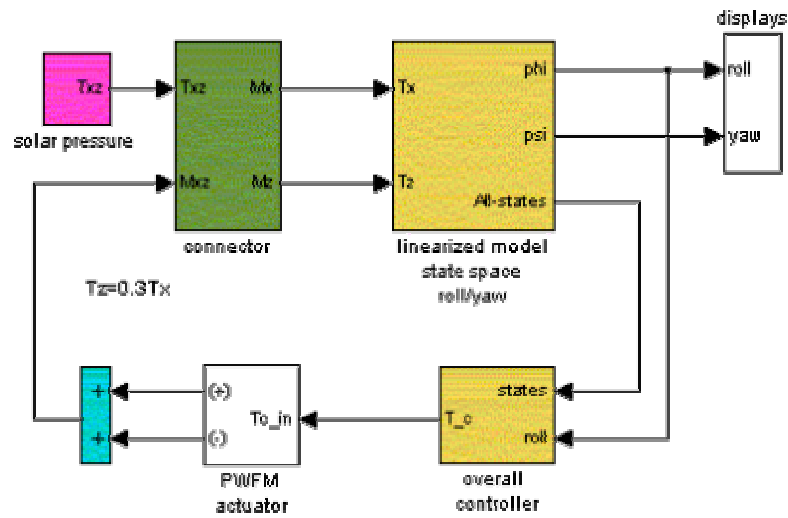


**Figure 39 Main roll/yaw control block diagram**

The main program is shown in Figure 39. Each sub-block is expanded in Figures 40-46. The integration method is set to variable step (ode23tb [stiff/TR-BDF2]) with relative tolerance  $10^{-5}$  to have fast and accurate numerical integration. Fixed step integration methods does not speed up the simulation, additionally setting appropriate step size is another problem. Larger step sizes, although speeds up the simulation, lacks accuracy to yield acceptable results. Hence best is to apply variable step size methods.

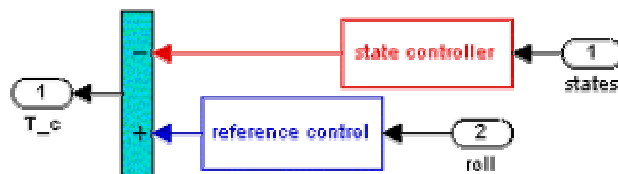


**Figure 40 Masked controller sub-block diagrams**

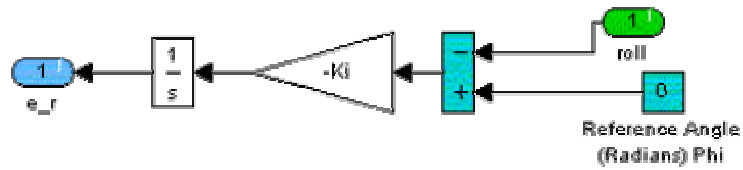


**Figure 41 Integral control and reference input (inside mask)**

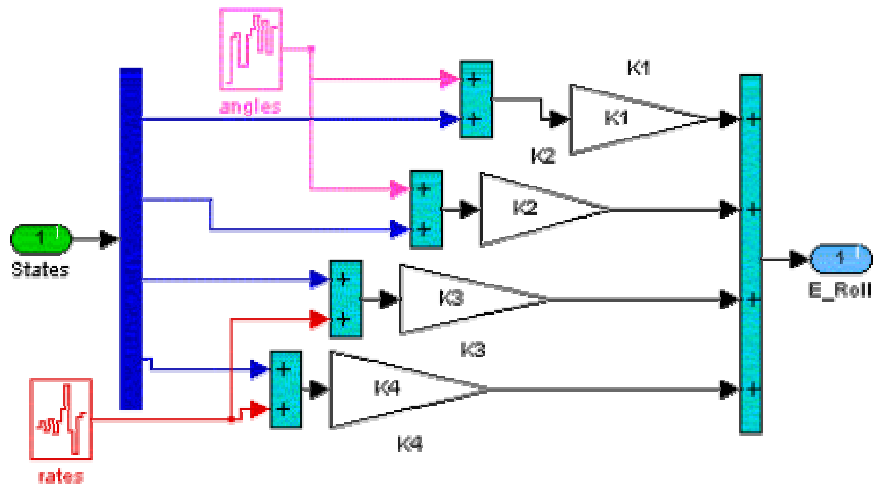
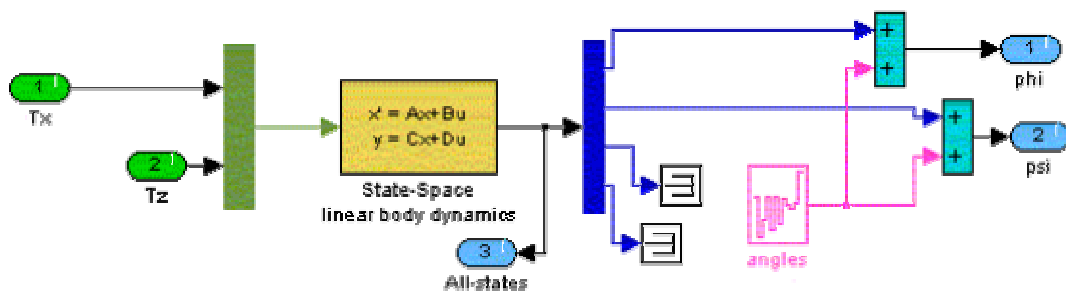


**Figure 42 State variable feedback controller (inside mask)**

Figures 40 and 42 show the controller gain and respective signal links. The white noise blocks producing random disturbance into measured attitude and rate signals represent measurement noise. Since we want the roll/yaw attitudes regulate about origin a zero constant block sets the reference-input signal. The controller gains are left as  $K_1$ - $K_4$  and  $K_i$  symbols to manipulate them easily both from workspace and from mask dialog boxes.



Solar Pressure Gradient is embedded into body dynamics equations  
Initial states: Roll, Pitch, Yaw Angles are not zero

**Figure 43 Satellite roll/yaw linear body dynamics in state space**

Satellite dynamics are represented via state-space formulation. However the actual output **C** and **D** matrices are modified to get all the state signals as outputs. Remember that all the states are measurable physical variables - angular rates and attitudes. For poleplacement design of feedback control, we used only the roll attitude direct measurement, to enable future studies with identical pole locations. Furthermore the **B** matrix is modified to enable two distinct torque effects on roll/yaw frames. Setting **B** to 2x4 matrix we can input the solar perturbation in z direction explicitly. Controllability is checked with the previously stated Matlab program list, and rank is found to be 5, which indicates controllable system. The overall system matrices inside above block of Figure 43 are:

**A**=4x4 system matrix with no alterations

**B**=[0 0; 0 0; 2.6525e-4 0; 0 2.4876e-4]

**C**=4x4 identity matrix

**D**=4x2 zero matrix

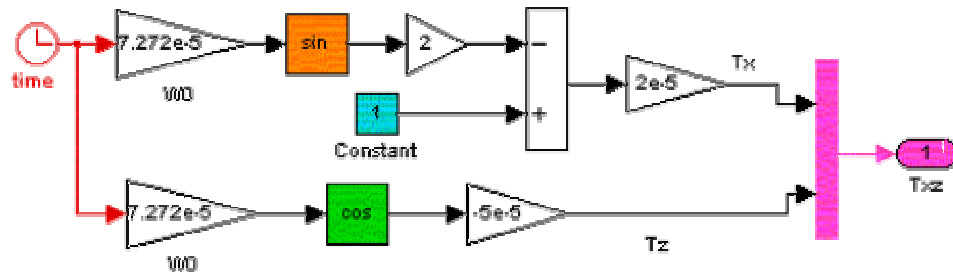


**Figure 44 Solar disturbance torque**

Pitch component is eliminated from the model representing the solar radiation disturbance.

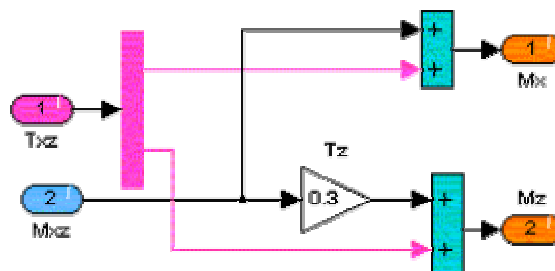


**Figure 45 Connector for disturbance and control torques**

To account for canted thruster yaw thrust effect is taken as,  $T_z=0.3 T_x$  as seen in Figure 45.

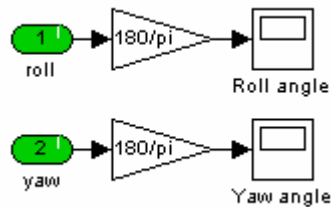


**Figure 46 Displays in degrees unit**

### 5.2.5 Linear Simulation Results with Fuel Consumption Minimising

Linear model is used to test various pole placement designs ensuring stable dynamics configurations in terms of transient and steady state performance. Among the determined pole locations satisfying these short and long term performance criteria, the most appropriate pole location minimizing fuel expenditure (=minimum control effort) is to be determined.

First the unmodulated feedback control is designed to determine the poles for transient and steady state performance. Hence it is assumed proportional gas jets are used as actuator. Various pole locations are picked and are tested, some results are shown in Tables 6-14. And the following set yielded acceptable performance. The simulations are run for 200,000 seconds. Total control effort is simply the integral of the control signal in absolute values. It is in direct relation with fuel consumption. Hence it is tried to find the most appropriate pole location to minimise the total control effort.

**Table 6 Pole placement Case 1**

Closed loop Poles @	-4.5	$-4 \cdot 10^{-3} \pm 1.5 \cdot 10^{-3}i$	$-10^{-4} \pm 10^{-5}i$	
Control Gains	$-6.5710 \cdot 10^1$	3.8203	$1.2144 \cdot 10^4$	$1.7247 \cdot 10^4$   $9.2214 \cdot 10^{-3}$
Roll limits	0.0456 °	-0.0455 °	Total Control Effort:	13.447
Yaw limits	1.865 °	-1.39 °		

**Table 7 Pole placement Case 2**

Closed loop Poles @	-5.5	$-5 \cdot 10^{-3} \pm 1.5 \cdot 10^{-3}i$	$-10^{-4} \pm 10^{-5}i$	
Control Gains	$-1.186 \cdot 10^2$	6.5853	$1.3463 \cdot 10^4$	$2.5986 \cdot 10^4$   $1.6829 \cdot 10^{-2}$
Roll limits	0.0425 °	-0.042 °	Total Control Effort:	13.584
Yaw limits	1.86 °	-1.4 °		

**Table 8 Pole placement Case 3**

Closed loop Poles @	-6.5	$-6 \cdot 10^{-3} \pm 1.5 \cdot 10^{-3}i$	$-10^{-4} \pm 10^{-5}i$	
Control Gains	$-1.9513 \cdot 10^2$	10.506	$1.4114 \cdot 10^4$	$3.7097 \cdot 10^4$   $2.7918 \cdot 10^{-2}$
Roll limits	0.0405 °	-0.0405 °	Total Control Effort:	13.7617
Yaw limits	1.86 °	-1.4 °		

**Table 9 Pole placement Case 4**

Closed loop Poles @	-8.5	$-8.5 \cdot 10^{-3} \pm 1 \cdot 10^{-3}i$	$-10^{-4} \pm 10^{-5}i$	
Control Gains	$-4.8253 \cdot 10^2$	24.889	$1.1774 \cdot 10^4$	$7.2279 \cdot 10^4$   $6.9911 \cdot 10^{-2}$
Roll limits	0.0381 °	-0.0405 °	Total Control Effort:	14.3079
Yaw limits	1.8534 °	-1.38 °		

**Table 10 Pole placement Case 5**

Closed loop Poles @	-10	$-10^{-2} \pm 1 \cdot 10^{-3}i$	$-10^{-4} \pm 10^{-5}i$	
Control Gains	$-7.7862 \cdot 10^2$	39.534	$8.2675 \cdot 10^4$	$1.0488 \cdot 10^5$   $1.1341 \cdot 10^{-1}$
Roll limits	0.0372 °	-0.0372 °	Total Control Effort:	14.7143
Yaw limits	1.8449 °	-1.3718 °		

**Table 11 Pole placement Case 6**

Closed loop Poles @	-4	$-3.510^{-3} \pm 1 \cdot 10^{-3}i$	$-10^{-4} \pm 10^{-5}i$	
Control Gains	-42.991	2.6285	$\frac{1.1322}{10^4}$	$\frac{1.3453}{10^4}$   $\frac{5.9511}{10^{-3}}$
Roll limits	0.0493 °	-0.0491 °	Total Control Effort:	13.4124
Yaw limits	1.8733 °	-1.398 °		

**Table 12 Pole placement Case 7**

Closed loop Poles @	-8	$-3.510^{-3} \pm 1 \cdot 10^{-3}i$	$-10^{-4} \pm 10^{-5}i$	
Control Gains	-85.981	5.2559	$\frac{2.2605}{10^4}$	$\frac{2.6950}{10^4}$   $\frac{1.1902}{10^{-2}}$
Roll limits	0.0493 °	-0.0491 °	Total Control Effort:	13.5406
Yaw limits	1.8733 °	-1.398 °		

**Table 13 Pole placement Case 8**

Closed loop Poles @	-5	$-510^{-3} \pm 1 \cdot 10^{-3}i$	$-10^{-4} \pm 10^{-5}i$	
Control Gains	$\frac{-1.0315}{10^2}$	5.7663	$\frac{1.2323}{10^4}$	$\frac{2.3335}{10^4}$   $\frac{1.4597}{10^{-2}}$
Roll limits	0.043°	-0.043°	Total Control Effort:	13.5592
Yaw limits	1.8591°	-1.385°		

**Table 14 Pole placement Case 9**

Closed loop Poles @	-5	$-3.710^{-3} \pm 1 \cdot 10^{-3}i$	$-10^{-4} \pm 10^{-5}i$	
Control Gains	-59.354	3.5703	$\frac{1.3917}{10^4}$	$\frac{1.7636}{10^4}$   $\frac{8.2473}{10^{-3}}$
Roll limits	0.0481°	-0.043°	Total Control Effort:	13.4611
Yaw limits	1.8591°	-1.385°		

All above Cases in Tables 6-14 have satisfactory time response histories. Three of the above sample Cases can be visualised in Figure 47 for response comparisons. (Initial attitude errors are  $\Delta\phi_0 = -.1^\circ$  and  $\Delta\psi_0 = 0.09^\circ$ )

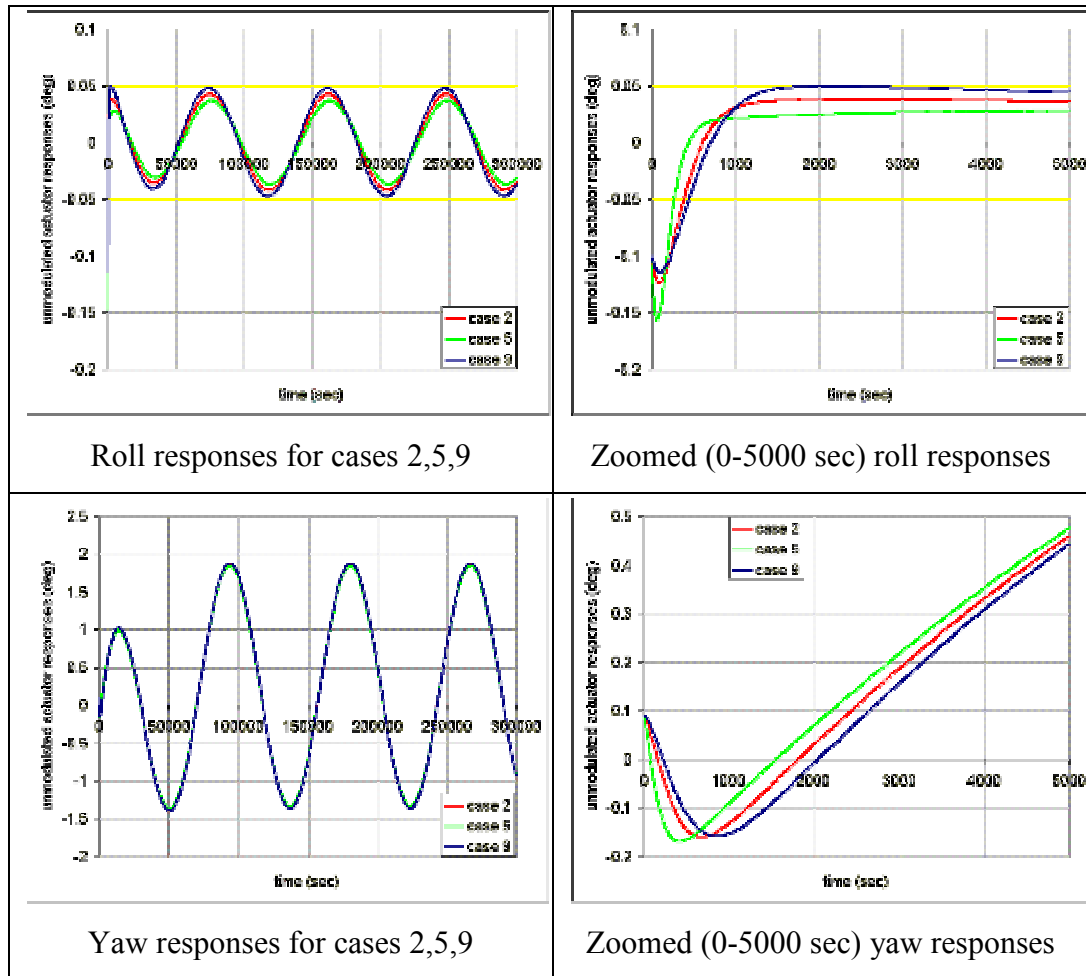


**Figure 47 Simulation results with unmodulated actuator for Cases 2, 5, and 9 of Tables 7, 10 and 14**

From above and many other observations we conclude that a pole placement that barely satisfies the transient and steady state requirements shall give minimum fuel consumption. However we shall keep in mind that on-off control is not a linear process hence relatively safe values shall be selected not to lose time response characteristics. Studying Tables 6 – 14 Case 1, Case 6, Case 8 and Case 9 are possible good candidates for modulated and nonlinear simulation, that satisfies transient and steady state response, and for fuel economy.

The system is controllable; hence poles can be placed anywhere on s-plane. Tables 6-14 shows several acceptable pole locations for proportional thruster controlled model All have satisfactory responses to external disturbances and initial attitude

bias of  $\pm 0.1^\circ$ . On the other hand the pole locations are not desirable to be more left-hand side than that of Tables 6-14 (faster pole assignment). Basic reason for that is faster the system, it is too hard to get the attitude within limits without fast oscillations. In summary pole assignments away from than the Tables 6-14 do not have satisfactory time histories, either have rapid oscillations or have continuous large overshoots about nominal attitude.

### 5.2.6 Linear Simulations with Pulse Width Modulated Actuator

Unlike proportional gas jet actuator model, pulse width modulated actuator generates pulse train. Hence computer simulations become sensitive to minimum and maximum step sizes of integration or activation. For non-modulated linear simulations it was possible to run the simulations long as 5-6 day periods, however for modulated simulations at most a quarter day simulation could be run, due to the computer memory and run-time restrictions.

In the modulated case, in addition to proper pole selection as before, proper sampling and thruster period are also important for fuel minimisation. Thruster activation period on the other hand is also critical to satisfy the transient response requirements. Thus we can not tolerate more than 0.05 degrees of deviation from nominal of zero degrees.

Among many trials of pole placement main observation is that, if the closed system is placed to relatively fast locations (more right hand side of s plane) it is harder to control the satellite with on-off actuators. The discrete actions of the thrusters excite fast oscillations for fast poles. Decreasing activation period somehow brings limited remedy, however overall fuel consumption is increased dramatically with small period and fast pole placement combination. Additionally since this combination requires too much of computer run-time and memory, it is not possible to simulate for long enough time to visualise long term response to solar radiation pressure.

On the other hand fast and relatively slow pole selections with long thruster periods is also tested. Selection of 10, 1, and 0.5 seconds of activation periods causes the satellite make large oscillations that forces the control signals to be enlarged. These large period selections consume too much fuel, also proper transient characteristics can not be obtained by these long period selections. Refer to Tables 6-14 and Figure 47 for unmodulated control simulations for selection of most appropriate pole assignment.

From the above experience in terms of fuel economy several tests are carried. Best illustrative results are listed at Table 15. Previously determined candidate pole locations are tested with candidate Pulse Width Modulator activation periods of 0.1, 0.25 and 0.4 seconds. The simulations are carried with  $\phi_0 = -0.1^\circ$  and  $\psi_0 = -0.09^\circ$  initial attitude angle errors. Table 15 and Figures 48-50 present these simulation results.

**Table 15 Parametric Search for Fuel Optimization**

<b>CASE 1</b>			<b>CASE 6</b>		
Period (sec)	Runtime	Net Control	Period (sec)	Runtime	Net Control
0.1	2000 sec	0.442854	0.1**	2000 sec	0.413818
0.25	2000 sec	0.457153	0.25**	2000 sec	0.417911
	5000 sec	0.909125		5000 sec	0.879415
0.4	2000 sec	0.759985	0.4**	2000 sec	0.593800
	5000 sec	1.318316		5000 sec	1.005206
<b>CASE 8</b>			<b>CASE 9</b>		
Period (sec)	Runtime	Net Control	Period (sec)	Runtime	Net Control
0.1 (NA)*	2000 sec	0.458948	<b>0.1</b>	2000 sec	<b>0.4206095</b>
0.25 (NA)*	2000 sec	0.496238	0.25	2000 sec	0.445752
	5000 sec	0.94694		5000 sec	0.91186
0.4 (NA)*	2000 sec	18386.47	0.4 (NA)*	2000 sec	<b>17476.03</b>
	5000 sec	49136.47	0.35	5000 sec	1.16481

\*NA means time response characteristics are not acceptable (very fast oscillations exist around nominal path).

\*\* System has a very small over shoot ( $\sim 0.0025^\circ$ ) between 1500-3000 seconds.

The above Table 15 indicates that the best selection will be the Case 9 with sampling period 0.1 second to provide minimum fuel expenditure. Even though Case 6 seems to have better fuel economy the long term modulated transient response is not preferable in comparison to Case 9. Further linear and nonlinear simulations use this selection of pole-placement design with optimised modulation period of 0.1 sec.

Figures 48-50 show respective time histories (0-5000 sec) of the four cases of Table 15. Case 9 and case 8 have almost same behaviour, however both are very sensitive to sampling period. Case 8 in any sampling period has very fast and small oscillations around its nominal path. Case 6 experiences noticeable overshoot, hence both case 6 and case 9 are not acceptable pole selections for modulated control. Linear simulation results in Figures 48-50 have the following initial conditions:  $\Delta\phi_0 = -0.1^\circ$ , and  $\Delta\psi_0 = 0.09^\circ$ .

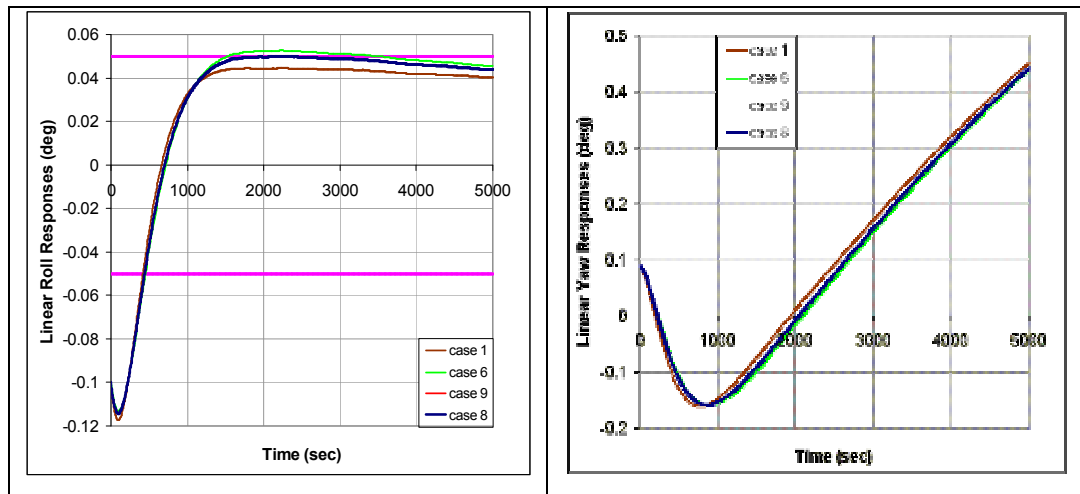


**Figure 48 Comparison of four cases of Table 15 with sampling period=0.1 sec**

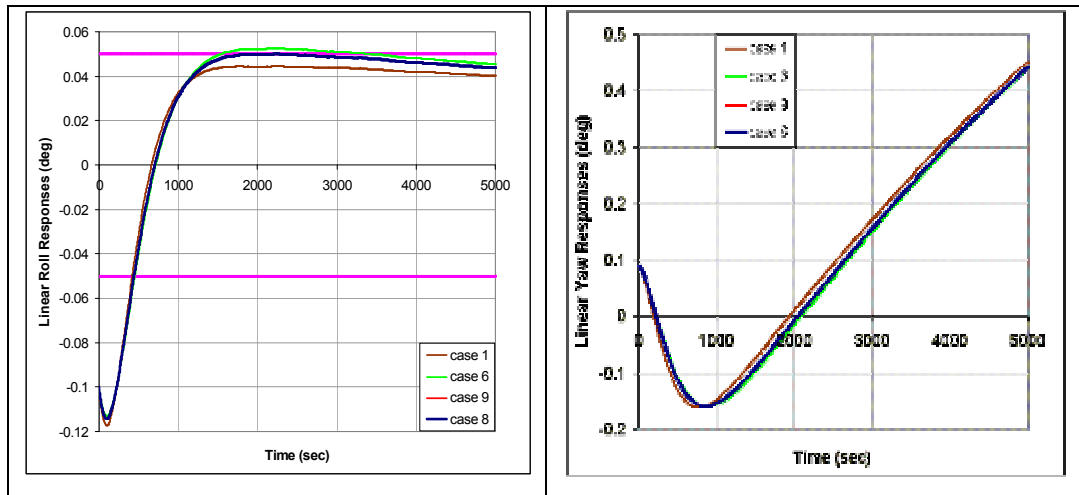


**Figure 49** Comparison of four cases of Table 15 with sampling period=0.25 sec

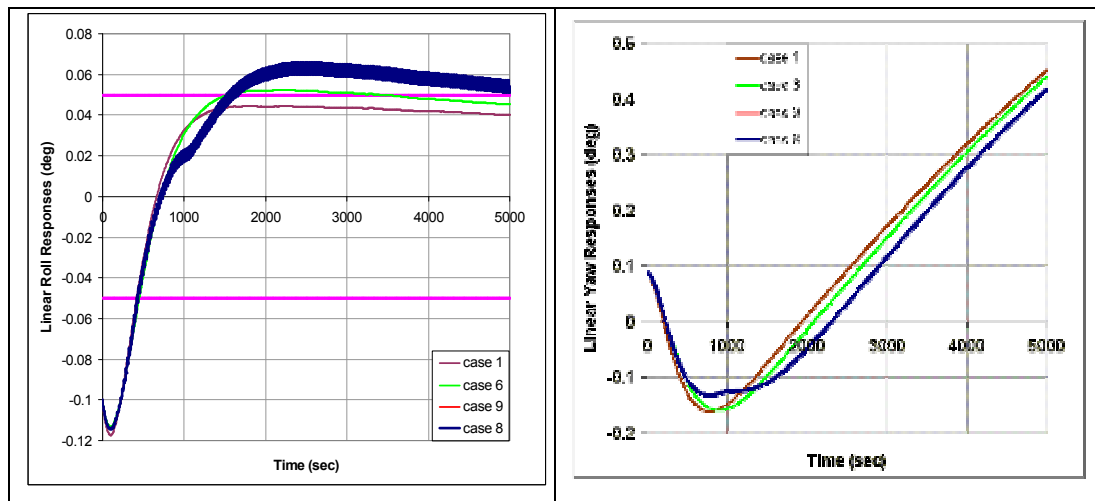


**Figure 50** Comparison of four cases of Table 15 with sampling period=0.4 sec

As noticed pulse width frequency modulation has dramatic effect on transient response characteristics. For the proportional thruster modelled simulations, relatively faster poles than that of Case 9 results in better (fast) control of satellite roll/yaw attitude. Fast pole placements to some limit have larger damping effect both for initial alignment error and for external disturbance torque in proportional thruster modelling. However application of a discrete modulation with fuel economy in consideration forced us to decide on relatively slow poles. Faster the modulated system poles are selected, the smaller the modulation-sampling period shall be. This is not feasible both for real actuators and for simulation capabilities of today's personal computers.

General result is that decreasing the sampling period is a means to reduce fuel expenditure. And poles just satisfying transient constraints shall accompany this minimum sampling period. Minimum sampling period is selected to be 0.1 sec., lesser periods are subject to saturation. Thrusters can be activated so small time as a few milliseconds. The thruster magnitude is very high comparing with proportional thruster model output, hence activation periods less than 0.1 seconds result in unreasonable small "on" times, which causes actual thrusters to produce more than the required torque, resulting in excessive fuel expenditure.

### **5.3 Nonlinear Simulation**

The feedback controllers are designed using linear body dynamics model in state space formulation. They are shown to be successful in linear models, however nonlinear model of the satellite best represents the real attitude behaviour. In this section we will test the optimised control system with nonlinear attitude model.

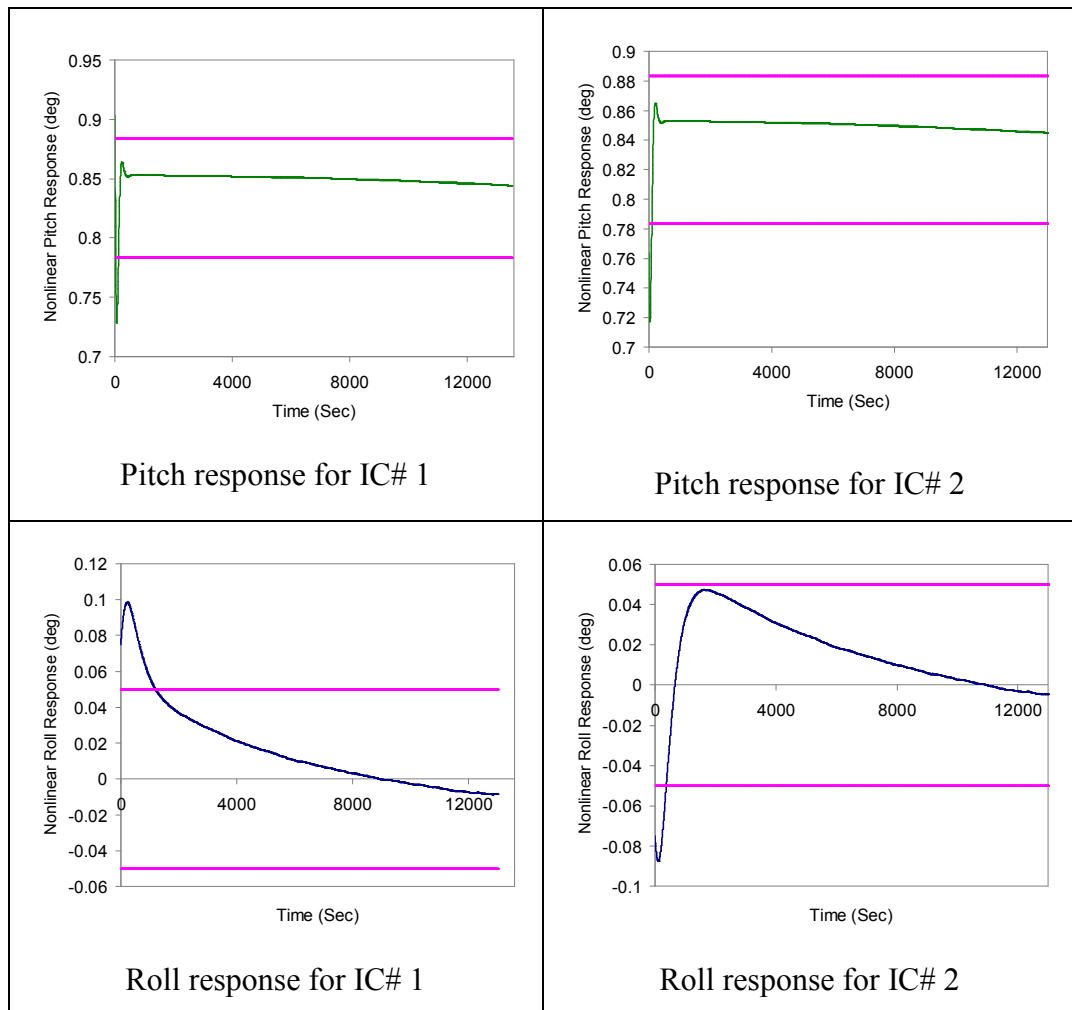
Two separate controllers are designed due to the uncoupled pitch motion equations in linear dynamics model. The nonlinear model on the other hand is fully coupled. This enables us to introduce thruster misalignment torque into pitch control output signal.  $10^{-5}$  Nm magnitude of internal perturbing torque is activated each time the roll thruster pair is at "on" state of pulse width modulation (PWM).

PWM with small periods (0.1 sec) slows down the linear model simulation, so that we could not have the long-term (1-5 days) simulations. Again this effect combining with nonlinear model's complexity, extremely slows down the computer simulation, and causes memory errors for long-term runs. Hence we again present the short-term responses. The proposed pitch PD Controller in combination with yaw/roll Servo Controller successfully suppresses the perturbations on satellite model. Especially pitch control dynamics is very fast in comparison to roll/yaw control.

### 5.3.1 Nonlinear System Responses with Controllers

Here we first present the simulation results showing satellite short-term response to above mentioned internal and external disturbing torques and to measurement errors. Then the nonlinear Simulink model is introduced with the controllers implemented. In comparison to the uncontrolled response presented in Appendix B, the controllers seem to be effective enough.

Figure 51 summarises pitch, roll, yaw responses of the controller with nonlinear model for 2 cases of initial attitude bias, and external/internal disturbances. First initial condition (IC# 1) has ( $\Delta\theta_0=-0.1^\circ$ ,  $\Delta\phi_0=+0.075^\circ$ ,  $\Delta\psi_0=-0.75^\circ$ ) attitude biases about nominal. The second initial condition (IC# 2) has ( $\Delta\theta_0=+0.1^\circ$ ,  $\Delta\phi_0=-0.075^\circ$ ,  $\Delta\psi_0=+0.75^\circ$ ) attitude biases about nominal.



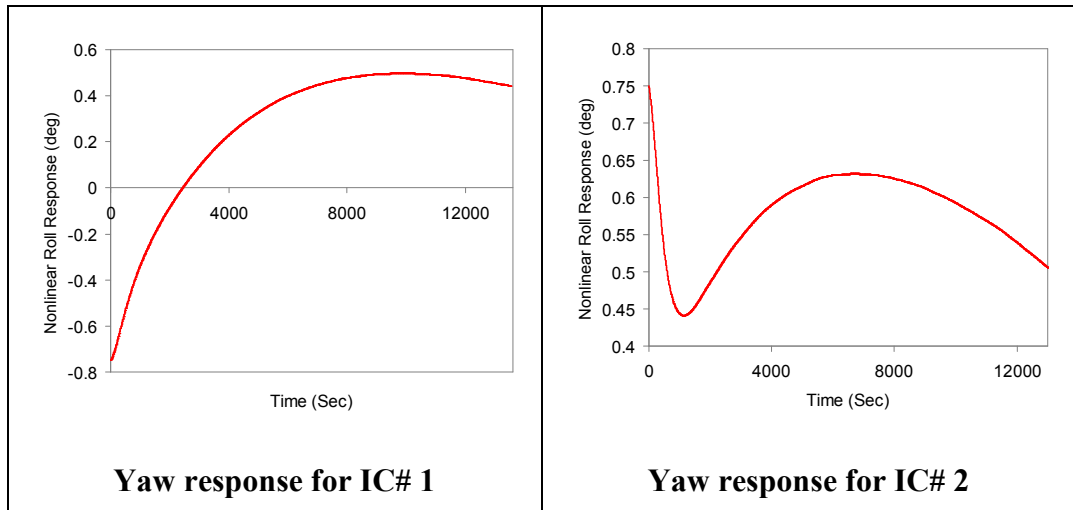


**Figure 51 Nonlinear simulation pitch-roll-yaw responses**

From several nonlinear simulations lasting for most to a quarter day, it may be concluded that the satellite attitude will be kept within requirements. The Roll/yaw controller is the one presented in Table 14, and the employed pitch controller is the one with gains ( $K_p=50$ ;  $K_d=2.5$ ).

Before going into detailed description of the nonlinear model with both controllers employed, linear and nonlinear simulation results are compared in Figures 52-54. It can easily be seen that nonlinear and linear responses are very similar.

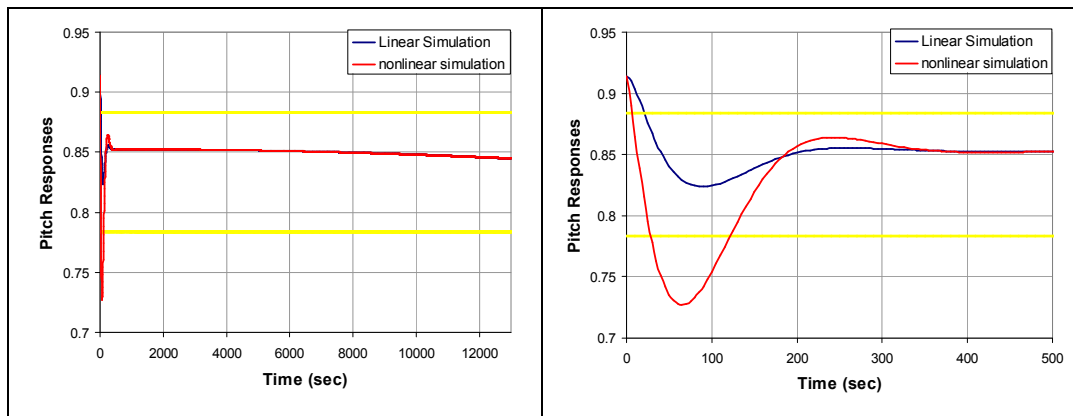


**Figure 52 Pitch response for 13000 sec and zoomed response for (0-500 sec)**

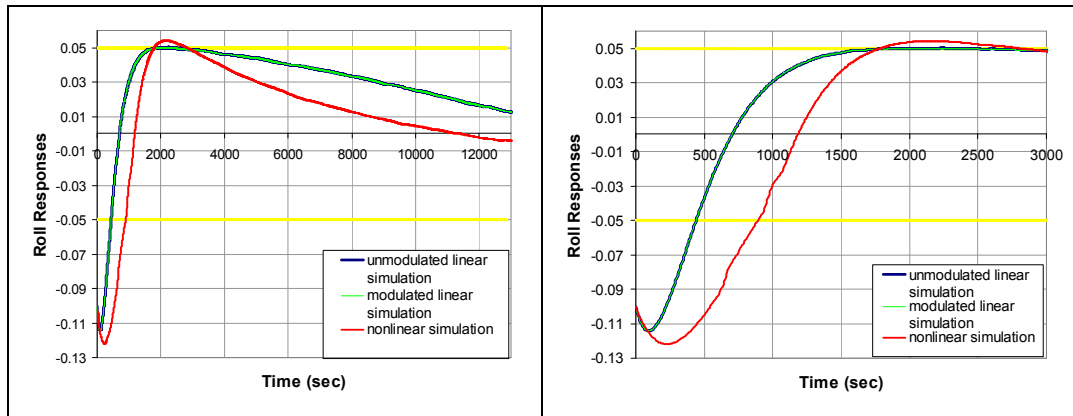


**Figure 53 Roll response for 13000 sec and zoomed response for (0-3000 sec)**

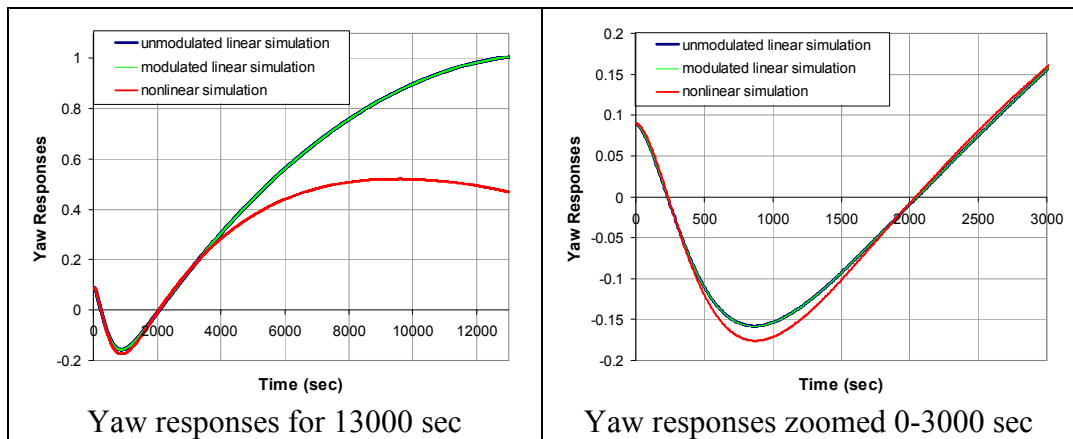


**Figure 54 Yaw response for 13000 sec and zoomed response for (0-3000 sec)**

As seen from Figures 52-54 linear modulated and unmodulated simulations have very close response characteristics. Nonlinear simulation on the other hand introduces small overshoots for pitch and roll controlled behaviour. Nonlinear pitch response can identically track the linear simulations' responses after 400 seconds showing that the pitch controller is very effective for both linear/nonlinear models. Roll/yaw responses; however have small deviations from linear simulation responses. 13000 seconds of simulations show that roll and yaw attitudes are kept within acceptable margins. Figures 52-54 are the simulation results in response to initial attitude errors of ( $\Delta\phi_0=-0.1^\circ$ ;  $\Delta\psi_0=0.09^\circ$ ;  $\Delta\theta_0=0.1^\circ$ ) from the nominal regulation values. Below figures show the thruster outputs, for comparison of saturated and correctly functioning actuator states.

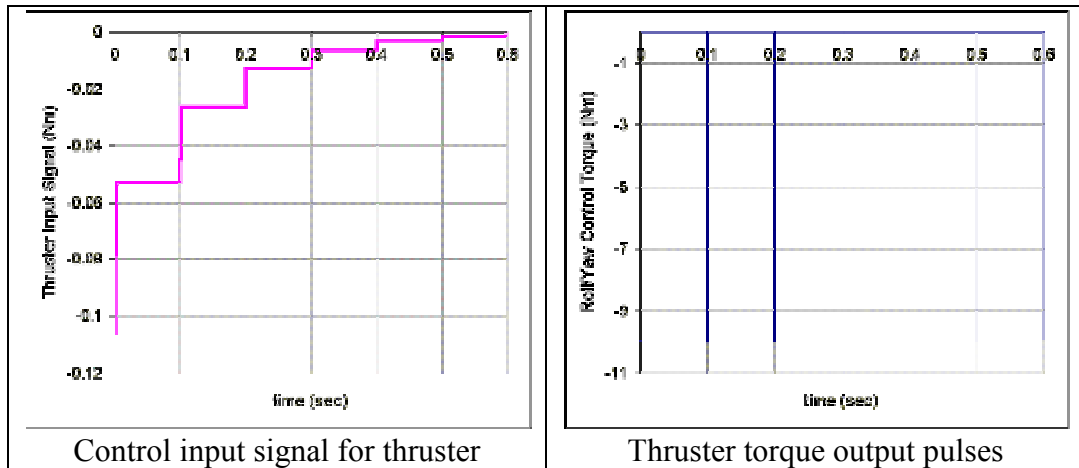


**Figure 55 Unsaturated thruster signals for pole placement design in Table 14 with 0.1 seconds of sampling and thruster activation period**

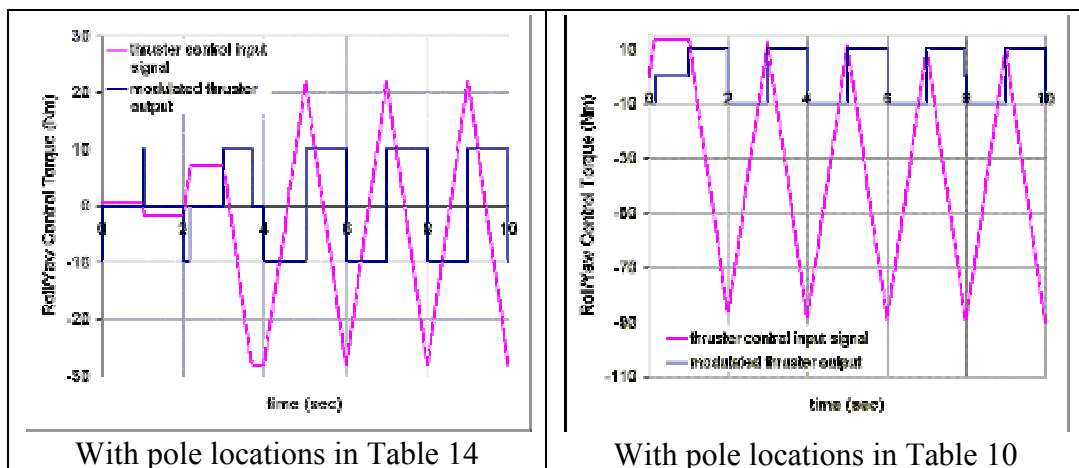


**Figure 56 Saturated thruster signals with 1 seconds of sampling and thruster activation period**

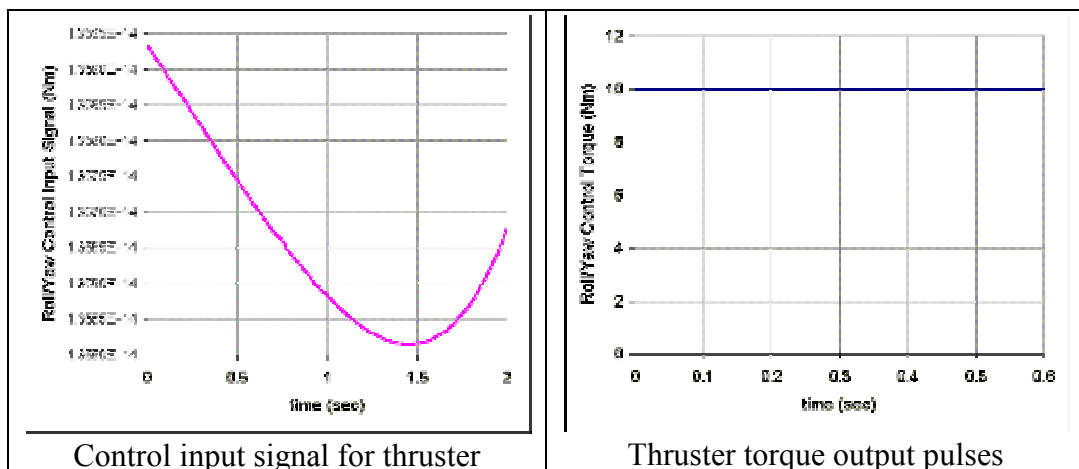


**Figure 57 Saturated thruster signals with 0.1 seconds of sampling and thruster activation period and with a very poor pole assignment**

Closed loop pole locations of Figure 57 are as follows:  $(-50; -3.7 \pm i; -1 \pm 0.1 i)$

### 5.3.2 Description of Nonlinear Simulink Model with Controllers

Below figures form the overall system of final simulation model:

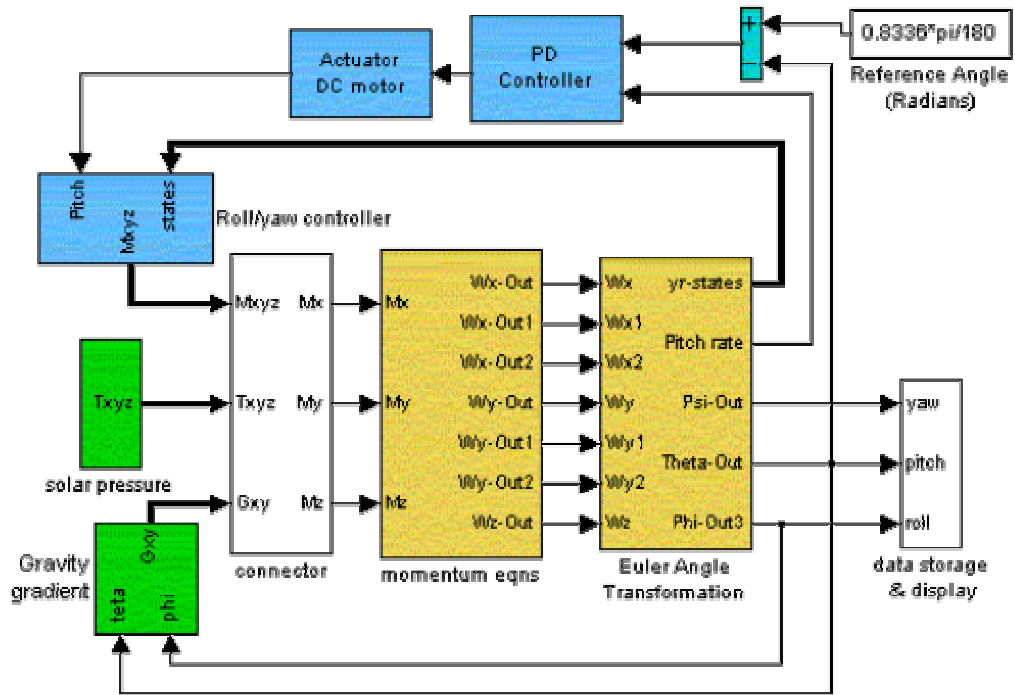


**Figure 58** The main block diagram for nonlinear model with both controllers employed

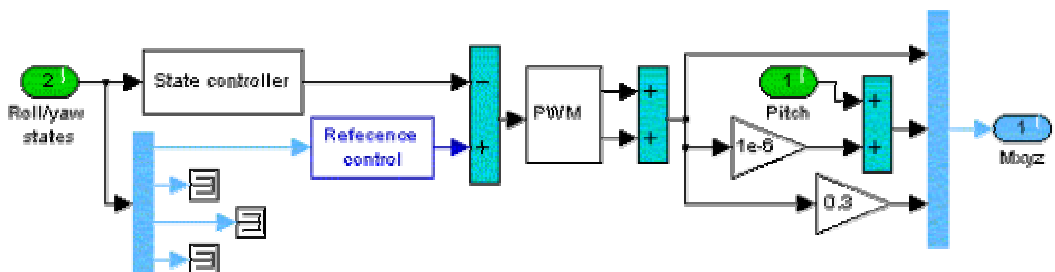


**Figure 59** Roll-yaw controller's block diagram

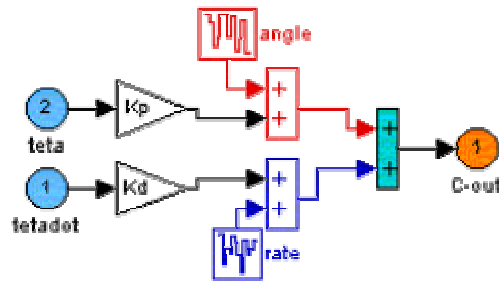


Figure 60 PD controller for pitch attitude regulation

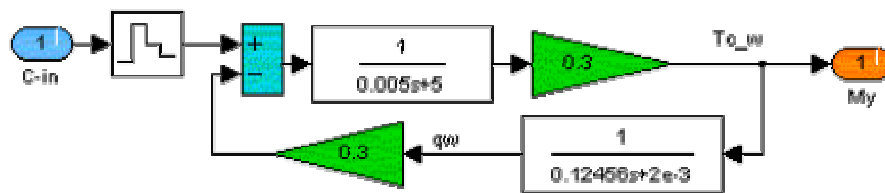


Figure 61 2<sup>nd</sup> order DC motor model

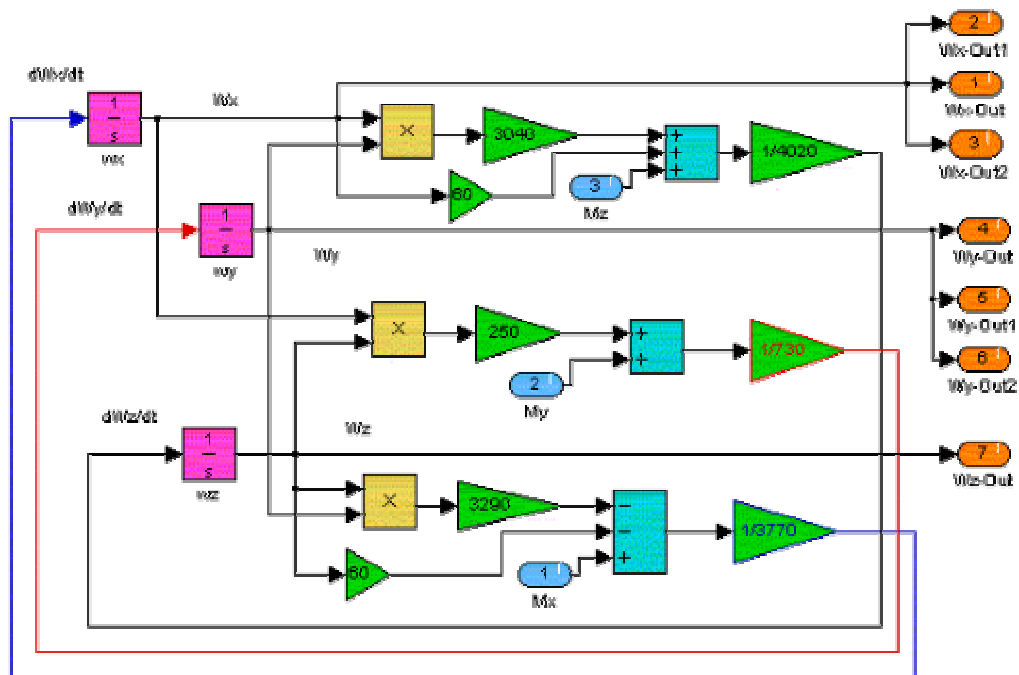


Figure 62 Momentum equations

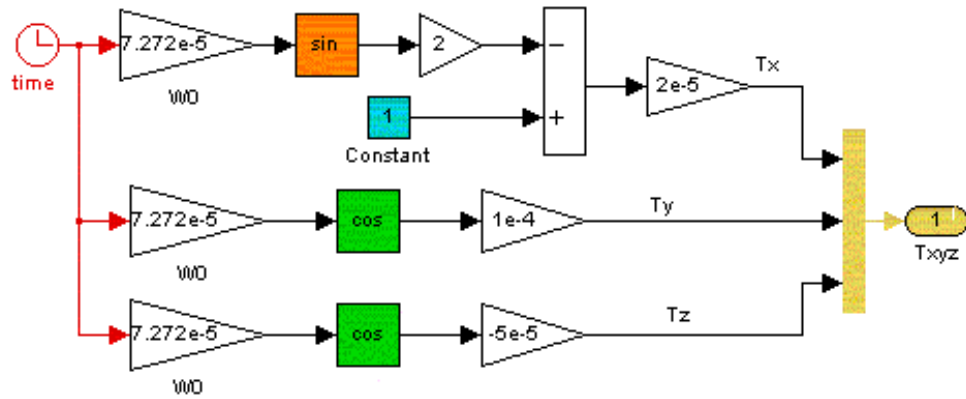


Figure 63 Solar radiation pressure disturbance

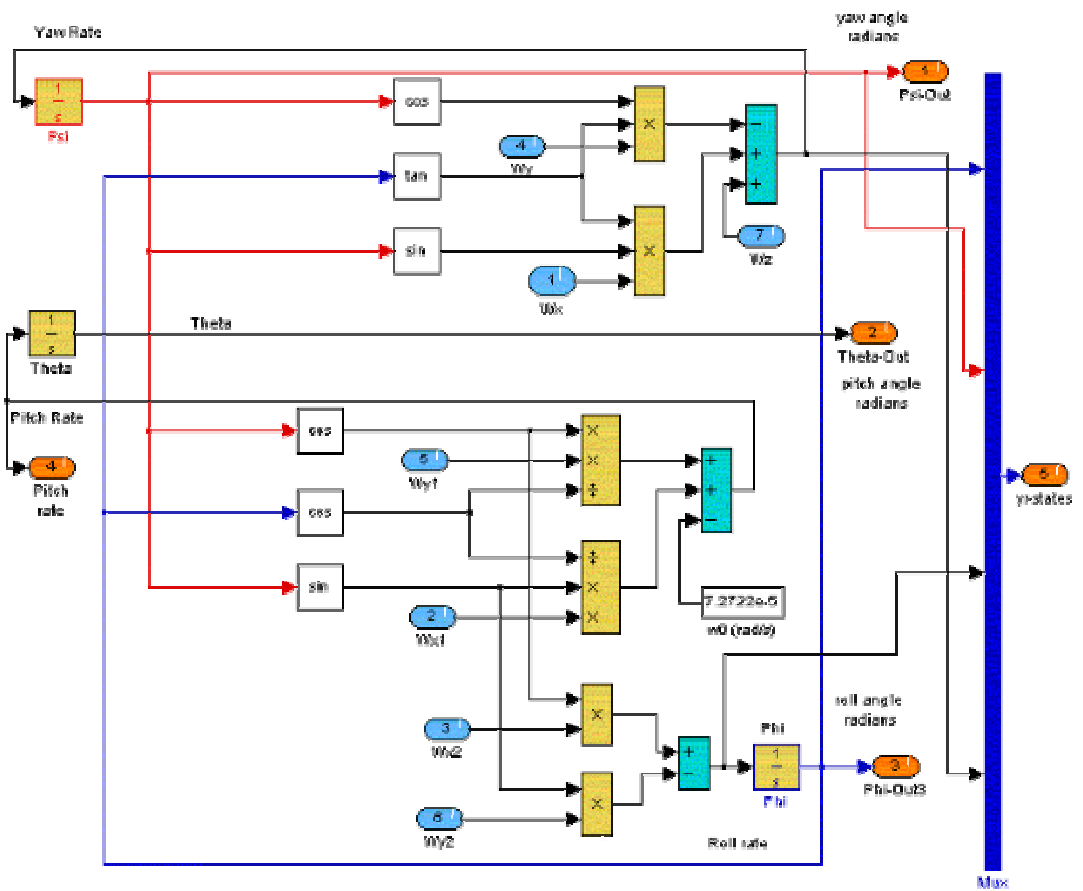
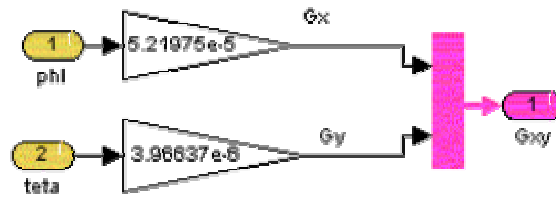
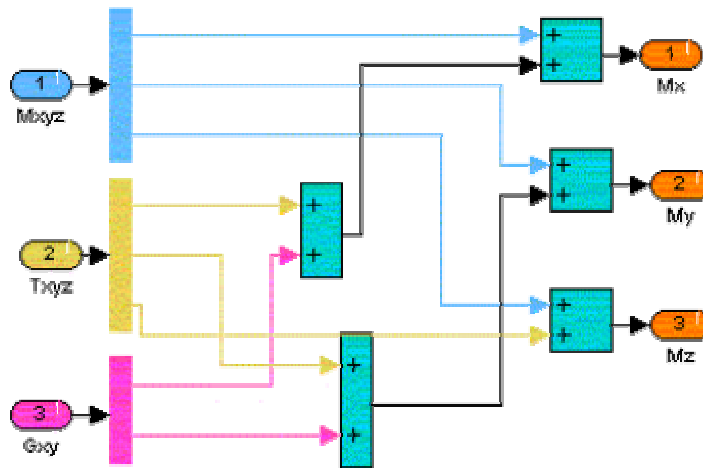


Figure 64 Euler angle transformation and links for state feedback



**Figure 65 Gravity gradient disturbance torque**



**Figure 66 Connector for disturbance and control torque signals**

The Pulse Width Modulator is derived from the default "pulse generator" masked block of Simulink. A "zero-order-hold" block samples the control signal ( $T_{c\_in}$ ) incoming to the actuator with same period of PWM thruster activation (PWM is modelled inside the masked blocks "positive/negative pulses").

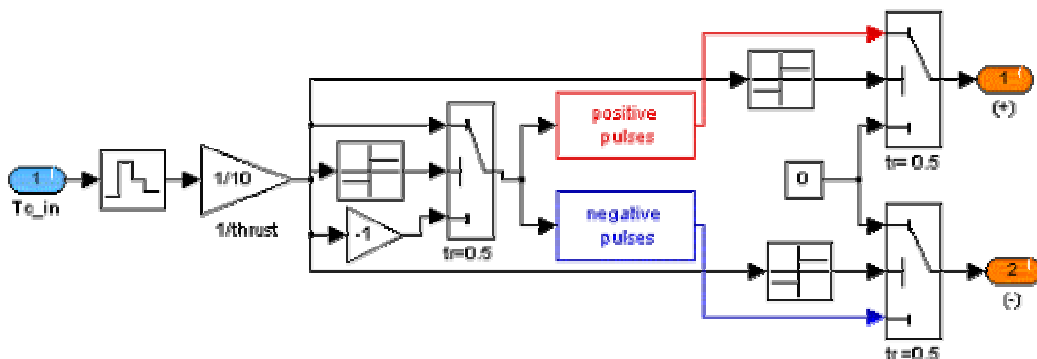


**Figure 67 Main PWM block, the thruster model**

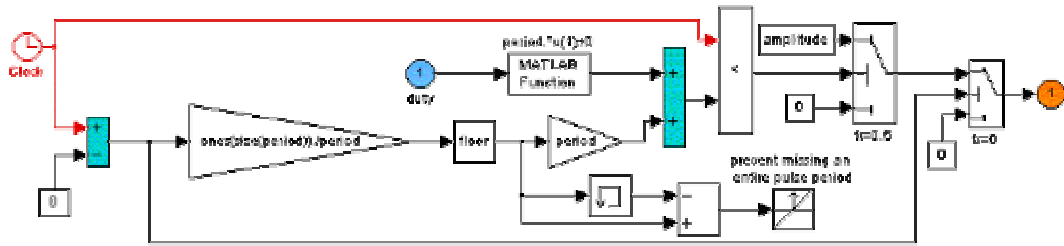


**Figure 68 PWM model inside the "positive/negative pulses" blocks**

PWM is derived from default Pulse Generator module of Simulink program. It is unmasked and "duty cycle" is modified as an external input signal.

The details of the roll/yaw feedback controller are in Figures 40-42. The controller is composed of a state feedback controller for stabilisation and an integral feedback for roll attitude regulation. The white noise modules of Simulink represent measurement errors. "Angles" and "rates" blocks of Figures 40-42 are the white noise blocks introducing random error signals into attitude measurement signals.

## CHAPTER VI

### SUMMARY AND CONCLUSION

In this thesis a design study is presented for attitude control of a geostationary satellite. The satellite dynamics model, types of actuators selected are very similar to that of TÜRKSAT 1B.

In the manuscript first a literature survey on satellite attitude control theories with a concentration on fuel minimisation is presented. Next the description of TÜRKSAT 1B attitude control system is given.

Nonlinear equations for satellite motion are obtained and a simulation program is written using Matlab-Simulink software. Using the program the satellite attitude response behaviour to initial alignment errors and to external/internal disturbing torques are simulated and presented. Concluding that satellite attitude is highly coupled and unstable, there is a need for an effective controller. Pitch attitude nominal value  $0.8336^\circ$  with  $\pm 0.05^\circ$  bias, and roll attitude zero nominal with same bias are the required performance parameters of the satellite controller.

The disturbances considered are due to solar radiation pressure and gravity gradient perturbing torques mostly. These disturbance torque models are integrated into Simulink model as well. Pitch control is realised by a strapdown momentum wheel and thrusters are used for roll/yaw control.

To design appropriate controllers, nonlinear equations of motion are linearised. It is observed that linear pitch motion is decoupled from the roll/yaw dynamics. Thus, two separate controllers, one for pitch attitude one for roll/yaw motion are designed.

Pitch control of satellite requires pitch rate measurement by rate gyros, and pitch attitude measurement with optical earth/sun sensors. TÜRKSAT 1B on the other hand do not use rate gyro measurements. Measurement of pitch rate enabled us to design a PD controller. Thus, an inner loop rate feedback is employed. The momentum wheel actuator is modelled as a second order DC motor model. The relation between control gains  $K_p$  and  $K_d$ , and the DC motor physical parameters are obtained root locus analysis to warrant a stable closed loop system. With the help of "Nonlinear Design Blockset" with several long-term simulation trials an appropriate pair of control gains are determined. With  $K_p=50$ ,  $K_d=2.5$  satellite pitch attitude is kept within limits in response to  $\pm 0.1^\circ$  initial angular placement error and long term external disturbances due to solar radiation pressure and gravity gradients.

Using a strapdown momentum wheel, the designed pitch controller achieved satisfactory regulation when tested with the linearised pitch attitude model.

Roll/Yaw linearised equations show that the motion is coupled between the two. That is, any torque on roll affects the yaw motion as well. This gives us a chance to align roll thrusters to have a limited constant torque component on yaw as well. Hence another yaw actuator becomes unnecessary, saving lots of weight and providing considerable fuel economy. With knowledge of TÜRKSAT 1B thruster activation and coupling levels, a new thruster similar to that of TÜRKSAT 1B is designed. Roll thruster with 10 Nm component on x- (roll) direction and 3 Nm component z-(yaw) direction is found to be satisfactory, less or higher component in yaw does not satisfy time response constraints with fuel economy.

For roll/yaw control integral plus state variable feedback controller is designed. This method has a state feedback controller in conjunction with integral controller

action acting with reference error signal. State feedback control requires measurement of both roll/yaw attitude angles and rates. The proposed controller is different from that of TÜRKSAT 1B. Measurement process is similar to that of pitch control case. Since we have four states, four state feedback control gains plus one integral control gain are our design parameters. Yaw motion is not actively controlled hence regulation with higher bias is acceptable as long as total yaw attitude does not exceed at most 10 degrees for the linearisation to be meaningful.

Pole placement is the technique to determine stable configuration of closed loop control. A Matlab m file is written using Ackermann's formulation for pole placement problem. Control gains are not unique for stabilization, they depend on where we want the closed loops to be. Several poles are studied for time response characteristics and fuel economy. It is observed that trying to have fast closed loop dynamics (placing poles too much left hand side) is not favourable. This exaggerates overshoots and saturates actuators. Also having relatively large imaginary roots, introduces fast oscillations into system that cause too much fuel consumption. Having purely real rooted poles do not have satisfactory long and short-term responses. All these unacceptable configurations on the other hand are stable unlike uncontrolled model. Finally appropriate region to place closed loop poles is determined, and detailed fuel economy search is done.

The thrusters are discrete devices, which causes the control problem to be much more difficult. Several pole locations determined from proportional thruster analysis are now tested with on-off actuator model. The period of thruster activation plus places of the closed loop system poles determines the optimum fuel consumption and attitude response characteristics. Long periods like 10 or even 0.5 seconds are found to be unacceptable, since they introduce short period oscillations to the system resulting in excessive fuel consumption and/or unacceptable attitude responses. Most appropriate sampling period with respective pole places satisfying time response and minimum fuel expenditure constraints are presented.

Final step is the application of optimised controllers to the nonlinear body dynamics model. The designed servo controller (roll/yaw) together with pitch controller is placed into nonlinear body dynamics Simulink model. The computer simulations took much more time in comparison to linear models. Additionally on linear model pitch motion is decoupled from yaw/roll dynamics, which is not valid for nonlinear model. Furthermore this fully coupled model enabled thruster misalignment internal disturbance to be modelled into Simulink. Hence overall disturbance effects become more difficult to overcome.  $10^{-5}$  Nm small discrete perturbing torque pulses are added to the pitch control output signal. The computational environment, as a result, becomes extremely difficult to handle. A Pentium II PC with relatively high memory was not able to handle long period (1-5 days) simulations. Hence only short-term responses are observed. In the future same study shall be carried out with a better computer to handle long-term simulations.

It is shown that the designed controllers were able to handle short-term responses successfully. They managed to suppress initial rate and angular placement errors and short-term solar pressure, and gravity gradient external disturbance torques, thrust misalignment, internal perturbation torques, and small measurement errors.

An extensive parametric study on control parameters for fuel minimisation is carried out. Total control effort (absolute integral of control signal) is directly related to fuel consumption. Hence the most appropriate pole placement and sampling period selection to minimise the total control effort is determined.

For future work we can note that, the robust control methods shall be investigated. The actual body dynamic characteristics of the satellite changes because of the fuel consumption and continuous rotation of the solar panels. Additionally structural modes are important, when there are large, flexible solar panels.

## REFERENCES

- [1] P. R. Eskobal, Methods of Orbit Determination, John Wiley and Sons, New York 1965
- [2] J. R. Wertz, Spacecraft Attitude Dynamics and Control, D. Reidel Publishing , Co., 1985
- [3] Uslu, Özge, "*Orbit Dynamics, Attitude Dynamics and Control Investigation into Possible Applications to TÜRKSAT*", M.S Thesis in Aeronautical Engineering, Middle East technical University, Ankara, January 1997.
- [4] K. J. Åström, Introduction to Stochastic Control Theory, Academic Press, 1970
- [5] Karşıdağ, Süleyman Tarkan, "*Model predictive control Using Neural Networks Applied to Flight Control*", M.S Thesis in Electrical and Electronics Engineering, Middle East technical University, Ankara, January 1999.
- [6] Kirk, Donald E., Optimal Control Theory; An Introduction, Prentice-Hall Inc, New Jersey, USA, 1970
- [7] Shin Whar Liu and Tarunraj Singh ,"*Fuel/Time optimal Control of Spacecraft Maneuvers*" , *Journal of Guidance, Control and Dynamics* , Vol. 20, No: 2 , pp. 394, 397 , 1997.
- [8] Karl D. Bilimoira and Bong Wie, "*Time Optimal Three-axis Reorientation of a Rigid Spacecraft*", *Journal of Guidance, Control and Dynamics*, Vol. 16, No: 3, 1993.

- [9] Hans Seyvald et al., "Minimum Fuel Spacecraft Reorientation", *Journal of Guidance, Control and Dynamics*, Vol. 17, No: 1, 1994.
- [10] Hari B. Hablani, "Pole Placement Technique for Magnetic Momentum Removal of Earth Pointing Spacecraft", *Journal of Guidance, Control and Dynamics*, Vol.20, No: 2, pp. 268-275, 1997.
- [11] A. L. Herman and B. A. Conway, "Optimal Spacecraft Attitude Control Using Collocation and Nonlinear Programming", *Journal of Guidance, Control and Dynamics*, Vol. 15 No: 5 pp. 1287-1289, 1992.
- [12] C. I. Byrnes and A. Isidori, "On the Attitude Stabilization of Rigid Spacecraft", *Automatica*, Vol. 27, No: 1, pp. 87-95, 1991.
- [13] Mark E. Pittelkau, "Optimal Periodic Control for Spacecraft Pointing and Attitude Determination", *Journal of Guidance, Control and Dynamics*, Vol.16, No:6, pp. 1078-1083, 1993.
- [14] H. Weiss, "Quaternion-Based Rate/Attitude Tracking System with Application to Gimbal Attitude Control", *Journal of Guidance, Control and Dynamics*, Vol.16, No: 4, pp. 609-616, 1993.
- [15] S. Nicosia and P. Tomei, "Nonlinear Observer and Output Feedback Control of Spacecraft", *IEEE Transactions on Aerospace and Electronic Systems*, Vol. 28, No: 4, pp. 970-977, 1992.
- [16] R. Venkatachalam, "Large Angle Pitch Attitude Maneuver of a Satellite Using Solar Radiation Pressure", *IEEE Transactions on Aerospace and Electronic Systems*, Vol. 29, No: 4, pp. 1164-1169, 1993.
- [17] J. G. Lee, et al., "Sliding-Mode Controller Design for Spacecraft Attitude Tracking Maneuvers", *IEEE Transactions on Aerospace and Electronic Systems*, Vol. 29, No: 4, pp. 1328-1332, 1993.
- [18] S. J. Doddds and A. B. Walker, "Sliding-Mode Control System for the Three-Axis Attitude Control of Rigid-Body Spacecraft with Unknown

Dynamics Parameters”, *International Journal of Control*, Vol. 54 No: 4, pp. 737-761, 1991.

- [19] A. G. Parlos and J. W. Sunkel, “Adaptive Attitude Control and Momentum Management for Large Angle Spacecraft Maneuvers”, *Journal of Guidance, Control and Dynamics*, Vol.15, No: 4, pp.1018-1028, 1992.
- [20] G. E. Piper and H. G. Kwatny, “Complicated Dynamics in Spacecraft Attitude Control Systems”, *Journal of Guidance, Control and Dynamics*, Vol.15, No: 4, pp. 825-831, 1992.
- [21] Y. Sharony and L. Meirovitch, “Accommodation of Kinematic Disturbances During Minimum Time Maneuvers of Flexible Spacecraft””, *Journal of Guidance, Control and Dynamics*, Vol.14, No: 2, pp.268-277, 1991.
- [22] M. Schwarzchild and S. Rajaram, “Attitude Acquisition System for Communication Spacecraft”, *Journal of Guidance, Control and Dynamics*, Vol.14, No: 3, pp.543-547, 1991.
- [23] John T. Garner, Satellite Control: A Comprehensive Approach, John Wiley and Sons, 1996
- [24] SCC/SCC-BU Operations Handbook, Part2, Aerospatiale Espace and Defence, 1993.
- [25] Türksat Engineering Training Documents, Aerospatiale Espace and Defence, 1993.
- [26] Vladimir A. Chobotov, Spacecraft Attitude Dynamics and Control, Krieger Publishing Co., Florida, 1991.
- [27] M. H. Kaplan, Modern Spacecraft Dynamics & Control, John Wiley & Sons, USA, 1976.

- [28] W. G. Hughes, "Space Vehicle Stabilization" Dynamics of Rockets and Satellites, Eds.: G.V. Groves, North-Holland Publishing Company, Amsterdam, 1965.
- [29] F. P. J. Rimrott, Introductory Attitude Dynamics & Control, John Wiley & Sons, USA, 1976.
- [30] A. E. Bryson, JR., Control of Spacecraft and Aircraft, Princeton University Press, Princeton, New Jersey, USA, 1994.
- [31] Katsuhiko Ogata, Modern Control Engineering, Prentice-Hall International Inc. USA, 1990.
- [32] Benjamin C. Kuo, Automatic Control Systems, Prentice-Hall International Inc. USA, 1991.

## APPENDIX A

### NONLINEAR BODY DYNAMICS BEHAVIOUR ANALYSES

#### A.1. Disturbance Effects Are Excluded

Here two cases where both initial angular placement and rate errors are imposed into the nonlinear Matlab-Simulink model are presented. The initial rate bias is referenced to earth rate, and the attitude errors are selected to be small values around the nominal values.

##### A.1.1. Simulations without the External Disturbance Torque

This section investigates the model behaviour in response to an initial attitude error and body rate bias. Three Cases of possible initial states are simulated and their respective attitude time histories are presented in Figures A1.

The initial bias angles are assigned to the integration blocks on the model. The initial conditions on Euler angles are inserted into integration blocks of the subsystem "Euler Angle Transformation", and the initial body rates are similarly implemented on the subsystem "Momentum Eqns". The following three cases are selected.

- *CASE 1*

$$\phi_0=0.1^\circ$$

$$\theta_0=0.2^\circ$$

$$\psi_0=0.5^\circ$$

$$\omega_x=\omega_0/5$$

$$\omega_y=\omega_0/8$$

$$\omega_z=\omega_0/13$$

Where  $\omega_0=2.272 \cdot 10^{-5}$  rad/s = 1 rev/day (earth rate)

- *CASE 2*

$$\phi_0 = -0.3^\circ$$

$$\theta_0 = -1.45^\circ$$

$$\psi_0 = 0.5^\circ$$

$$\omega_x = -\omega_0/5$$

$$\omega_y = -\omega_0/8$$

$$\omega_z = \omega_0/13$$

- *CASE 3*

$$\phi_0 = 0.3^\circ$$

$$\theta_0 = 1.45^\circ$$

$$\psi_0 = -0.5^\circ$$

$$\omega_x = \omega_0/5$$

$$\omega_y = \omega_0/8$$

$$\omega_z = -\omega_0/13$$

As noticed from the above Euler angle initial magnitudes, these values are larger than the nominal regulation limits for the automatic control system ( $\pm 0.05^\circ$  from nominal on all attitude angles). Also initial body rates are referenced to the earth rate. Much larger initial body rate errors exaggerates the deviations much more drastically.

The following attitude behaviours are observed in response to above defined Cases:

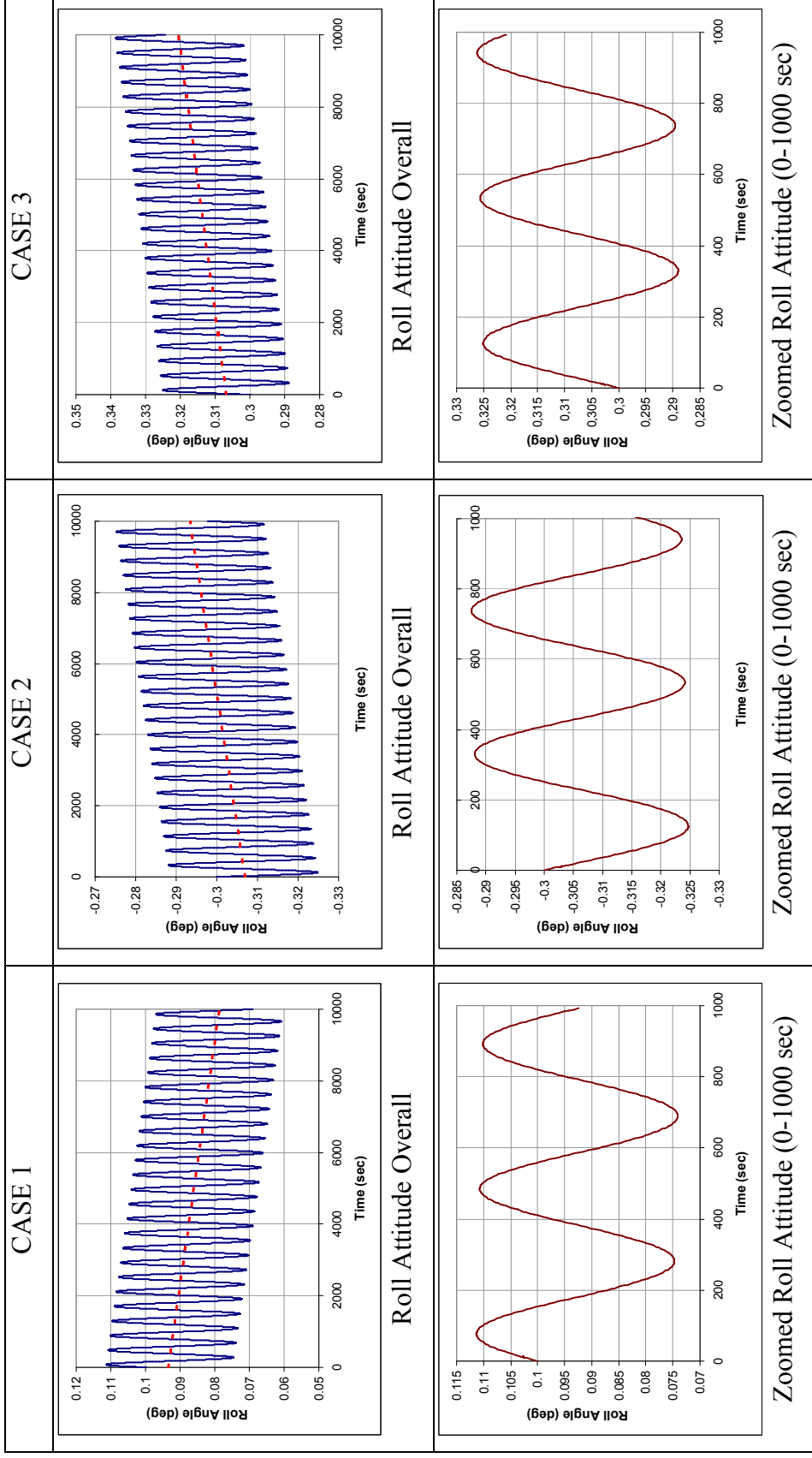


**Figure A1 Roll behaviour in response to the initial attitude angle and rate errors**

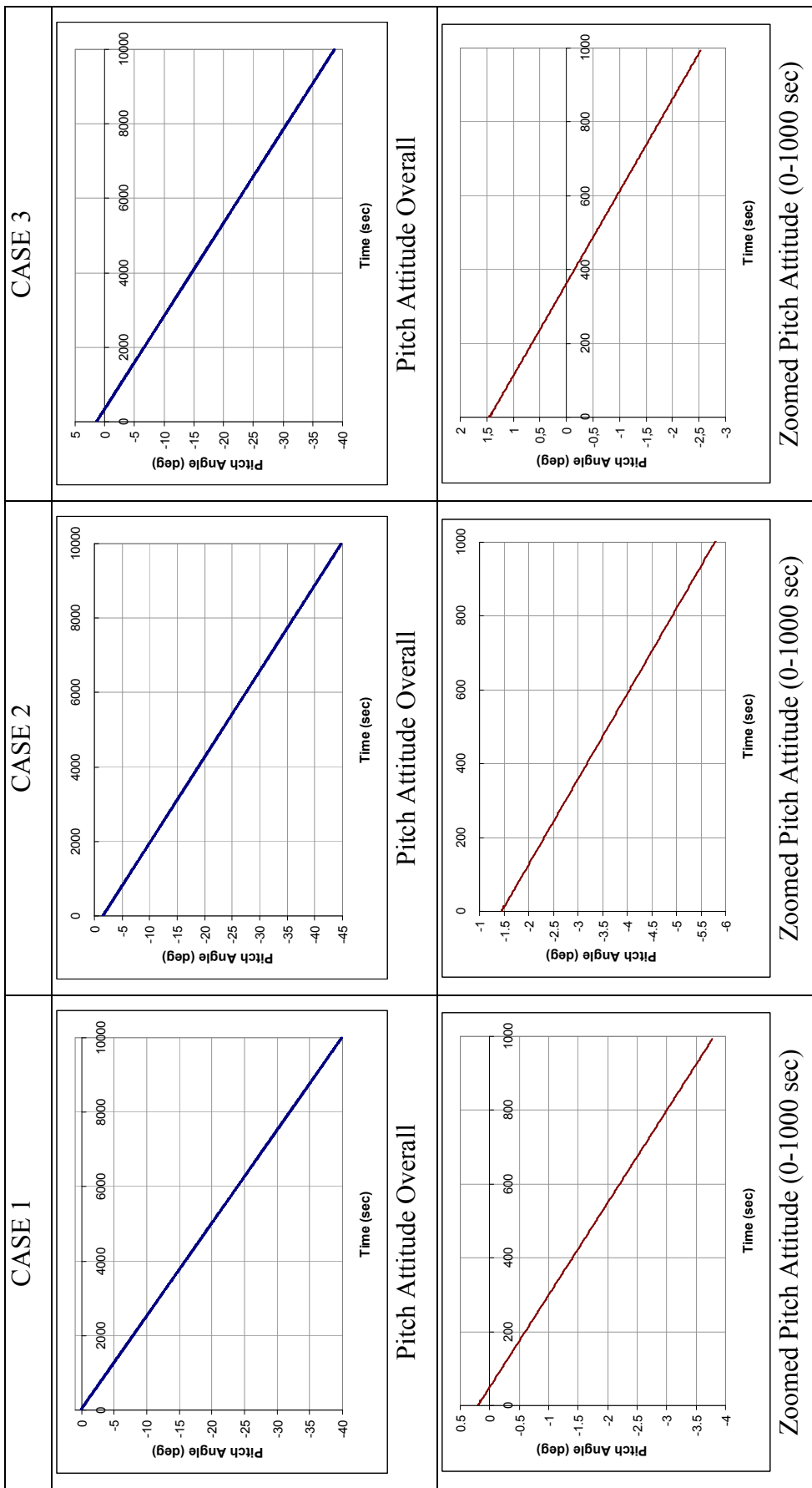


Figure A2 Pitch behaviour in response to the initial attitude angle and rate errors

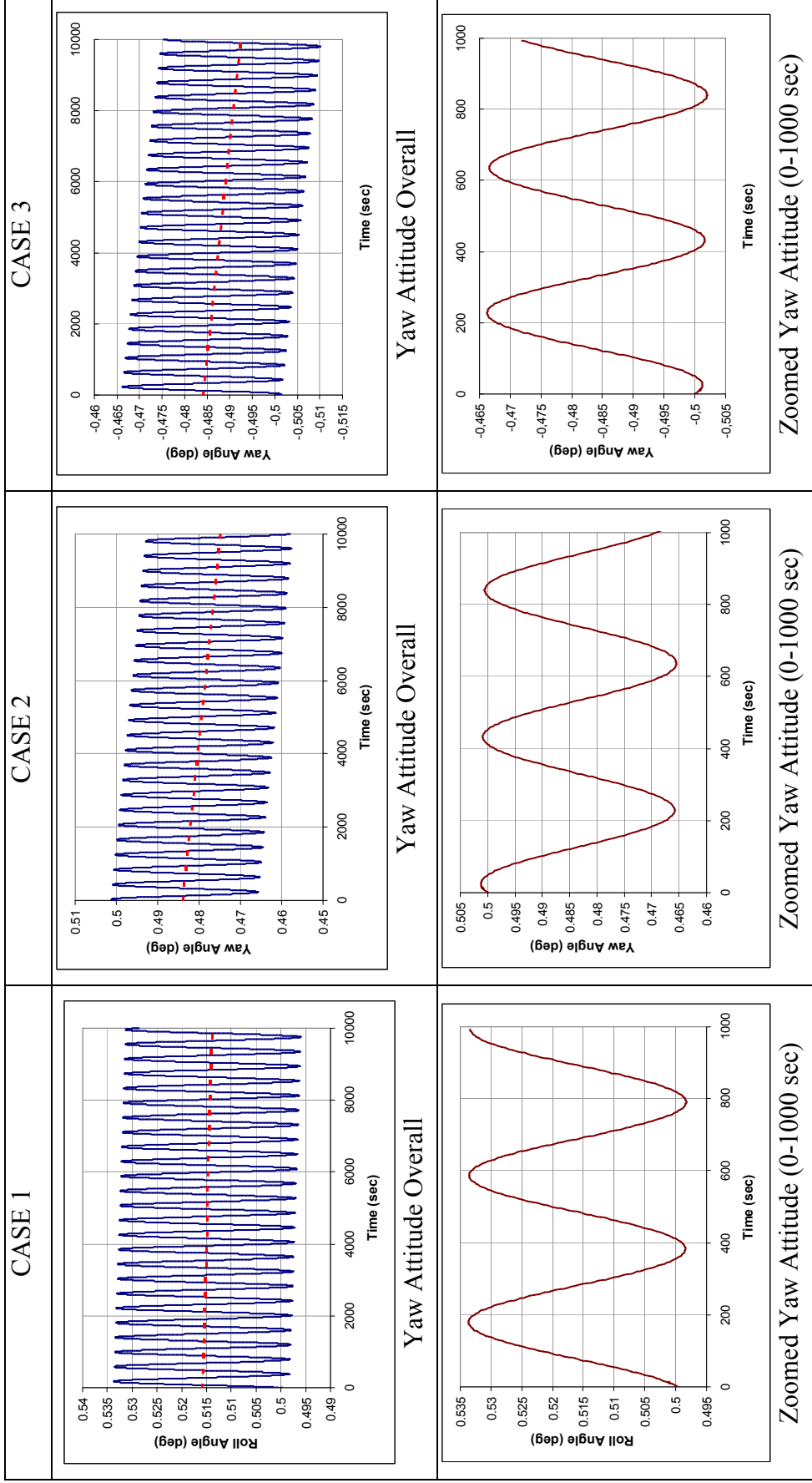


Figure A3 Yaw behaviour in response to the initial attitude angle and rate errors

Figures A1-A3 represent the simulation results for undisturbed model response to initial errors. The observed general behaviour is that yaw and roll responses are oscillatory with constant around a linearly changing average value. The pitch response, on the other hand, is linearly increasing in magnitude. This behaviour is also observed with similar initial error selections on angular rate and positions. But much larger rate and angle biases exaggerates this behaviour; however this thesis does not study larger angle maneuvers, hence the larger initial biases are not investigated further in detail. In Appendix B the un-disturbed dynamics model is linearised and the eigenvalues that are responsible for oscillations are extracted. The coupling between roll/yaw is the basic reason why both dynamics are oscillatory. Their oscillation periods are very close as follows:

## A.2. Simulations with Disturbance Torque Models Included

This case again excludes any control torques but includes the solar radiation pressure and gravity gradient disturbances. Also initial angular rate and position biases still exist. Figures A4 to A6 represent the satellite model response to these disturbing torques.

CASE A: The model has the following initial bias at Euler Angles:

$$\phi_0=0.1^\circ \qquad \theta_0=1.45^\circ \qquad \psi_0=0.25^\circ$$

The initial body rates are common for all the three cases:

$$\omega_x=\omega_0/5 \qquad \omega_y=\omega_0/8 \qquad \omega_z=-\omega_0/13$$

CASE B: The model has the following initial bias at Euler Angles:

$$\phi_0=-0.3^\circ \qquad \theta_0=-1.45^\circ \qquad \psi_0=-0.5^\circ$$

CASE C: The model has the following initial bias at Euler Angles:

$$\phi_0=0.1^\circ \qquad \theta_0=-1.45^\circ \qquad \psi_0=0.5^\circ$$

Changing sign of  $\omega_y$  has no noticeable influence on pitch behaviour. Changing signs of  $\omega_x$ ,  $\omega_z$ , has noticeable effect only together with magnitude and signs of respective Euler angles. The behaviour of the attitude most dominantly depends on initial Euler Angle signs and magnitudes. The initial Euler Angle and body rate bias magnitudes are selected similar to that of the undisturbed model response analysis.

In Figure A5, it is observed that pitch attitude is highly unstable, and shows fast divergent characteristics without oscillations. In Figures A4 and A6 it is observed that roll and yaw motions are coupled and unstable.

The mathematical parameters used for the simulation are as follows:

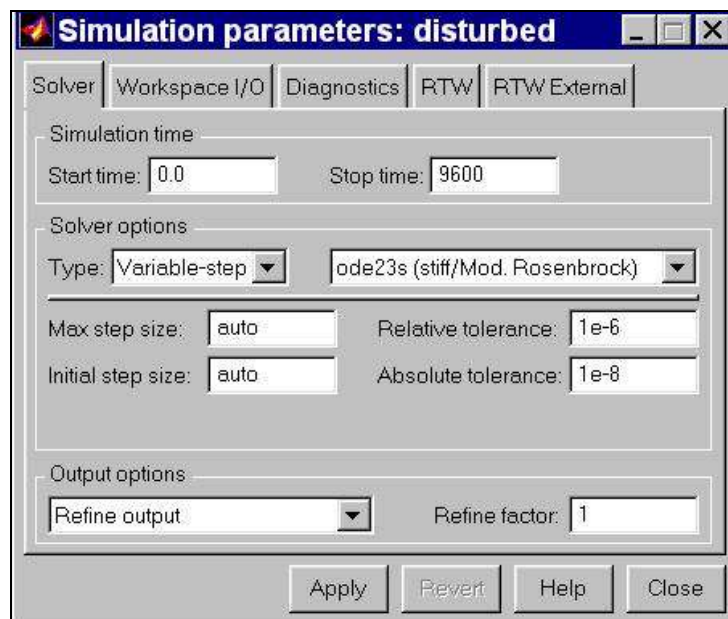


**Figure 69 Mathematical parameters of the simulation**

Oscillatory behaviour is observed at initial stages of the simulation except for pitch attitude. The model is linearised in Appendix B to investigate the nature of the system matrix's eigenvalues, the imaginary roots are located that are responsible from the oscillatory responses in nonlinear simulation.

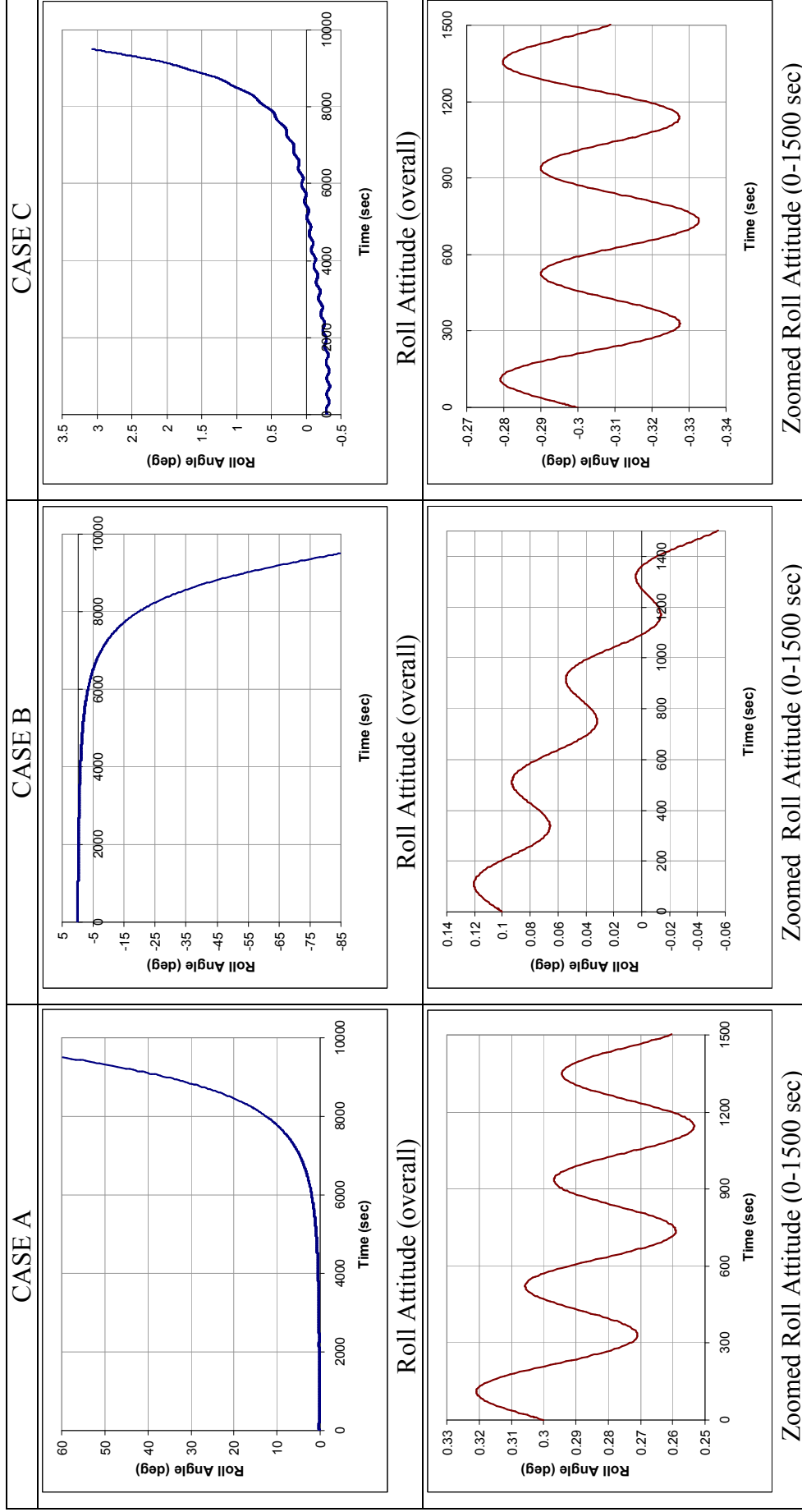
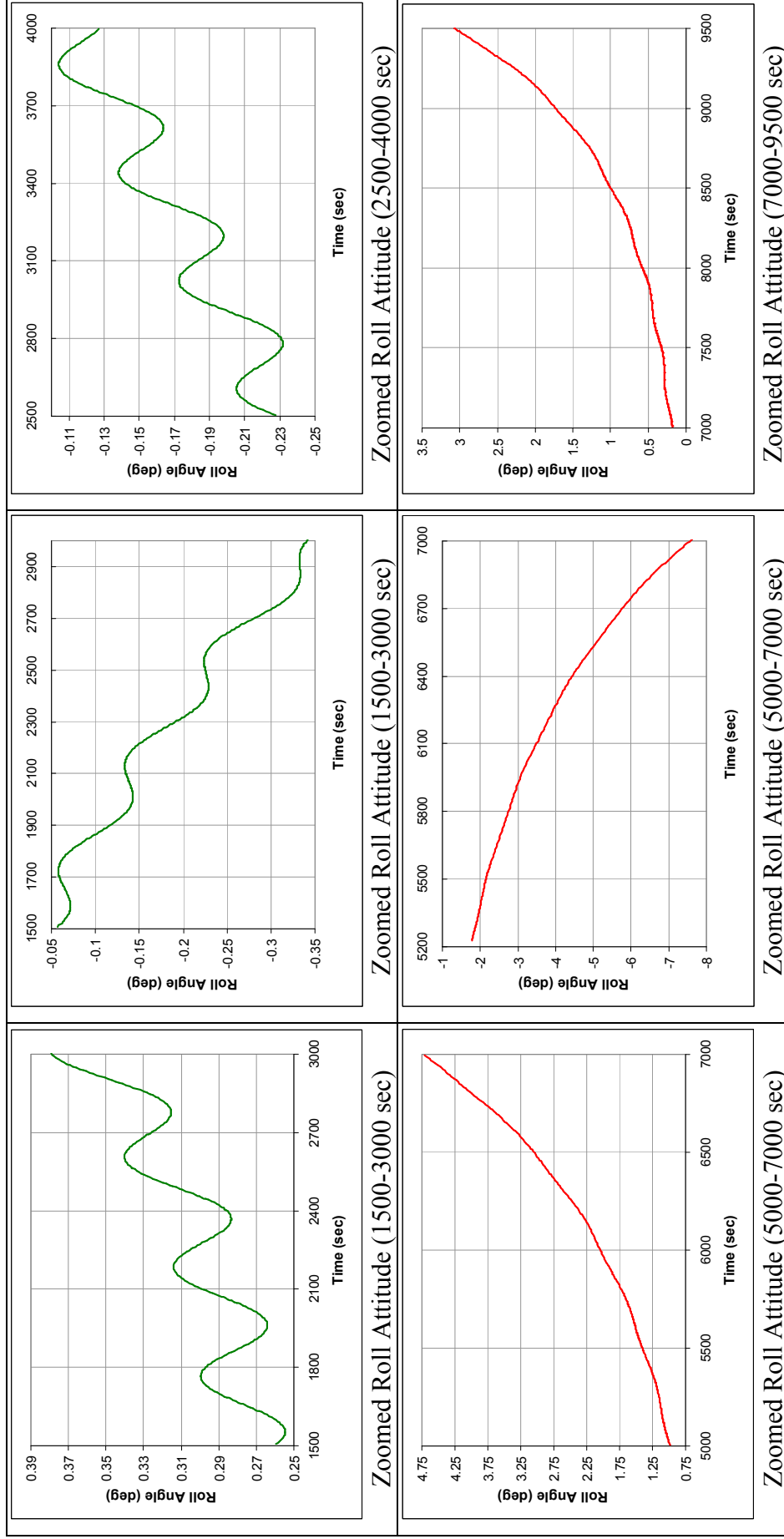


**Figure A4 Roll attitude in response to the initial attitude angle and rate errors and to external disturbance torque**



**"Figure A4 Continues" Roll attitude in response to the initial attitude angle and rate errors and to external disturbance torque**

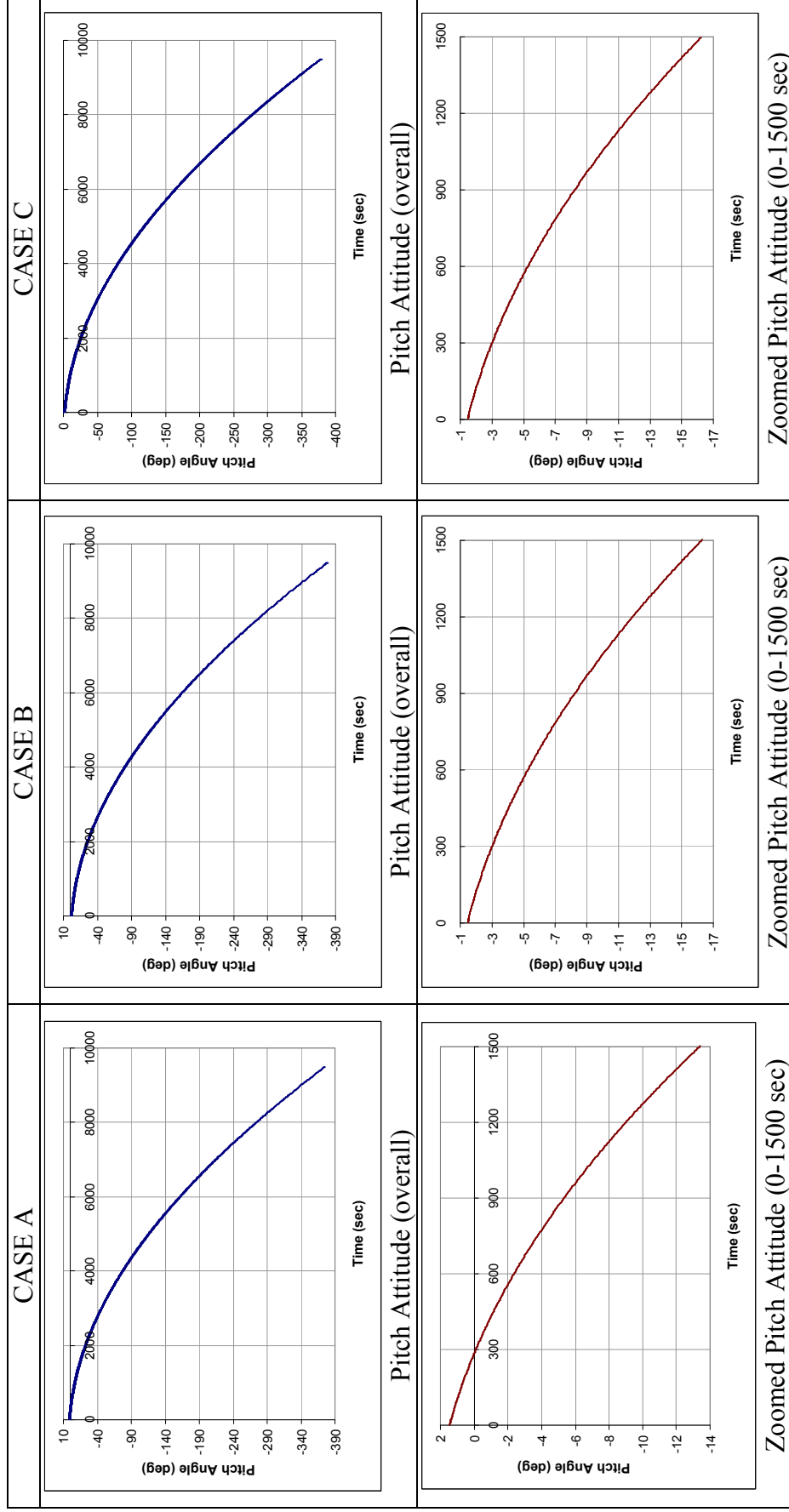


**Figure A5 Pitch attitude in response to the initial attitude angle and rate errors and to external disturbance torque**

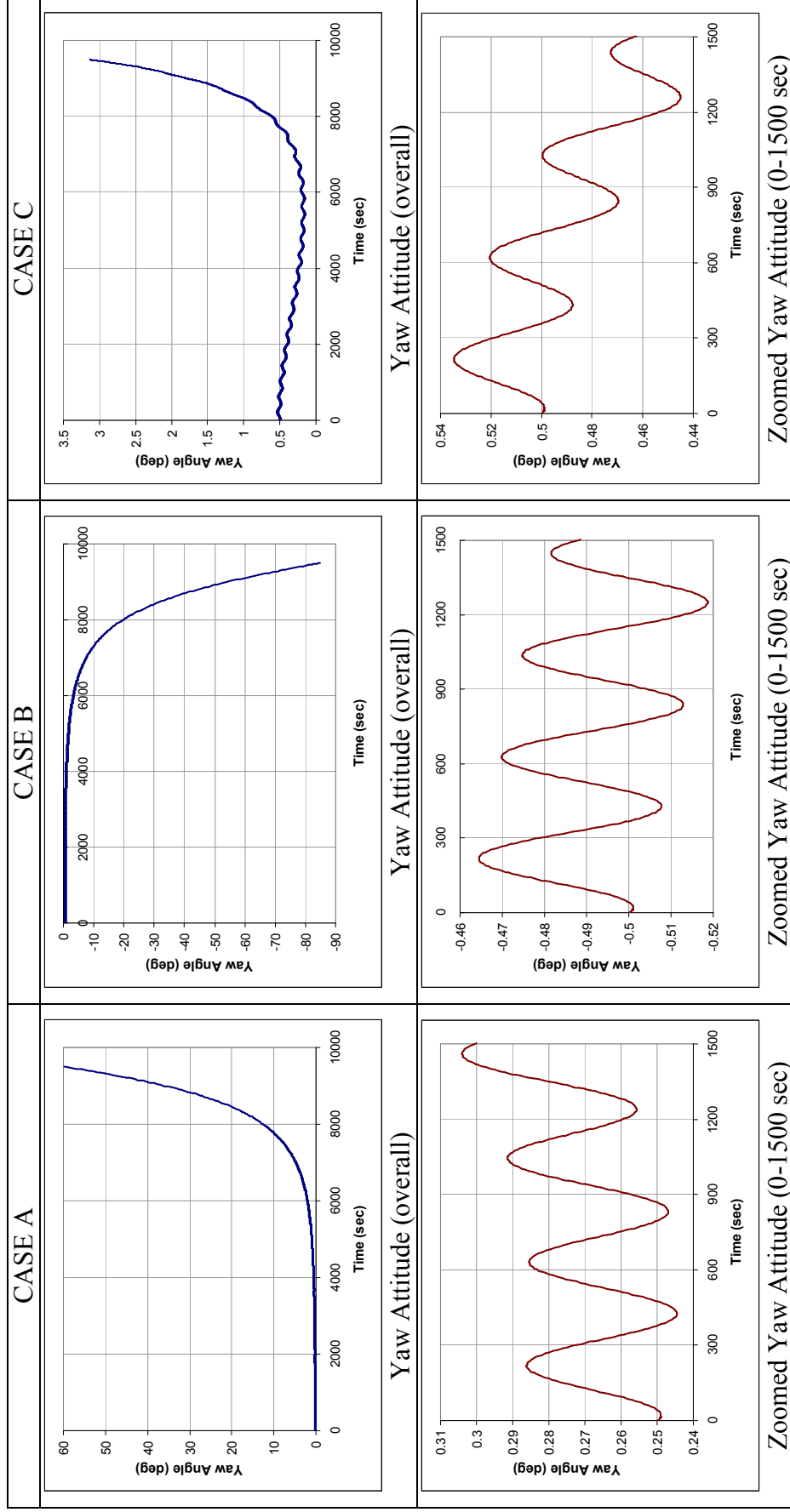


**Figure A6 Yaw attitude in response to the initial attitude angle and rate errors and to external disturbance torque**

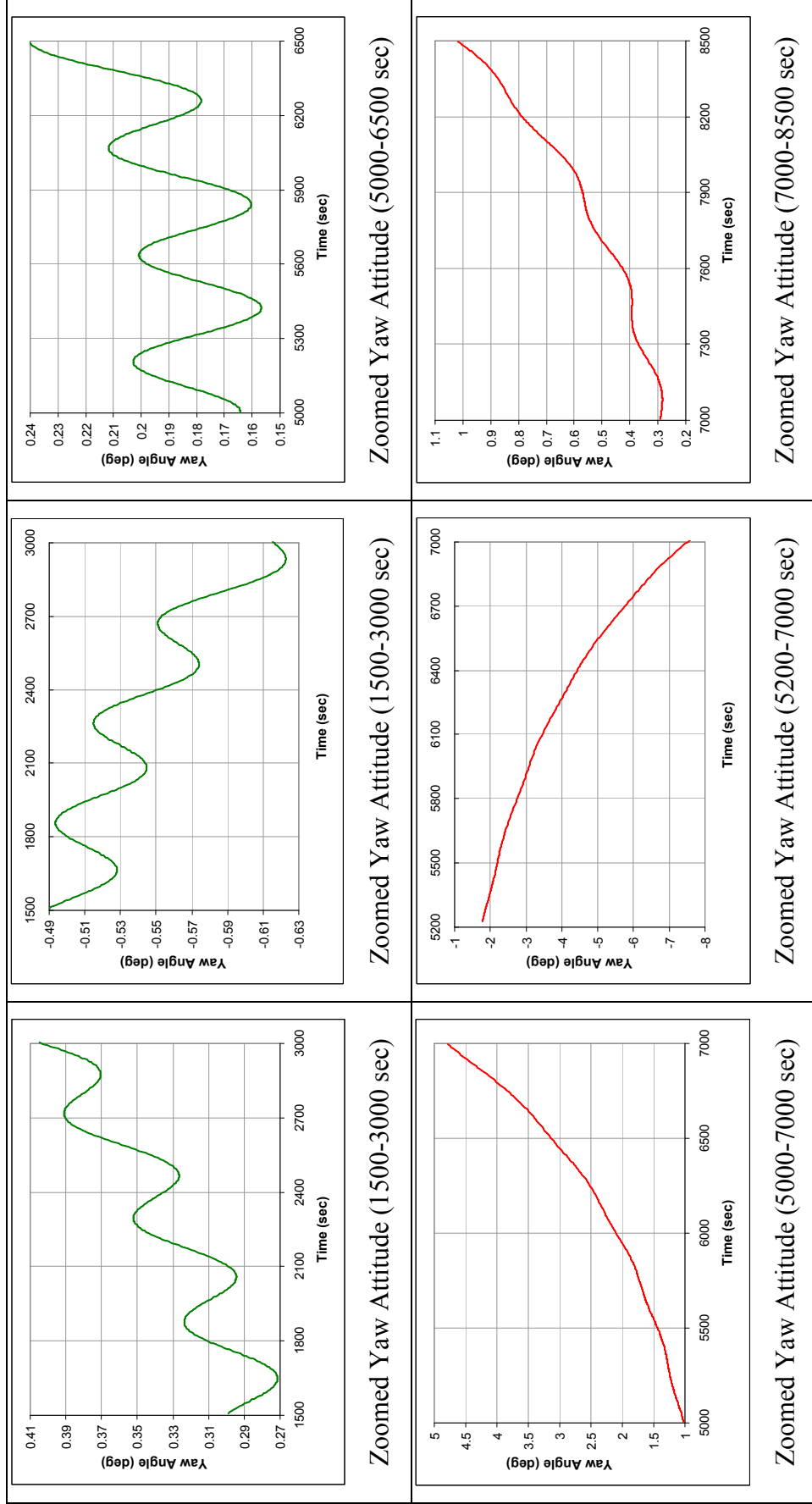


**Figure A6 "continued" Yaw attitude in response to the initial attitude angle and rate errors and to external disturbance torque**

## APPENDIX B

### LINEARISED ATTITUDE DYNAMICS MODELS

The equations representing the attitude dynamics are highly nonlinear. This Appendix shows two methods of linearisation of these equations (Equations 4.14 and 4.18). Case 1 is the manual linearisation and Case 2 is linearisation by Matlab program. The second method is used for check and representation of alternative means. For linearisation only the solar radiation pressure disturbance model is taken into account due its dependence on the body attitude angles. Finally as mentioned in Appendix A, the undisturbed Simulink model is also linearised by Matlab to extract the eigenvalues causing the oscillations.

#### B.1. CASE 1; Manual Linearisation

Let's remember the Euler transformation, Momentum, and the Gravity Gradient Disturbance equations respectively:

$$\begin{bmatrix} \omega_x \\ \omega_y \\ \omega_z \end{bmatrix} = \begin{bmatrix} \dot{\phi} \cos(\psi) + (\dot{\theta} + \omega_0) \sin(\psi) \cos(\phi) \\ -\dot{\phi} \sin(\psi) + (\dot{\theta} + \omega_0) \cos(\psi) \cos(\phi) \\ \dot{\psi} - (\dot{\theta} + \omega_0) \sin(\phi) \end{bmatrix} \quad (4.14)$$

Repeated)

$$T_x = 3770\dot{\omega}_x + 3290\omega_y\omega_z + 60\omega_z \quad (4.18.a \text{ Repeated})$$

$$T_y = 730\dot{\omega}_y - 250\omega_x\omega_z - \dot{h}_w \quad (4.18.b \text{ Repeated})$$

$$T_z = 4020\dot{\omega}_z - 3040\omega_x\omega_y - 60\omega_x \quad (4.18.c \text{ Repeated})$$

$$\begin{bmatrix} G_x \\ G_y \\ G_z \end{bmatrix} = \begin{bmatrix} -3\omega_0^2(I_y - I_z)\phi \\ -3\omega_0^2(I_x - I_z)\theta \\ 0 \end{bmatrix} = \begin{bmatrix} 5.0958 \cdot 10^{-6} \phi \\ 3.8722 \cdot 10^{-7} \theta \\ 0 \end{bmatrix} \quad (4.26 \text{ and } 4.28 \text{ Repeated})$$

These three equations represent the body dynamics that that is to linearised.

### B.1.1. Assumptions for Linearisation

In units of radians,  $\phi$ ,  $\theta$ ,  $\psi$  and their changes  $\tilde{\phi}$ ,  $\tilde{\theta}$ ,  $\tilde{\psi}$  are small angles (much less than 10 degrees) hence their multiplication can be neglected. Also again in radians units, cosine and sine functions of these angles can be linearised as:  $\text{Cos}(\tilde{\phi}, \tilde{\theta}, \tilde{\psi}) \approx 1$  and  $\text{Sin}(\tilde{\phi}, \tilde{\theta}, \tilde{\psi}) \approx (\tilde{\phi}, \tilde{\theta}, \tilde{\psi})$ .

With the above assumptions the above set of equations simplifies and can easily be combined together.

### B.1.2. Linearisation

Euler equations and their first derivatives simplify to:

$$\begin{bmatrix} \omega_x \\ \omega_y \\ \omega_z \end{bmatrix} \approx \begin{bmatrix} \dot{\tilde{\phi}} + \omega_0 \tilde{\psi} \\ \dot{\tilde{\theta}} + \omega_0 \\ \dot{\tilde{\psi}} - \omega_0 \tilde{\phi} \end{bmatrix} \quad (\text{B.1})$$

and

$$\begin{bmatrix} \dot{\omega}_x \\ \dot{\omega}_y \\ \dot{\omega}_z \end{bmatrix} \approx \begin{bmatrix} \ddot{\tilde{\phi}} + \omega_0 \dot{\tilde{\psi}} \\ \ddot{\tilde{\theta}} \\ \ddot{\tilde{\psi}} - \omega_0 \dot{\tilde{\phi}} \end{bmatrix} \quad (\text{B.2})$$

Combining the above set of equations:

$$T_x + 5.0958 \cdot 10^{-6} \tilde{\phi} = 3770(\ddot{\tilde{\phi}} + \omega_0 \dot{\tilde{\psi}}) + 3290(\ddot{\tilde{\theta}} + \omega_0)(\dot{\tilde{\psi}} - \tilde{\phi} \omega_0) + 60(\dot{\tilde{\psi}} - \tilde{\phi} \omega_0) \quad (\text{B.3 a})$$

$$T_y + 3.872 \cdot 10^{-7} \tilde{\theta} = 730 \ddot{\tilde{\theta}} - 250(\ddot{\tilde{\phi}} + \dot{\tilde{\psi}} \omega_0)(\dot{\tilde{\psi}} - \tilde{\phi} \omega_0) \quad (\text{B.3 b})$$

$$T_z = 4020(\ddot{\tilde{\psi}} - \omega_0 \dot{\tilde{\phi}}) - 3040(\ddot{\tilde{\phi}} + \dot{\tilde{\psi}} \omega_0)(\dot{\tilde{\psi}} - \tilde{\phi} \omega_0) - 60(\ddot{\tilde{\phi}} + \dot{\tilde{\psi}} \omega_0) \quad (\text{B.3 c})$$

Plugging in the  $\omega_0 = 2.2722 \cdot 10^{-5}$  rad/sec and performing respective summations and equating the control torques to zero we obtain the following equation set:

$$0 = \begin{bmatrix} 3770 & 0 & 0 \\ 0 & 730 & 0 \\ 0 & 0 & 4020 \end{bmatrix} \begin{bmatrix} \ddot{\tilde{\phi}} \\ \ddot{\tilde{\theta}} \\ \ddot{\tilde{\psi}} \end{bmatrix} + \begin{bmatrix} 0 & 0 & 60.16 \\ 0 & 0 & 0 \\ -60.01 & 0 & 0 \end{bmatrix} \begin{bmatrix} \dot{\tilde{\phi}} \\ \dot{\tilde{\theta}} \\ \dot{\tilde{\psi}} \end{bmatrix} + \begin{bmatrix} -1.37 \cdot 10^{-3} & 0 & 0 \\ 0 & -3.87 \cdot 10^{-7} & 0 \\ 0 & 0 & -1.36 \cdot 10^{-3} \end{bmatrix} \begin{bmatrix} \tilde{\phi} \\ \tilde{\theta} \\ \tilde{\psi} \end{bmatrix} \quad (\text{B.4})$$

The equation representing pitch attitude can be extracted from above set, since it is independent of the other attitude angles.

$$0 = 730 \ddot{\tilde{\theta}} - 3.8722 \cdot 10^{-7} \tilde{\theta} \quad (\text{B.5})$$

The roll and yaw attitudes are coupled.

$$0 = \begin{bmatrix} 3770 & 0 \\ 0 & 4020 \end{bmatrix} \begin{bmatrix} \ddot{\tilde{\phi}} \\ \ddot{\tilde{\psi}} \end{bmatrix} + \begin{bmatrix} 0 & 60.1604 \\ -60.0091 & 0 \end{bmatrix} \begin{bmatrix} \dot{\tilde{\phi}} \\ \dot{\tilde{\psi}} \end{bmatrix} + \begin{bmatrix} -1.37 \cdot 10^{-3} & 0 \\ 0 & -1.36 \cdot 10^{-3} \end{bmatrix} \begin{bmatrix} \tilde{\phi} \\ \tilde{\psi} \end{bmatrix} \quad (\text{B.6})$$

Also the equation (B.4) can be represented 6x6 set of first order of differential equations. To reduce the second order differentials we define new variables:

**Table 16 Variables for Reduction of Order of Equation A2.4**

$x_1 = \tilde{\phi}$	$x_4 = \dot{\tilde{\phi}}$
$x_2 = \tilde{\theta}$	$x_5 = \dot{\tilde{\theta}}$
$x_3 = \tilde{\psi}$	$x_6 = \dot{\tilde{\psi}}$

Then the system governing equations of satellite motions in linear form of input-output relation becomes;  $\dot{\mathbf{x}} = \mathbf{Ax} + \mathbf{Bu}$  :

$$\begin{bmatrix} \dot{x}_1 \\ \dot{x}_2 \\ \dot{x}_3 \\ \dot{x}_4 \\ \dot{x}_5 \\ \dot{x}_6 \end{bmatrix} = \begin{bmatrix} 0 & 0 & 0 & 1 & 0 & 0 \\ 0 & 0 & 0 & 0 & 1 & 0 \\ 0 & 0 & 0 & 0 & 0 & 1 \\ 3.6310^{-7} & 0 & 0 & 0 & 0 & -1.595810^{-2} \\ 0 & 5.4310^{-10} & 0 & 0 & 0 & 0 \\ 0 & 0 & 3.3910^{-7} & 1.49310^{-2} & 0 & 0 \end{bmatrix} \begin{bmatrix} x_1 \\ x_2 \\ x_3 \\ x_4 \\ x_5 \\ x_6 \end{bmatrix} + \begin{bmatrix} 0 & 0 & 0 \\ 0 & 0 & 0 \\ 0 & 0 & 0 \\ 2.652510^{-4} & 0 & 0 \\ 0 & 1.369910^{-3} & 0 \\ 0 & 0 & 2.487610^{-4} \end{bmatrix} \begin{bmatrix} T_x \\ T_y \\ T_z \end{bmatrix} \quad (\text{B.7})$$

and the output matrix relation is  $\mathbf{y} = \mathbf{Cx} + \mathbf{Du}$ :

$$\begin{bmatrix} \tilde{\phi} \\ \tilde{\theta} \\ \tilde{\psi} \end{bmatrix} = \begin{bmatrix} 1 & 0 & 0 & 0 & 0 & 0 \\ 0 & 1 & 0 & 0 & 0 & 0 \\ 0 & 0 & 1 & 0 & 0 & 0 \end{bmatrix} \begin{bmatrix} x_1 \\ x_2 \\ x_3 \\ x_4 \\ x_5 \\ x_6 \end{bmatrix} + \begin{bmatrix} 0 & 0 & 0 \\ 0 & 0 & 0 \\ 0 & 0 & 0 \end{bmatrix} \begin{bmatrix} T_x \\ T_y \\ T_z \end{bmatrix} \quad (\text{B.8})$$

This format is now comparable with the numerical linearisation by Matlab of the next section B.2.

### B.1.3. Stability Analysis

#### B.1.3.1. Pitch Attitude

The characteristic equation is;

$$730 \lambda^2 - 3.8722 \cdot 10^{-7} = 0 \quad (\text{B.9})$$

Then the eigenvalues are;

$$\lambda_{(1,2)0} = \pm 2.3031 \cdot 10^{-5}. \quad (\text{B.10})$$

This denotes that pitch attitude is unstable because of the positive real root.

#### B.1.3.2. Roll and Yaw Attitudes

The characteristic equation obtained from the coupled roll and yaw attitude equation (B.6) is:

$$0 = \begin{bmatrix} 3770 & 0 \\ 0 & 4020 \end{bmatrix} \lambda^2 + \begin{bmatrix} 0 & 60.1604 \\ -60.0091 & 0 \end{bmatrix} \lambda + \begin{bmatrix} -1.3701 \cdot 10^{-3} & 0 \\ 0 & -1.3633 \cdot 10^{-3} \end{bmatrix} \quad (\text{B.11})$$

$$\begin{bmatrix} 3770\lambda^2 - 1.37011 \cdot 10^{-3} & 60.16042\lambda \\ -60.00913\lambda & 4020\lambda^2 - 1.36332 \cdot 10^{-3} \end{bmatrix} \begin{bmatrix} \tilde{\phi} \\ \tilde{\psi} \end{bmatrix} = 0 \quad (\text{B.12})$$

Then the determinant of the 2x2 matrix shall be zero;

$$15155400 \lambda^4 + 3604.473 \lambda^2 + 1.868 \cdot 10^{-6} = 0 \quad (\text{B.13})$$

Then the eigenvalues are the roots of Equation B.13):

$$\lambda_{(3,4)} = 0 \pm 1.5422 \cdot 10^{-2} i \quad \text{and} \quad \lambda_{(5,6)} = 0 \pm 2.2764 \cdot 10^{-5} i \quad (\text{B.14 a , b})$$

The above eigenvalues  $\lambda_{(1-6)}$  (equations B.10 and B.14) are also identically the eigenvalues of the system matrix **A** of equation (B.7). Both the eigenvalues of roll and yaw attitudes have imaginary that causes the system be oscillatory. The real roots are at the origin that makes the roll/yaw motion marginally stable; that is if no initial rate bias and/or external disturbance exist, the satellite model stays at equilibrium or at the initially positioned angles. The control system shall deal with this stability problem as well by replacing appropriate poles and zeros.

## **B.2. CASE 2; Linearisation by Matlab**

The model is arranged with only the solar radiation pressure disturbance model as in the manual linearisation case. The command "linmod" is used to linearise the model. Here is the short description of the command usage on Matlab:

```
» help linmod
```

```
LINMOD Obtains linear models from systems of ord. diff. equations (ODEs).
[A,B,C,D]=LINMOD('SYS') obtains the state-space linear model of the
system of ordinary differential equations described in the
block diagram 'SYS' when the state variables and inputs are set
to zero.
```

```
[A,B,C,D]=LINMOD('SYS',X,U) allows the state vector, X, and
input, U, to be specified. A linear model will then be obtained
at this operating point.
```

The name of the Simulink model is "distmodel.mdl" and the Matlab output is:

```
» [a, b, c, d]=linmod('distmodel')
```

```
a =
```

```

0      0      0      0      1.000e+00      0
0      0      0      1.000e+00      0      0
0      0      0      0      0      1.000e+00
0      5.3044e-10      0      0      0      0
1.3517e-09      0      0      0      0      -1.5915e-02
0      0      0      0      1.4925e-02      0

```

b =

```

0      0      0
0      0      0
0      0      0
0      1.3699e-003      0
2.6525e-004      0      0
0      0      2.4876e-004

```

c =

```

1  0  0  0  0  0
0  1  0  0  0  0
0  0  1  0  0  0

```

d =

```

0  0  0
0  0  0
0  0  0

```

The state-space matrices **a**, **b**, **c**, **d** with the relation  $\dot{\mathbf{x}} = \mathbf{ax} + \mathbf{bu}$  and  $\mathbf{y} = \mathbf{cx} + \mathbf{du}$  where **x** is the state, **y** is the output and **u** are the control vectors respectively. The state ordering is a bit different than that of manual linearisation case.

The eigenvalues of the system matrix are:

```
» eigenvalues=eig(a)
```

```
eigenvalues =
```

```

0
2.3031e-005
-2.3031e-005
0
0 +1.5412e-002i
0 -1.5412e-002i

```

The above calculated system eigenvalues are very close to results of the manual linearisation case whose eigenvalues are defined by (B.10) and (B.14 a ,b). The

minor differences in magnitudes are due to numerical approach of Matlab. Most significant difference of Matlab's linearisation is that, it excluded the yaw angle from yaw rate differential equation. Hence one pair of roll/yaw eigenvalues obtained are at the origin, whereas manual computation yielded purely imaginary values. As a result manually linearised model more closely follows the nonlinear model and it is employed to develop control laws.

The Simulink model "distmodel.mdl" is:

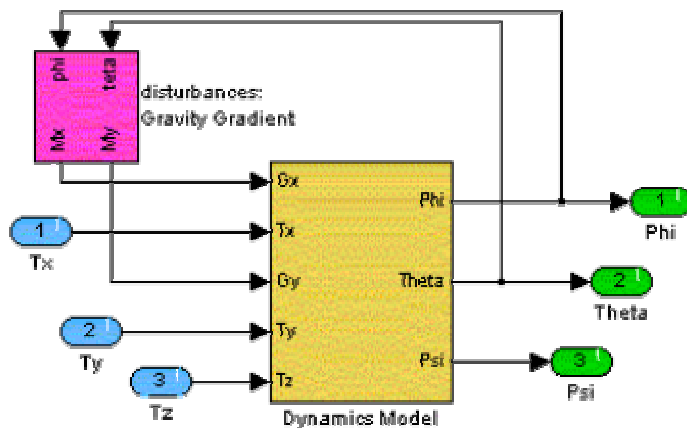


Figure 70 Main Simulink model to be linearised

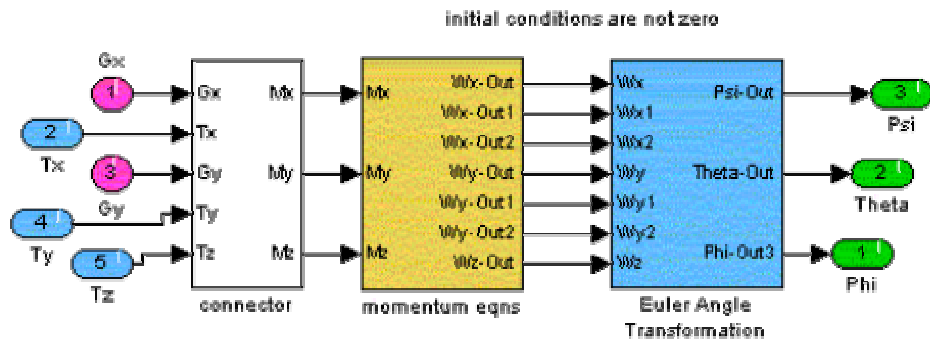
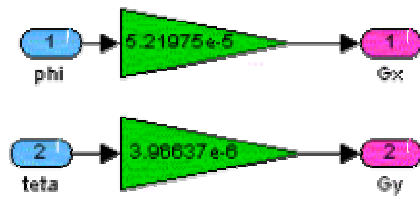
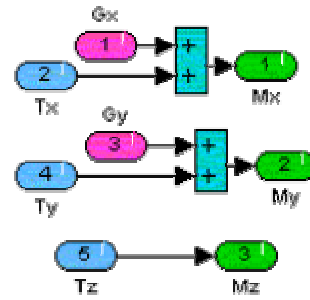


Figure 71 Subsystem "Dynamics Model"



**Figure 72 Gravity gradient perturbation torque model**



**Figure 73 Connector Subsystem**

The "Dynamics model" includes the momentum and the Euler equation sets, which were investigated in detail at Chapter 4.

### B.3. Linearisation of the Simulink Model that Excludes External Disturbance Torque Model

To analyse the dynamical behaviour represented at Appendix A with Figure A1-A3 the relevant Simulink model is also linearised to see the system eigenvalues:

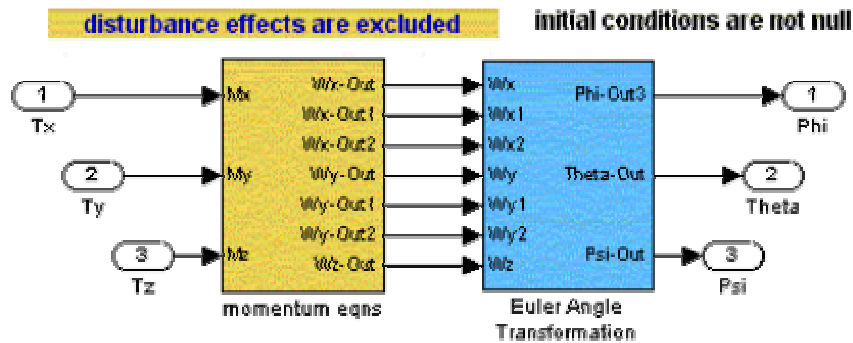


**Figure 74 Undisturbed Simulink model for linearisation**

And the Matlab linearisation is:

```
[k, l, m, n]=linmod('undistmodel')
```

k =

```

0      0      0      0      1.0000e+000      0
0      0      0 1.0000e+000      0      0
0      0      0      0      0      1.0000e+000
0      0      0      0      0      0
0      0      0      0      0      -1.5915e-002
0      0      0      0      1.4925e-002      0

```

l =

```

0      0      0
0      0      0
0      0      0
0      1.3699e-003      0
2.6525e-004      0      0
0      0      2.4876e-004

```

m =

```

1  0  0  0  0  0
0  1  0  0  0  0
0  0  1  0  0  0

```

n =

```

0  0  0
0  0  0
0  0  0

```

And the respective system eigenvalues are:

» eigenvalues=eig(k)

eigenvalues =

```

0
0
0 +1.5412e-002i
0 -1.5412e-002i
0
0

```

For the linearised system of equations the above imaginary roots are responsible from the oscillations. However the linearised model can not observe the continuous increase in the total magnitude on all attitudes.

#### **B.4 Short Discussion on Linearisations in terms of Stability**

Investigating the non-linear attitude model that is subject to the external disturbances and initial biases, the critical nature of oscillations is observed. The imaginary eigenvalues of the linearised models represent this oscillatory behaviour. Comparing the manual derivation of the linear dynamics model and the Matlab linearised model, they agree on eigenvalues. The small changes in the eigenvalues are due to numerical approaches. Both linearisation analyses agree on the observed non-linear dynamics simulations of the Appendix A. The instability in roll-pitch-yaw attitudes, and nature of oscillations in roll-yaw attitudes are best represented by the manual linearised equations. For the controller design studies manual linearisation results are used.